AFCRL-70-0581

MATHEMATICAL ANALYSIS AND COMPUTER ORIENTED ENVIRONMENTAL STUDIES

by

Donald J. Armstrong
John A. Carbone
Edward D. Conway
Peter W. Lindstrom
Carolyne M. Mandell

Analysis & Computer Systems, Inc.
Building 6, Second Avenue, Northwest Park
Burlington, Massachusetts 01803

Contract No. F19628-70-C-0029

Final Report

Period Covered: September 1969 through August 1970

September 1970

Contract Monitor: Vincent J. Mazzio, Analysis and Simulation Branch

Prepared
for

AIR FORCE CAMBRIDGE RESEARCH LABORATORIES
AIR FORCE SYSTEMS COMMAND
UNITED STATES AIR FORCE
BEDFORD, MASSACHUSETTS 01730

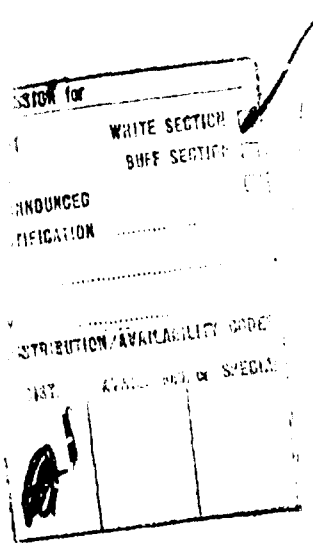

Qualified requestors may obtain additional copies from the Defense Documentation Center. All others should apply to the Clearinghouse for Federal Scientific and Technical Information.

AFCRL-70-0581

MATHEMATICAL ANALYSIS AND COMPUTER ORIENTED ENVIRONMENTAL STUDIES

by

Donald J. Armstrong
John A. Carbone
Edward D. Conway
Peter W. Lindstrom
Carolyne M. Mandell

Analysis & Computer Systems, Inc.
Building 6, Second Avenue, Northwest Park
Burlington, Massachusetts 01803

Contract No. F19628-70-C-0029

Final Report

Period Covered: September 1969 through August 1970

September 1970

Contract Monitor: Vincent J. Mazzio, Analysis and Simulation Branch

Prepared
for

AIR FORCE CAMBRIDGE RESEARCH LABORATORIES
AIR FORCE SYSTEMS COMMAND
UNITED STATES AIR FORCE
BEDFORD, MASSACHUSETTS 01730

ABSTRACT

This report is the concluding scientific report to record the status and progress of Scientific Analytical Investigations, the preparation of Computer Programs, Data Reduction, and the development of mathematical and computer techniques in support of Environmental Research and other various aspects of the physical sciences concerning the upper atmosphere.

During the year covered by this report, the 50 completed programs ranged in complexity and size from conversion of programs from one language or computer system to another, to analysis and development of a large system of analytical programs.

FOREWORD

These computer programs are the results of analytical research performed for:

The Analysis and Simulation Branch (SUYA)
Computation Center AFCRL
Air Force Cambridge Research Laboratories
Bedford, Massachusetts 01730

The computer programs contained in this report may be obtained from the above organization, upon request by referencing the appropriate project number and problem number listed at the end of each program description.

TABLE OF CONTENTS

SECTION 1

INTRODUCTION

This report documents the efforts under subject contract.

Each program documented herein describes what was done rather than a detailed program writeup.

Upon request, a complete program description may be made available to interested parties (see FOREWORD). The program descriptions are lengthy and very detailed, and may be used to follow the complete flow and operation of each program.

SECTION 2

RAINFALL, SOIL MOISTURE AND TRAFFICABILITY IN THE VICINITY OF SAIGON

1. INTRODUCTION

Trafficability, the ability of a soil to permit the movement of vehicles, is a function of soil strength. Soil strength is related to soil moisture, which in turn is related to many other variables such as soil type, drainage and vegetation. For the preparation of an accurate estimate of the effect of climatology on soil strength conditions, a long-time record of soil moisture measurements is required. For most places in the world no such record exists. In this study, equations developed for estimating soil moisture in sandy silt of the type found in low terraces in the Saigon area are used, in conjunction with a 22-year record of daily rainfall observations, to generate a soil moisture record. From knowledge of soil moisture-strength relations a soil strength record is generated. This record is used to estimate the probability of vehicle "go" (the ability to execute severe maneuvers over the soil without becoming immobilized) for given types of vehicles on any given day of the year. The data generated in this study are first estimates intended for guidance in planning military operations.

2. RAINFALL

Daily rainfall observations taken at Saigon over the 22-year period from 1947 through 1968 were sorted, by 7-day periods, to obtain the relative frequency of daily rainfall for several categories of rainfall amounts. The frequencies are plotted in Figure 1. The frequencies for each 7-day period are based on 154 observations (7 daily observations multiplied by 22 years of record). The pronounced seasonal character of rainfall in Saigon is clearly evident. From 6 Jan to 1 Apr. more than 9 out of every 10 days are without rain, while from 25 May through 20 Oct. less than 3 out of every 10 days are without rain. From about 10 June to 8 Oct. more than 1 in. of rain can be expected on 1 out of 10 days. During the 22-year period there were 9 days when more than 4 in. of rain was observed.

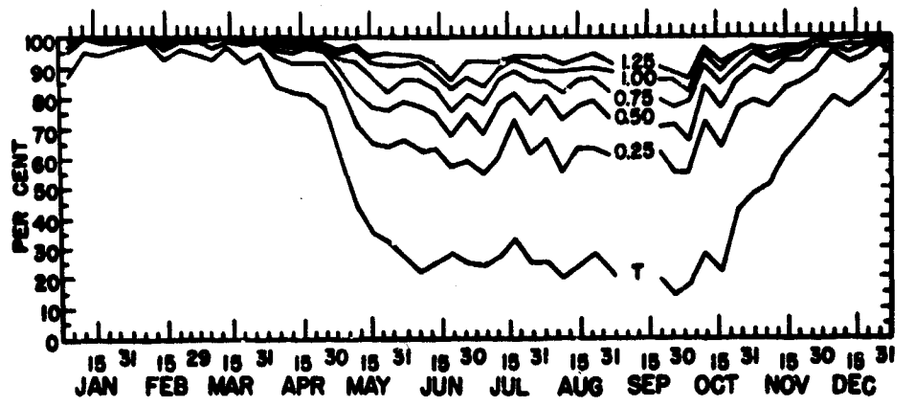

Figure 1. Relative Frequency of Daily Rainfall; ≤Trace, ≤0.25, ≤0.50, ≤0.75, ≤1.00, and ≤1.25 in. at Saigon

Since trafficability is often affected more by prolonged rainfall than by single showers, Figure 2 was prepared to depict the total rainfall that might be expected over a 5-day period. For example, the probability of observing 5 consecutive days without rain is about 85% in February and 1% from 23 May through 24 Oct. During the 22-year period there were 6 five-day periods when more than 8 in. of rainfall was observed.

Figure 3 depicts average daily rainfall and average rainfall on a day with more than a trace of rain. The curves were drawn freehand. For example, Figure 3 shows that almost three times as much rain falls on a rainy day in June or September as on a rainy day in January, and that less rainfall occurs near 1 Aug. than near 15 June or 15 Sept.

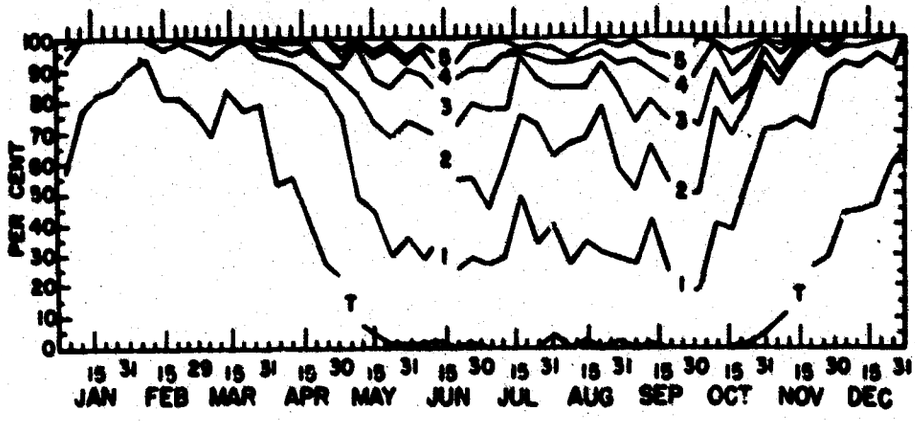

Figure 2. Relative Frequency of Total Rainfall During a Five-Day Period; ≤Trace, ≤1.00, ≤2.00, ≤3.00, ≤4.00, and ≤5.00 in. at Saigon

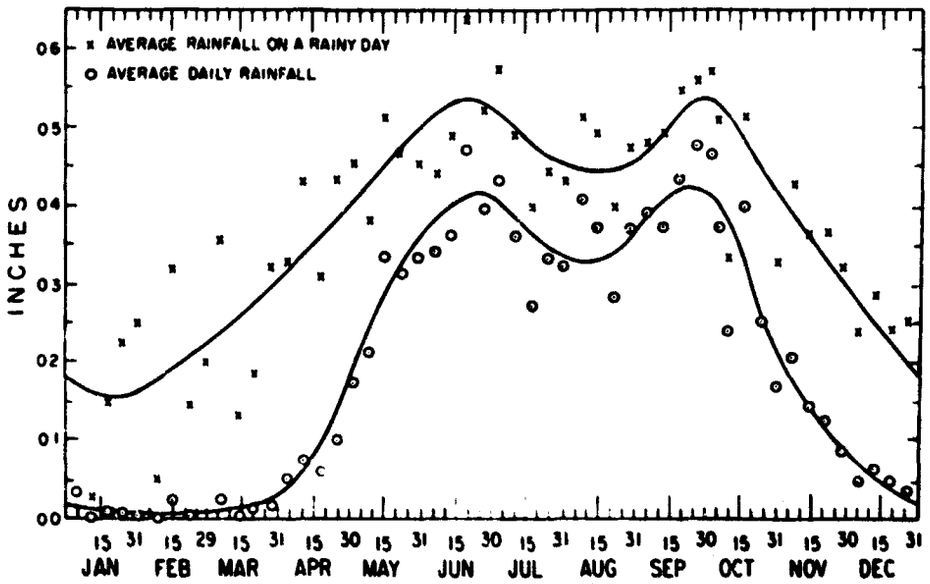

Figure 3. Average Daily Rainfall and Average Rainfall on a Day With More Than a Trace at Saigon

3. SOIL MOISTURE COMPUTATIONS

Since there was no available long-time record of soil moisture measurements taker in the vicinity of Saigon, daily soil moisture was computed with the use of equations developed for estimating moisture from rainfall amounts (Carlson and Horton, 1959), and from relations derived from an analagous soil at site PD241 in Thailand (Kennedy et al., 1967). The soil, a sandy silt, was assumed to be similar to that found in low terraces near Saigon Measurements have shown that even in the absence of rainfall over long periods this soil retains at least 0.62 in. of moisture in the 0- to 6-in. layer and 0.61 in the 6- to 12-in layer. This is termed the Field-Minimum moisture content. The Field-Maximum moisture content of the soil, the highest recurring moisture the soil can attain, was 2.38 in. in the 0- to 6-in. layer and 2.05 in. in the 6- to 12-in. layer. If rainfall equalled or exceeded 0.10 in. in one day, moisture was added to the soil (accretion) until the Field-Maximum was reached. If rainfall was not observed, or if less than 0.10 in occurred, moisture was lost from the soil (depletion) until the Field-Minimum was reached.

Observations have shown that depletion is a function of moisture content in excess of the Field-Minimum. Figure 4 depicts sixty-order least-squares fits to

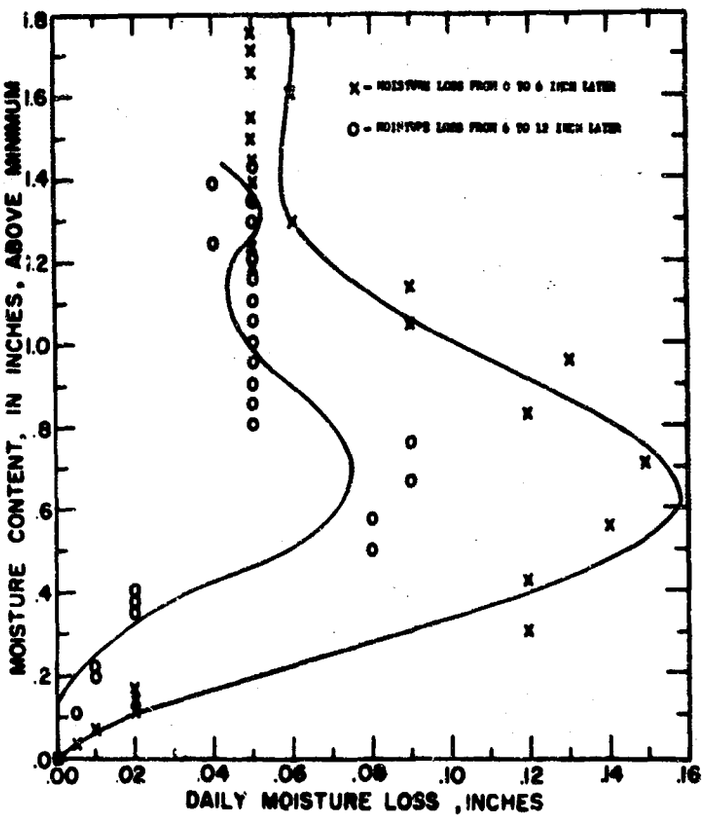

Figure 4. Daily Moisture Loss as a Function of Moisture Content in Excess of Field Minimum

measured depletion from sandy silts for the 0- to 6-in. and 6- to 12-in layers. Equations are provided in Sections 3.2 and 3.3. Depletion from the upper layer is more rapid than depletion from the lower layer. Accretion was assumed to be a simple linear function of the amount of daily rainfall.

The method of generating daily estimates of soil moisture from daily rainfall observations is as follows:

3.1 Notation

C = Moisture Content (inches), 0- to 6-in. Layer

d = Day

R = Rainfall (inches)

Z = Available Storage (inches), 0- to 6-in. Layer

A = Constant Coefficient

X = Moisture Content (inches) above Field Minimum, 0- to 6-in. Layer

M = Moisture Content (inches), 6- to 12-in. Layer

Y = Moisture Content (inches) above Field Minimum, 6- to 12-in. Layer

S = Available Storage (inches), 6- to 12-in. Layer

3.2 Computation of Soil Moisture in the 0- to 6-in. Layer

Step 1. Assume that the soil moisture on 31 Dec. 1946 was 0.62 in. in the 0- to 6-in. layer, and 0.61 in. in the 6- to 12-in. layer

Step 2. Compute the soil moisture on 1 Jan. 1947 using Eq. (1), Eq. (2), or Eq. (3), depending upon how much rain (R_d) was observed on 1 Jan. 1947 (rain during 24-hr. period previous to observation).

$$C_{d+1} = C_d - \left(\sum_{i=1}^{4} A_i X^i\right) \quad \text{if } R_d < 0.10, \tag{1}$$

$$C_{d+1} = C_d + 0.47R_d - 0.01 \quad \text{if } (S_d + Z_d) \geq R_d \geq 0.10, \tag{2}$$

$$C_{d+1} = C_d + 0.75Z_d - 0.05 \quad \text{if } R_d \geq (S_d + Z_d), \tag{3}$$

where:

$S_d = 2.05 - M_d$
$Z_d = 2.38 - C_d$
$X_d = C_d - 0.62$

$$\sum_{i=1}^{6} A_i X = 0.030X + 1.894X^2 - 4.103X^3 + 3.257X^4 - 1.107X^5 + 0.133X^6.$$

3.3 Computation of Soil Moisture in the 6- to 12-in. Layer

Step 3. Compute the soil moisture on 1 Jan. 1947, using Eq. (4), Eq. (5), or Eq. (6), depending upon how much rain (R_d) was observed on 1 Jan. 1947 (rain during 24-hr. period previous to observation).

$$M_{d+1} = M_d - \left(\sum_{i=1}^{6} A_i^i \, Y^i \right) \quad \text{if } R_d < 0.10, \tag{4}$$

$$M_{d+1} = M_d + 0.22 R_d - 0.01 \quad \text{if } (S_d + Z_d) \geq R_d \geq 0.10, \tag{5}$$

$$M_{d+1} = M_d + 0.60 S_d - 0.02 \quad \text{if } R_d \geq (S_d + Z_d), \tag{6}$$

where:

$$Y_d = M_d - 0.61$$

$$\sum_{i=1}^{6} A_i^i \, Y^i = -0.054Y - 0.083Y^2 + 3.057Y^3 - 6.625Y^4 + 5.069Y^5 - 1.316Y^6.$$

3.4 Generation of Soil Moisture Record and Frequencies

Step 4. Compute soil moisture for 0- to 6-in. and 6- to 12-in. layers on 2 Jan. 1947, using the rainfall observed on 2 Jan. 1947 as R_d and the C_{d+1} value computed in Step 2 as C_d, and the M_{d+1} value computed in Step 3 as M_d.

Step 5. Repeat Steps 2 and 3 until moisture content values are generated for every day of the 22-year period.

Step 6. For each 7-day period (1 to 7 Jan., 8 to 14 Jan., and so forth), find the relative frequency of days when the moisture content is in each of the following categories for each of the two layers.

(a)	0.70	(j)	1.60	
(b)	0.80	(k)	1.70	
(c)	0.90	(l)	1.80	
(d)	1.00	(m)	1.90	
(e)	1.10	(n)	2.00	
(f)	1.20	(o)	2.10	
(g)	1.30	(p)	2.20	
(h)	1.40	(q)	2.30	Omit for 6- to 12-in. layer
(i)	1.50	(r)	2.40	

4. SOIL MOISTURE PROBABILITIES

Daily soil moisture estimates computed for the 22-year period from 1947 through 1968 were sorted, by 7-day periods, to obtain the relative frequency of several categories of soil moisture amounts. Figure 5 shows the frequencies for the 0- to 6-in. layer and Figure 6 shows the frequencies for the 6- to 12-in layer. Frequencies for each 7-day period are based on 154 estimates of soil moisture.

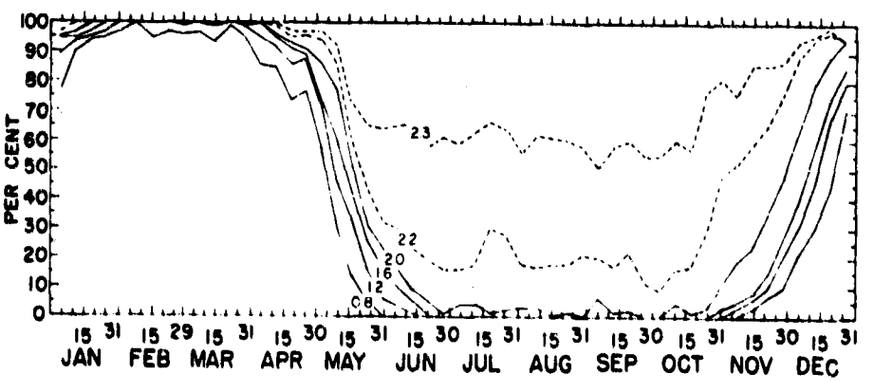

Figure 5. Relative Frequency of Moisture in the 0- to 6-in. Layer of Soil; ≤0.8, ≤1.2, ≤1.6, ≤2.0, ≤2.2 and ≤2.3 in.

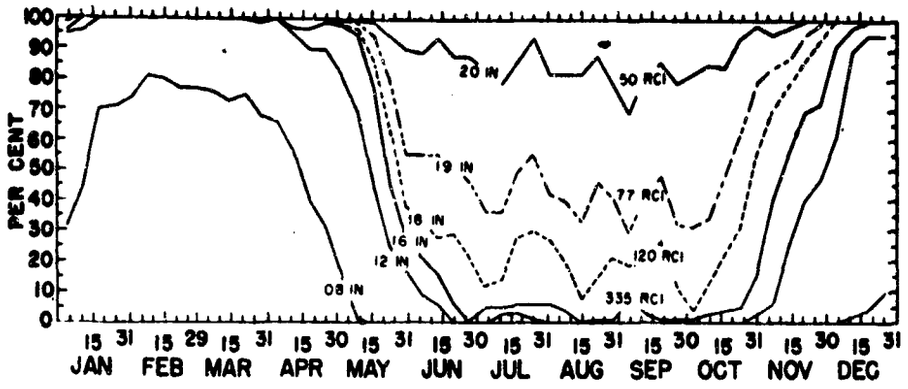

Figure 6. Relative Frequencies of Moisture and Rating Cone Index (RCI) in the 6- to 12-in. Layer of Soil. Moisture: ≤0.8, ≤1.2, ≤1.6, ≤1.8, ≤1.9, and ≤2.0 in. RCI: ≥50, ≥77, ≥120, and ≥335

5. SOIL STRENGTH-VEHICLE MOBILITY RELATIONS

Trafficability is a function of the mass shear strength of a critical soil layer. The mass shear strength is expressed in terms of rating cone index (RCI), which is a measure of the probable strength of the soil under a moving vehicle. The depth of the critical layer varies with the weight and type of vehicle and soil profile, but it is generally the layer located 6 to 12 in. below the surface. The RCI may be compared to the minimum cone index required for 50 passes of a specific vehicle, called its vehicle cone index (VCI). If the RCI of a soil is higher than the VCI of a particular vehicle, 50 such vehicles can be expected to travel successfully in the same straight-line path, or one vehicle can be expected to execute severe maneuvers without becoming immobilized. A system has been developed for classifying vehicles according to their VCI (Departments of the Army and Air Force, 1968). A condensation of the system for standard military vehicles is shown in Table 1.

Table 1. Condensed Classification of Vehicles According to Vehicle Cone Index (VCI) (contd)

Category	VCI Range	Vehicle and Vehicle Types
2	30-49	Engineer and high-speed tractors with comparatively wide tracks and low contact pressures. Examples: VCI of D7 engineer tractor = 40; VCI of M114 armored personnel carrier = 37.
3	50-59	Tractors with average contact pressures, tanks with comparatively low contact pressures, and some trailed vehicles with very low contact pressures. Example: VCI of M48 medium tank = 52.
4	60-69	Most medium tanks, tractors with high contact pressures, and all-wheel-drive trucks and trailed vehicles with low contact pressures. Example: VCI of M135, 2-1/2-ton truck = 62.
5	70-79	Most all-wheel-drive trucks, a great number of trailed vehicles, and heavy tanks. Example: VCI of 1-1/2-ton, 4x4 dump truck = 73.
6	80-99	A great number of all-wheel-drive and rear-wheel-drive trucks, and trailed vehicles intended primarily for highway use. Example: VCI of 1/2-ton, 4x2 pickup truck = 88.
7	100 or greater	Rear-wheel-drive vehicles and others that generally are not expected to operate off roads, especially in wet soils. Example: VCI of 5-ton, 4x2 dump truck = 119.

A listing of vehicle cone indexes for military vehicles and a discussion of the procedures for computing vehicle cone indexes, and a more detailed discussion of trafficability terms are included in Departments of the Army and Air Force (1968).

6. SOIL MOISTURE VERSUS SOIL STRENGTH

The relation between soil moisture and soil strength, in terms of rating cone index, for the 6- to 12-in. layer of soil is shown in Table 2.

The data in Table 2 were derived from measurements at the site in Thailand that was used in the derivation of the moisture relations discussed in Section 3, Soil Moisture Computations. If RCI from Table 2 is substituted for moisture values in Figure 6 the graph can be used to show the relative frequency of RCI equal to or greater than a given value. Thus, during the rainy period from the end of May through

Table 2. Relation Between Soil Moisture and Soil Strength in Terms of Rating Cone Index (RCI) for the 6- to 12-in. Layer of Soil

Water Content (in.) 6- to 12-in. Layer	RCI
< 1.50	> 590
1.50	590
1.50	440
1.60	335
1.65	260
1.70	198
1.75	155
1.80	120
1.85	95
1.90	77
1.95	62
2.00	50
2.05	40

the end of September, moistures of 2.0 in. or less or RCI's of 50 or more occur 80 to 90 percent of the time, and moistures of 1.8 in or less or RCI's of 120 or more occur 10 to 30 per cent of the time.

7. PROBABILITY OF VEHICLE "GO"

The RCI may be related to the minimum cone index requirements of "go" for a vehicle, and so in Figure 7 graphs of VCI were substituted for the graphs

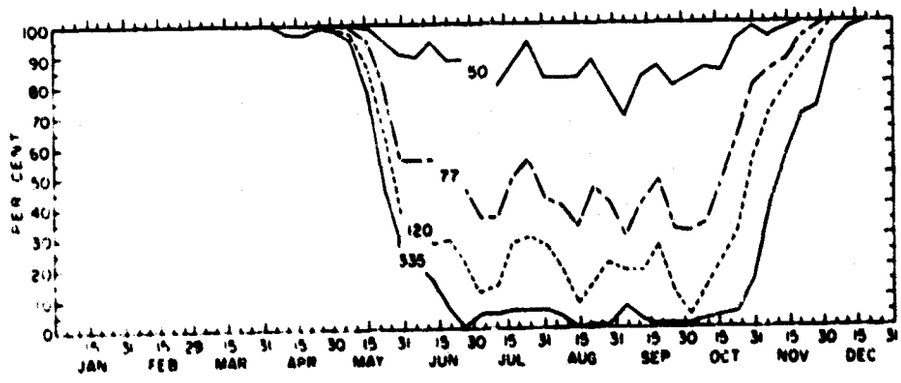

Figure 7. Probability of "Go" for Vehicles With Vehicle Cone Index (VCI) of 50, 77, 120, and 335

of RCI shown in Figure 6. Figure 7 shows that during the rainy season vehicles with a VCI of 50 will have an 80- to 90- percent probability of "go" (or conversely, 10- to 20- percent probability of "no go") and that vehicles with a VCI of 120 will have a 10- to 30- percent probability of "go" (or conversely, a 70- to 90- percent probability of "no go").

8. LIMITATIONS OF STUDY

Caution should be exercised in drawing conclusions on trafficability in the Saigon area from the graphs presented herein. The graphs were developed for only one of several soils in the area, specifically a sandy silt found in low terraces. Other soils within the area include: (1) alluvial and marine clays, similar to the soils in the lowlands of the Mekong delta; these clays remain wet and have poor trafficability throughout the rainy season; (2) clays and sandy clays on hills; these clays generally have good trafficability even during the rainy season; and (3) silty clays in narrow valleys on terraces and hills; these clays are trafficability problems when wet. The area also includes clays and organic soils of mangrove swamps and marshes, which remain soft, and sands of river terraces and ridges, which remain firm throughout the year. These other soils were not analyzed because of limitations of time and money. The sandy silt terrace soil was chosen for analysis because it is one of the predominant soils in the area, and because, of all the predominant soils, it provides one of the lowest bearing strengths (RCI) under wettest conditions.

It should be recognized that the charts in this paper are based on rainfall and therefore are not applicable to soils subjected to irrigation. Areas of irrigated rice paddies, commonly found on low terraces, would normally have higher percentages of high moistures and low strengths and a lower probability of "go" for a given vehicle than those shown on the charts.

The probabilities of vehicle "go - no-go" are applicable only to soil conditions on flat terrain. The slope and such natural obstacles as drainageways, scarps, dense vegetation, and microrelief features as well as such man-made obstacles as railroad embankments, canals, and so forth, are not considered in the mobility evaluations.

Project Number: 8624

Problem Number: 1675

Researcher: Mr. I. Lund

SECTION 3

CORRELATIONS BETWEEN AREAL PRECIPITATION AND GEOPOTENTIAL HEIGHT

This study was performed to identify predictors which might be used to replace, or supplement, persistence in conditional climatologies of precipitation, and to provide at least partial answers to the following questions:

a. Are geopotential height observations better predictors of daily areal precipitation than persistence?

b. Which geopotential height observations are most highly correlated with areal precipitation?

c. How do predictors of areal precipitation vary with respect to the geographical location of the predictant stations?

d. Over how long a period of time are height observations significantly correlated with areal precipitation?

To accomplish this end, computer programs were written to correlate geopotential heights, geostrophic vorticities, and thicknesses between surfaces, at 499 grid-points over one-half of the Northern Hemisphere, extending from 10 degrees E westward to 170 degrees W, at 200, 500, and 850-mb with precipitation observed over areas in California, Central United States, and Eastern United States on 401 January and February days.

The daily total precipitations observed between 0000 LST and 2400 LST, at 10 stations in each of three areas, was used as the predictand. The stations are listed on the following page and the areas are shown in Figure 1.

	EAST	CENTRAL	CALIFORNIA
1.	Concord, N. H.	Burlington, Ia.	Red Bluff
2.	Boston, Mass.	DesMoines, Ia.	Chico
3.	Hartford, Conn.	Dubuque, Ia.	Colusa
4.	Albany, N. Y.	Columbia, Mo.	Brooks
5.	New York, N. Y.	Kansas City, Mo.	Sacramento
6.	Harrisburg, Pa.	St. Louis, Mo.	Stockton
7.	Philadelphia, Pa.	Springfield, Mo.	Modesto
8.	Atlantic City, N. J.	Peoria, Ill.	Merced
9.	Baltimore, Md.	Wichita, Kan.	Fresno
10.	Washington, D. C.	Tulsa, Okla.	Angiola (Corcoran)

The data include all January and February days from 1962 through 1969.

The total precipitation observed at the 10 stations, in each area, during the period from 1 January through 22 February for the years 1962 through 1969, a sample of 424 days, was correlated with the precipitation observed from one to six days later. The results were:

DAYS	EAST	CENTRAL	CALIFORNIA
1	0.01	0.20	0.53
2	-0.09	-0.00	0.20
3	-0.03	-0.01	0.16
4	-0.04	-0.08	0.12
5	-0.02	-0.05	0.11
6	-0.06	0.04	0.14

Heights of the 200, 500 and 850-mb surfaces at the 499 grid points shown in Figure 1 were studies. Data was available for 401 of the possible 424 days between 1 January and 22 February for the years 1962 through 1969. Geopotential heights at each surface, height difference (thickness) between surfaces, and geostrophic vorticities were correlated with precipitation. The vorticities were simply the sum of the heights at the four surrounding grid points minus four times the height at the center point.

More than 90,000 correlation coefficients were computed to prepare 189 maps depicting relationships between height data and subsequent precipitation. Examples of these maps are shown in Figures 2, 3, 4, and 5. The highest correlation coefficient found on each map is given in Table 1.

Since precipitation values used in this study are not normally distributed in a statistical sense, the method proposed by Lund (1970) was used to test the significance of the coefficients.

The frequency distribution of the 424 daily California precipitation values is shown in Figure 6. The values greater than zero were fitted to a normal distribution. The resulting curve,

$$\hat{Y} = 0.301X - 4.378X^2 + 12.817X^3 - 9.065X^4 + 2.656X^5 - 0.279X^6 \quad \text{when } X \geq 0.4 \text{ and } \hat{Y} = 0, \text{ when } X < 0.4$$

where $\hat{Y}$ is an estimate of California precipitation and X is a normal number, is also shown in Figure 6. Equation above was used to generate 8020 bogus precipitation values (see Figure 7). Also, see Figure 8 for the plot of the largest of the 499 coefficients obtained with each of the 20 sets of bogus values.

The frequency distribution of the 424 daily East precipitation values and a least squares curve fit to the data,

$\hat{Y}' = 0.103+0.173X_1+1.237X_1^3+0.171X_1^4-0.251X_1^5+0.041X_1^6$, when $X_1 \geq -0.3$, and

$Y = 0$, when $X_1 < -0.3$,

where $\hat{Y}'$ is an estimate of East precipitation and X_1 is a normal number is shown in Figure 9. See Figure 10 for the highest correlation coefficient obtained from the 20 sets of 499 coefficients each when bogus values were used. Results from Central United States were obtained in a similar manner.

The following tentative answers were received from this study.

1. A single well-chosen geopotential height observation is a better predictor of future daily precipitation than persistence.

2. 850-mb heights are usually better predictors than observations taken at higher altitudes.

3. Predictors are found in areas expected by experienced synoptic weather forecasters rather than some distant unsuspected location.

4. The statistical significance of correlations between height observations and California precipitation exceeds the 5% level for all periods of less than five days.

Project Number: 8624

Problem Number: 1446

Researcher: Mr. I. Lund

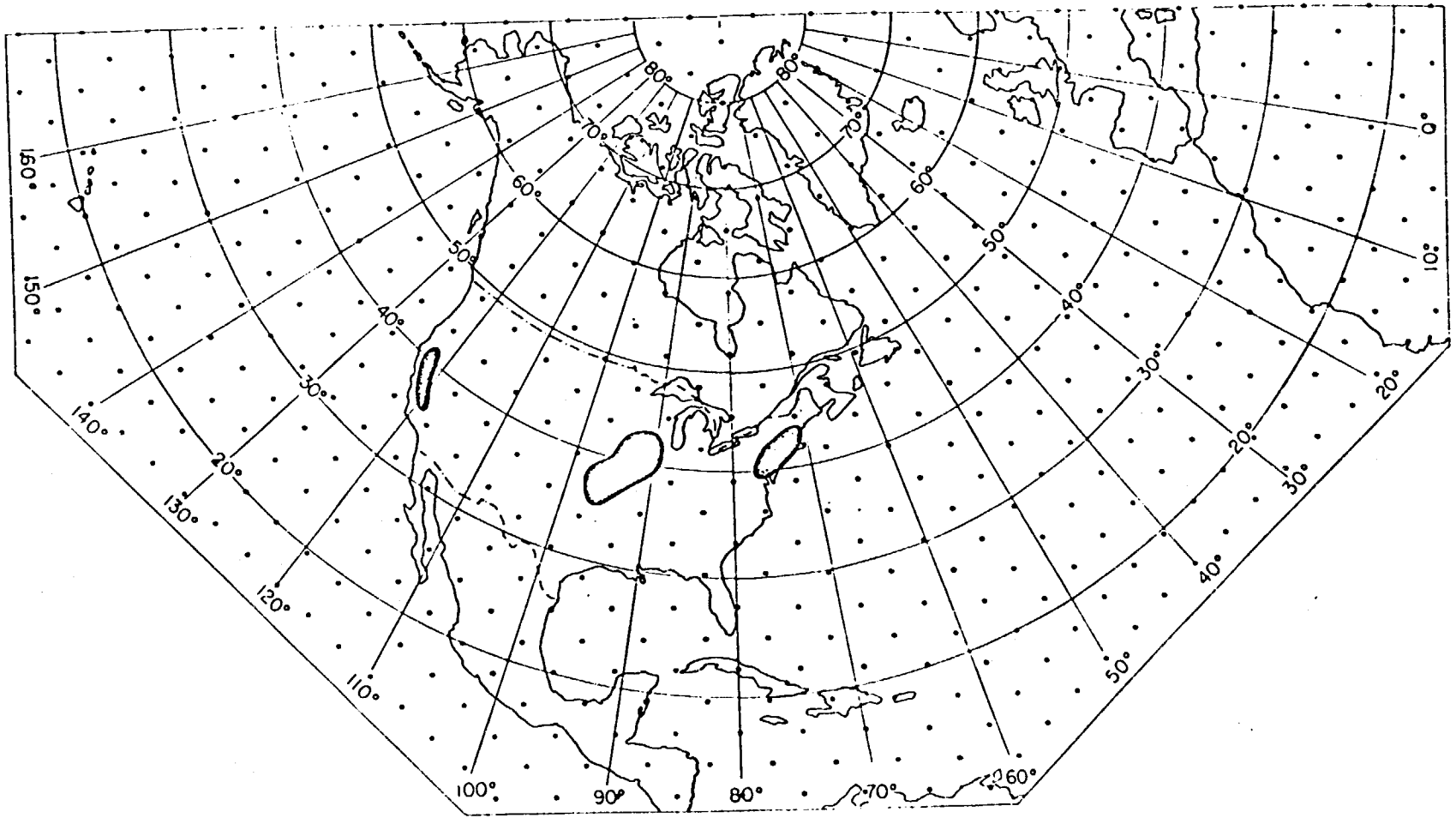

Fig. 1 Location of the three precipitation areas and the 499 grid-points over which geopotential heights were obtained.

AFCRL PHOTO 40-3

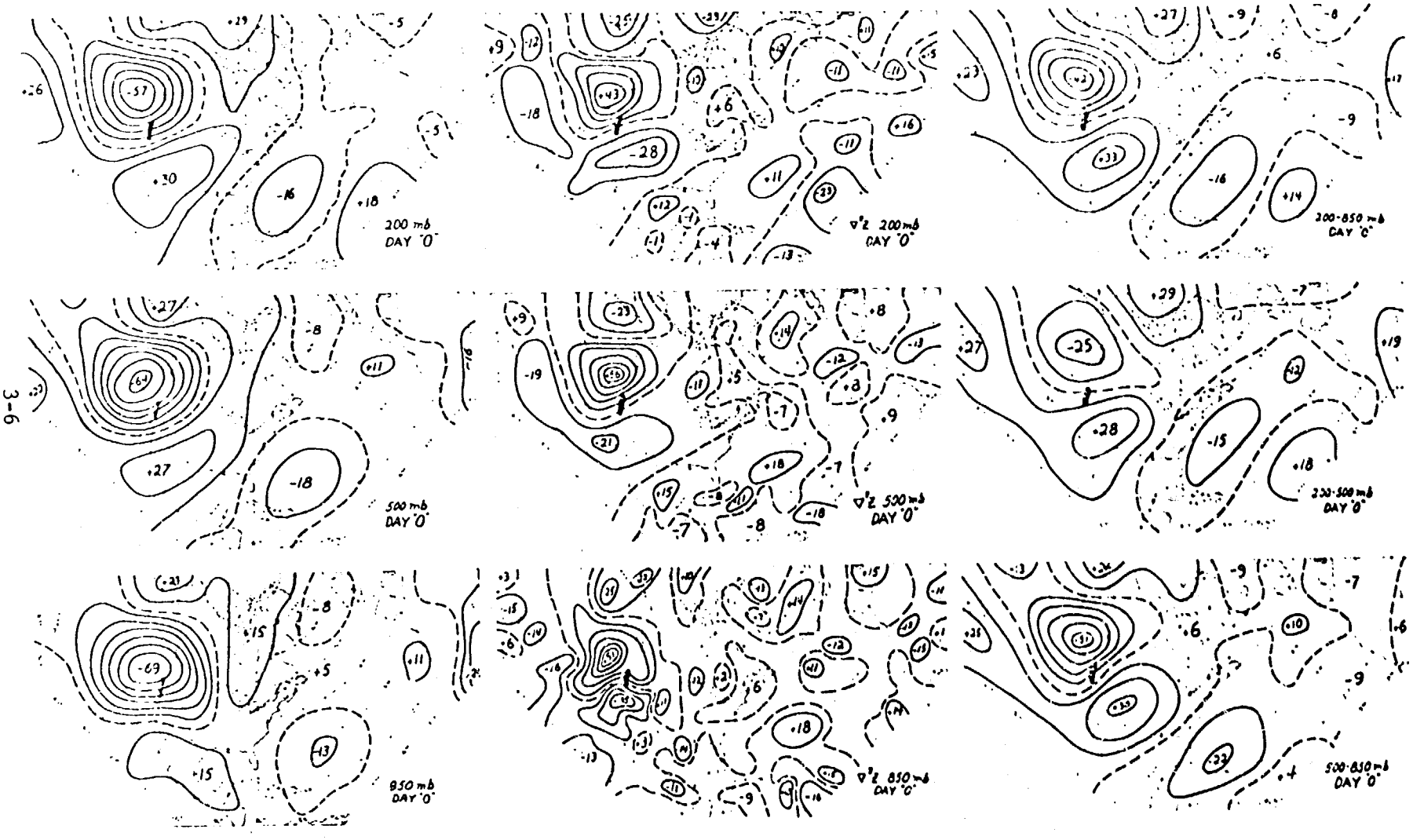

Fig. 2 Correlations between 01,CO LST geopotential heights (left column), geostrophic vorticities (center column), height differences (right column) and total precipitation observed between CCCOLST and 21,COLST at 10 stations in California (darkened area), on 101 January and February days.

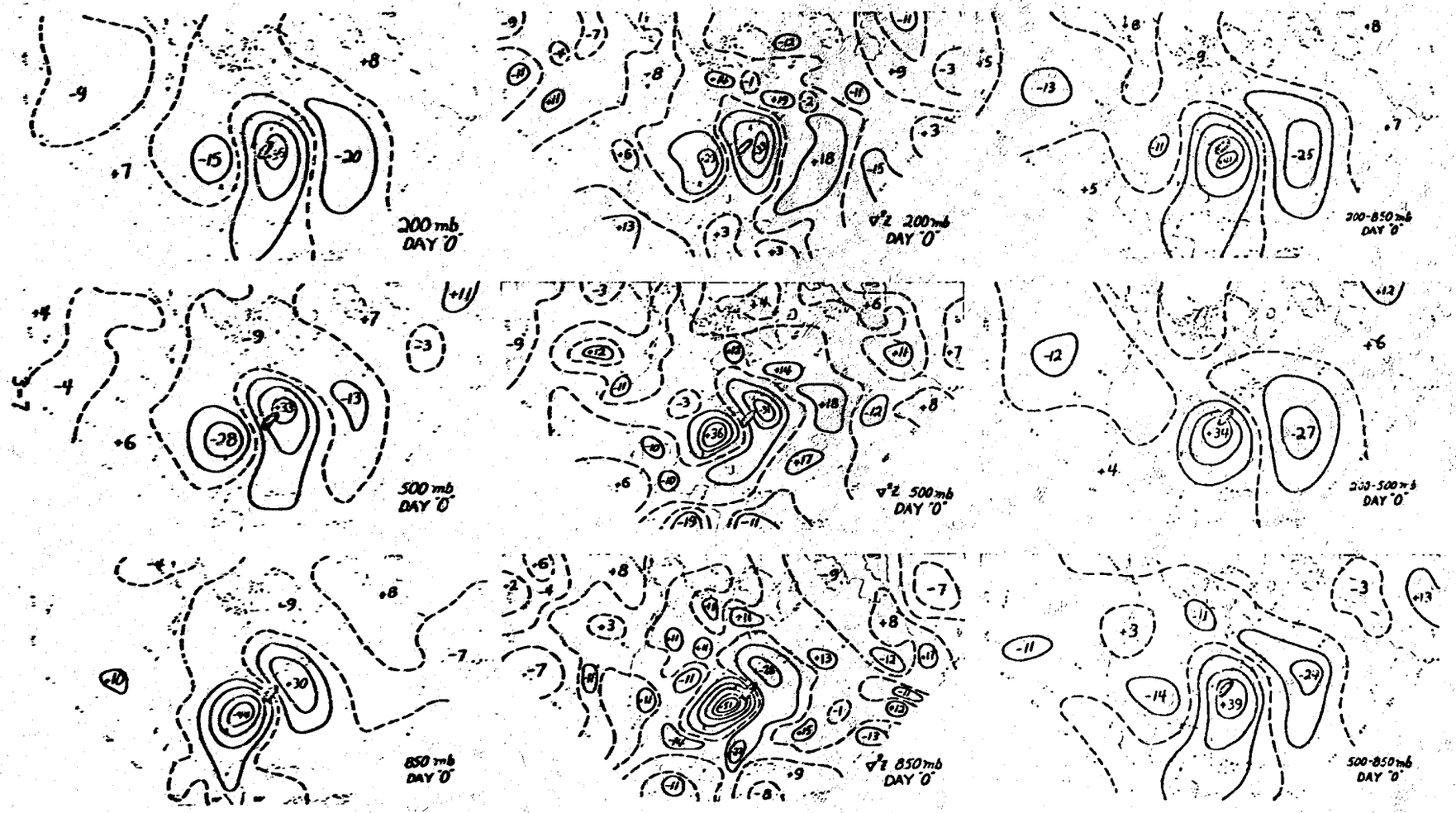

Fig. 3 Correlations between 07CCLST geopotential heights (left column), geostrophic vorticities (center column), height differences (right column) and total precipitation observed between CCCOLST and 24COLST at 10 stations in Eastern United States (darkened area), on 101 January and February days.

Fig. 1: Correlations between 04COLST geopotential heights (left column), geostrophic vorticities (center column), height differences (right column) and total precipitation observed between 00COLST and 24COLST two days later (44 to 68 hours after the heights were observed) at 10 stations in California (darkened area), on 401 January and February days.

Fig. 5 Correlations between 0700LST geopotential heights (left column), geostrophic vorticities (center column), height differences (right column) and total precipitation observed between 0000LST and 2400LST two days later (41 to 65 hours after the heights were observed) at 10 stations in Eastern United States (darkened area), on 401 January and February days.

Table 1. The highest correlation coefficient observed on each of the 189 maps. The largest value in each row is underlined.

		HEIGHT(Z)			VORTICITY($\nabla^2 Z$)			THICKNESS (T)		
								200	200	500
Area	Pay/Surface	200	500	850	200	500	850	850	500	850
East	0	-.36	-.33	-.44	-.33	.35	.51	.41	.34	.39
Central	0	-.41	-.39	-.35	-.35	.26	.33	.34	-.24	.35
Calif.	0	-.57	-.64	-.69	.43	.55	.51	-.42	.29	-.51
East	1	-.21	-.27	-.31	.22	.26	.34	.20	-.18	.24
Central	1	.27	-.32	-.37	.25	.22	.32	.25	-.19	-.31
Calif.	1	-.49	-.54	-.55	-.36	.35	.39	-.36	.30	-.42
East	2	-.19	-.22	-.21	.22	.19	.19	-.20	-.18	-.19
Central	2	-.25	-.26	-.26	.23	.25	-.20	-.24	-.17	-.29
Calif.	2	-.37	-.40	-.42	.31	.27	.27	.29	.27	-.33
East	3	-.17	-.17	-.17	.21	.18	.19	-.17	-.18	-.15
Central	3	-.24	-.24	-.23	.25	.26	.21	-.26	-.18	-.31
Calif.	3	-.29	-.29	-.30	.27	-.19	-.20	.27	.24	-.26
East	4	-.18	-.18	-.17	-.16	-.17	-.16	-.19	-.15	-.20
Central	4	-.22	-.20	-.21	.23	.20	.20	-.22	.17	-.25
Calif.	4	-.24	-.24	-.23	.24	-.19	.18	.23	.22	.24
East	5	-.19	-.16	-.14	.16	.16	-.16	-.19	-.17	-.19
Central	5	-.16	-.19	-.19	.20	.20	.19	-.15	-.12	-.16
Calif.	5	-.24	.22	-.21	-.21	.21	-.18	.25	.23	.26
East	6	-.13	-.11	-.15	.15	-.14	-.16	-.16	-.16	-.15
Central	6	-.15	-.19	-.18	-.17	.14	-.18	-.15	-.18	.14
Calif.	6	.21	-.19	-.20	.22	-.18	-.18	.24	.22	.21

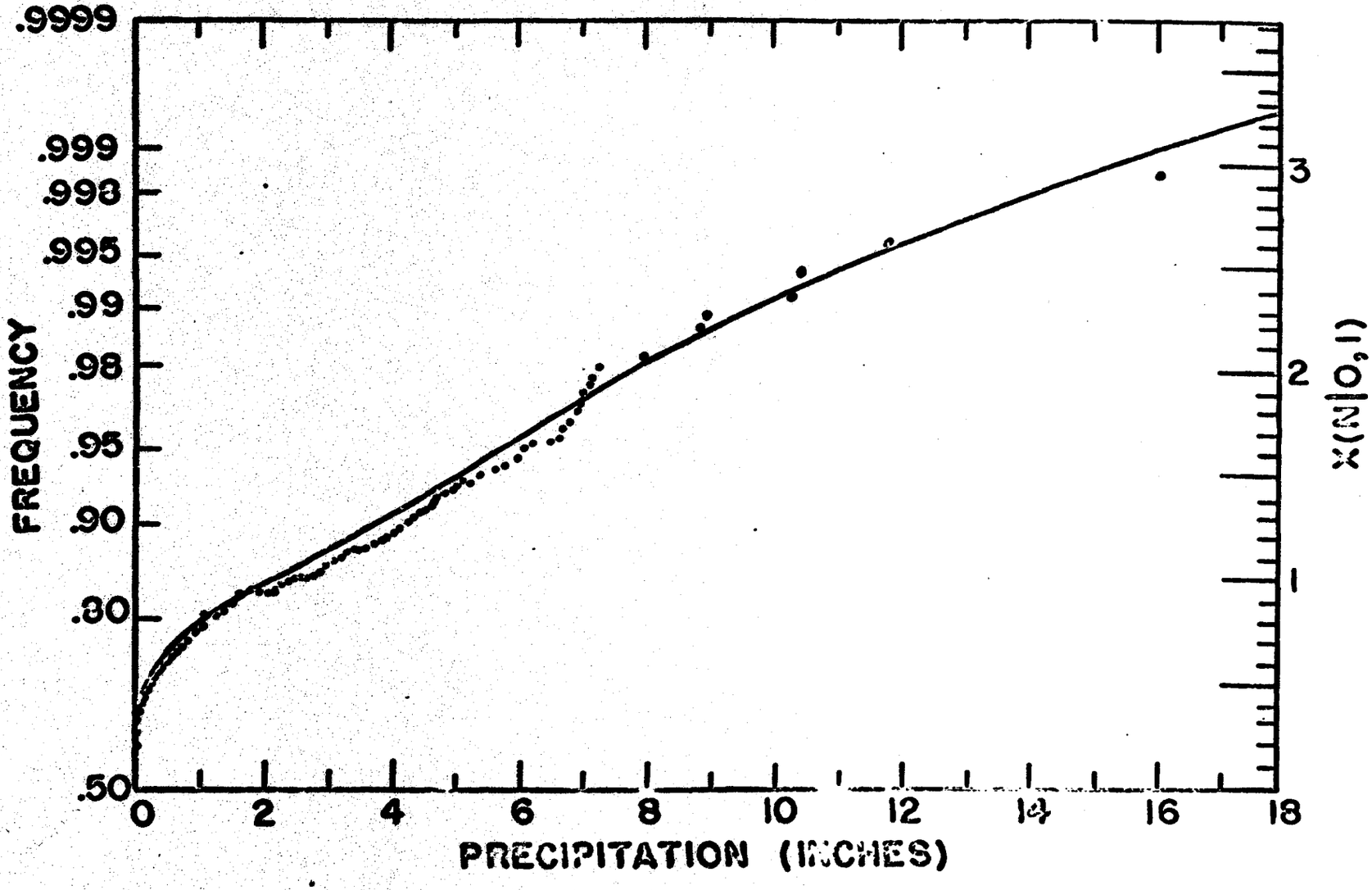

Fig. 6 Frequency distribution of the 424 daily 10-station total 1 January- 22 February precipitation values for California (1962-1969). The curve is a least-squares fit to normalized values Equation (2).

AFCRL PHOTO 40-1

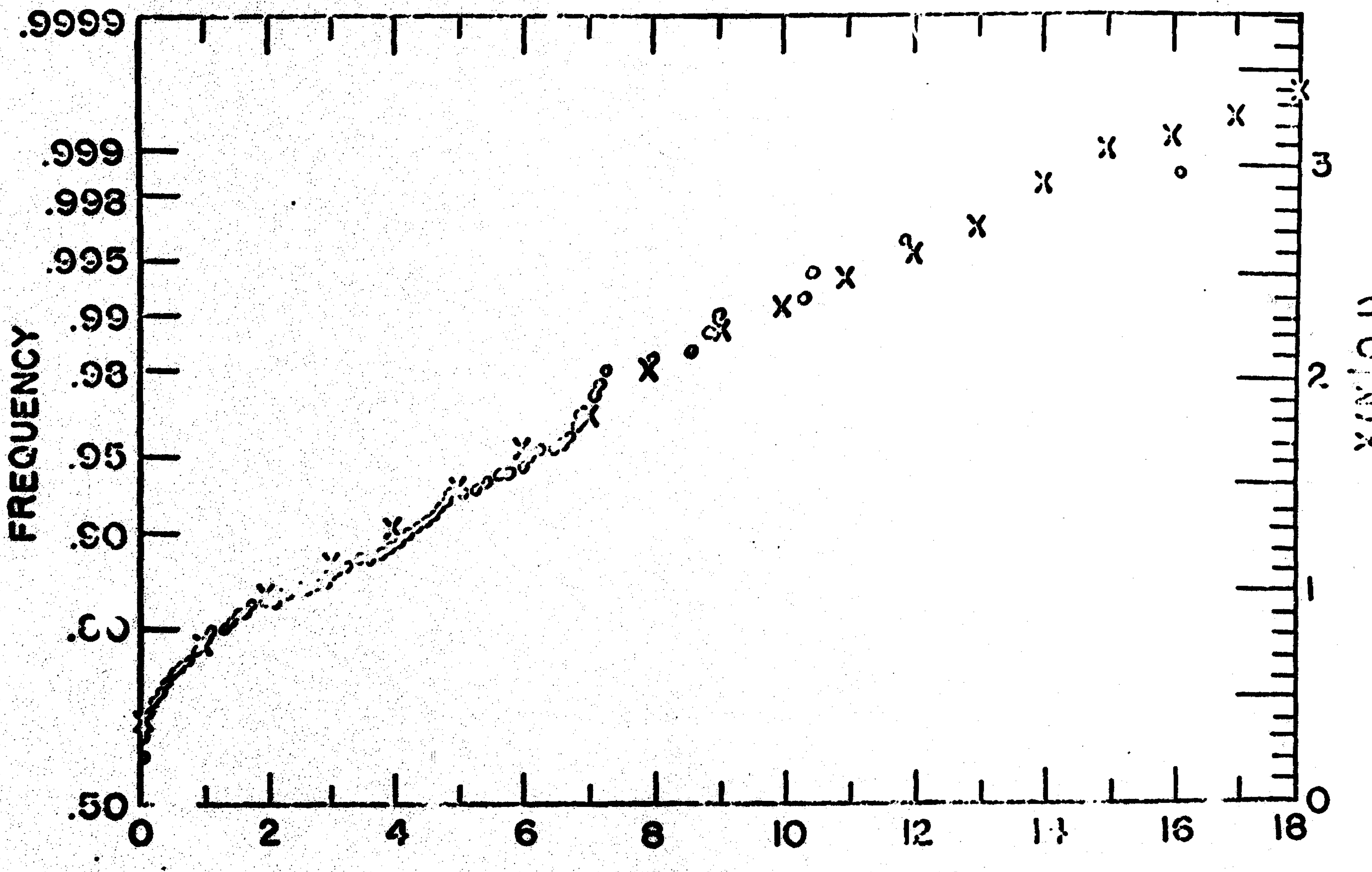

Fig. 7 Frequency distribution of the 124 California precipitation values (dots) and of 8020 bogus precipitation values (X's) generated from 8020 random normal numbers through use of Equation (2).

AFCRL PHOTO 40-103

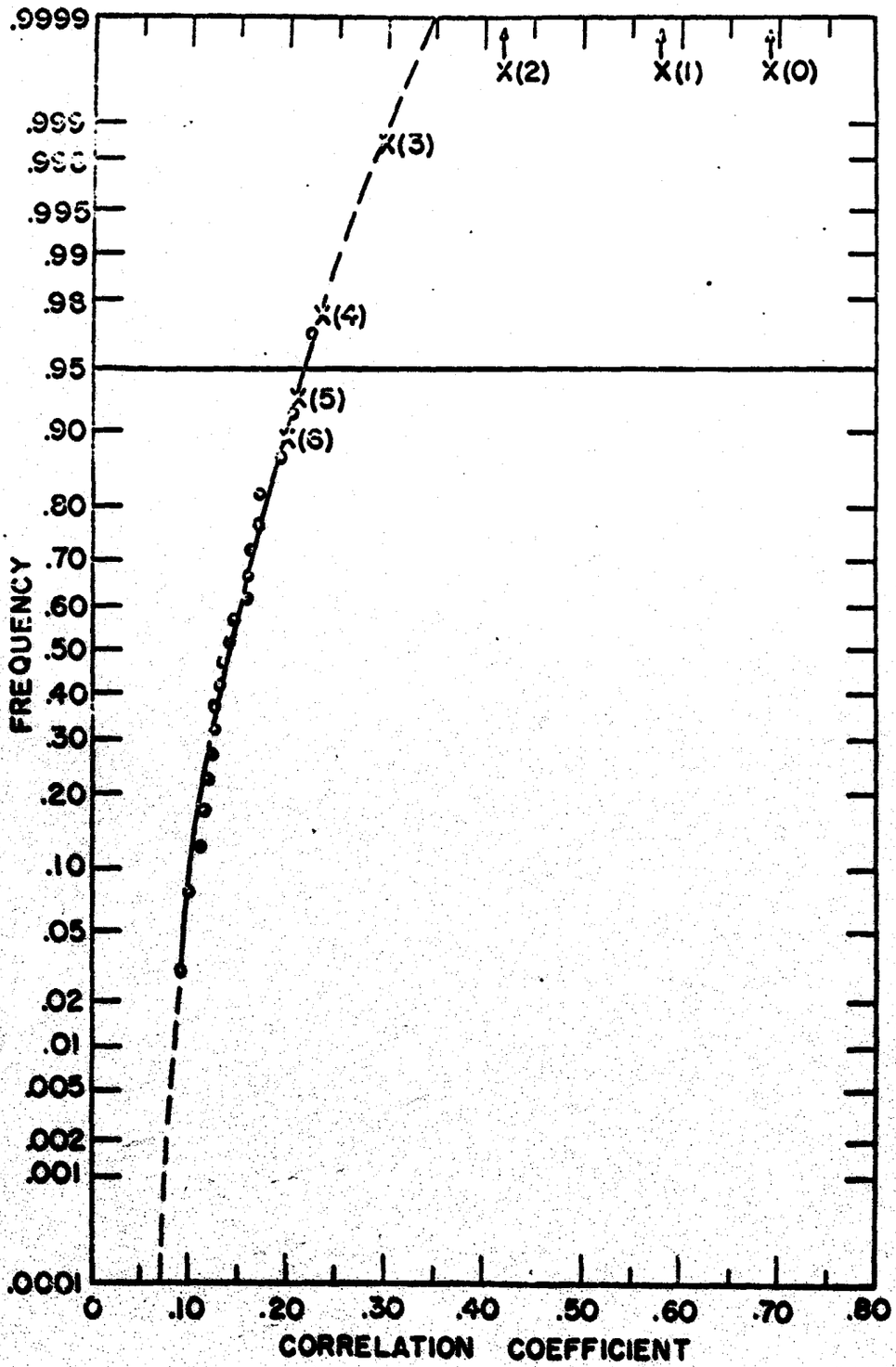

Fig. 6 Frequency distribution of the highest of 154 correlations on each of 20 charts of correlations between 850-mb heights and boyta precipitation values (dots), and corresponding correlations between the same 850-mb heights and actual observed California precipitation (X's) on the same day (0), and (1) through (6) days after the heights were observed.

SECTION 4

STUDIES OF CLOUDS AND WEATHER OVER SEA

I. Introduction

The aim of these studies is to improve the forecasting of cloudiness and weather occurences over Southeast Asia (SEA) during the southwest monsoon enabled by the supplemental use of data derived from satellites. Studies range from the development of simple empirical relationships which can currently be applied in the preparation of forecasts to more basic studies which are required for understanding the weather of the area.

II. The Weather Radar Index & Its Use

A radar index, RI, was developed and calculated for each hour to provide a measure of precipitation activity over SEA. The index as calculated in 1969 represented the percental coverage of radar echoes whose radius was 50 nautical miles centered at the four stations of Tan Son Nhut, Ubon, Udorn, and Pleiku. To assess the accuracy of the index, a comparison between computed areas of echoes as photographed on the PPI scope and computed areas from radar echoes (RAREPS) was initiated. This comparison was first done using data from Miami during summer showery conditions; and, later polarcid transparencies of ground clutter patterns and the PPI scope at antenna elevations of 0 degrees and 4 degrees were made available from Ubon and Udorn during an eight day period in September 1969. The Miami data were supplied as scope photography tracings which were planimeterized to determine total echo area within a 50 nautical mile radius of the radar. The SEA data was projected and drawn onto computer generated plots of the appropriate RAREPS. Areas of the outlined echoes were then calculated by using an area calculator, which is an electrical

device which counts the number of small squares intercepted by a conducting pencil as the operator runs it over the areas. From correlation coefficients between the measured and reported indices: 0.69 for 60 cases at Miami, 0.63 for 113 cases at Ubon, and 0.66 for 150 cases at Udorn, the regression lines found for each relationship were as follows:

Miami: $RI_{photo} = 0.56\ (RI_{RAREP}) + 6.96$

Ubon: $RI_{photo} = 0.46\ (RI_{RAREP}) + 2.04$

Udorn: $RI_{photo} = 0.28\ (RI_{RAREP}) + 0.64$

Thus, on the average the RAREP calculations grossly overestimate the true RI.

In order to test for human variability when taking RAREP readings, an analysis of variance was done on the differences between the RAREP radar index and the photography radar index for six operators at Ubon. The results showed that one operator underestimated the radar coverage by an average of 2% of the 50 nautical mile circle, while other operators overestimated by averages as great as 8%. Using the F distribution the averages for the six operators are found to be different at the 1% level of significance. These differences may not be due solely to the individual observers interpretations of observation but could arise from the time interval between RAREP and photograph being often as much as 15-20 minutes. The gain settings and photographic exposure were presumed reasonably consistent although since the true values are uncommon this could allow for another degree of variability.

In order to eliminate any significant errors from indices computed from the RAREPS and since the true index varied considerably from hour to hour, the index was averaged for use over twelve-hourly or at least three-hourly periods. Previously, an RI was emphasized as an index of aerial coverage of rain and not a good index of the amount of rainfall within the area. Thus, a study was conducted using the Tan Son Nhut precipitation record and RI's for that station over the summer months of 1966-68. On an hourly basis, a correlation of 0.72 between RI vs. rain occurence was found using a sample of 244 cases. The correlation was 0.68 for RI vs. the number of hours of rainfall less than or equal to 0.0 mm; and a correlation of 0.58 vs. the number of hours of rainfall over 0.5 mm. When the data from four stations within 50 miles were used, a correlation of 0.82 was found between the RI and hours of rain, thus substantiating the view that an RI represents the frequency or probability of rain better than the amount of rainfall.

From these findings, the degree of activity with regard to aerial rainfall coverage is expressed as a tertile 1, 2, or 3 day. The part of the day considered is from 1230 to 2330 LT, although other periods could have been used if desired. The average RI's for this 12-hourly period are determined for each station, Tan Son Nhut, Pleiku, Ubon and Udorn. September's RIs have been added for 1967 and 1968 at Pleiku, Ubon, and Udorn; while Tan Son Nhut also includes June through August 1966. The average daily RI's for each station are then ranked and divided into thirds. The highest third, TERTILE 1, represents active days while days in TERTILE 2 are considered average and days in TERTILE 3 are considered inactive. Since these classes are relative, the large average over-estimates of RI that are known to exist are unimportant.

III. Relationship Between Cloudiness, Current and Subsequent Radar Indices

New correlation coefficients of noontime cloudiness and coordinates of the maximum correlation values.

Expansion of the data sample to include Septembers of 1967 and 1968 required that noontime APT pictures for these months be prepared and read. The data were then smoothed over 4° X 4° overlapping squares as before, added to the accumulated sample of 1969 data and correlated with subsequent radar indices as before. New coordinates of the center of the 4° X 4° squares which gave the highest correlations at key locations, the value of the correlation coefficient and number of days used are shown in Table 1. This data is one of several variables used to yield a forecast of activity.

IV. Relationships Between Large Scale Pressure Distribution and Subsequent Radar Index

Previous analysis on this data was done using an average RI for the SEA peninsula area. Each days' 1230-2330 LT average RI was an average of the combined RI of Tan Son Nhut, Pleiku, Ubon and Udorn. However, the findings from day to day correlations between the widely separated stations were as low as +0.16, thus to possibly secure more significant results, all analysis was performed with respect to activity at a single station at a time. Analysis was done in detail for Tan Son Nhut and to a lesser extent for Udorn. Also, the data used in the analysis was expanded to include September of 1967 and 1968. The area of the analysis was also expanded to cover the Northern Hemisphere in order to show planetary wave patterns if they truly exist. Other new data consisted of 00Z MSL (mean sea level) grid point pressures that covered an area extending from about 80°E to 160°E and 0° to 15°N. These pressures were read to 0.2 millibars from maps prepared by the Hong Kong Royal Observatory, and were then adjusted to heights at 1000 millibars

to provide an aerial extension to the hemispheric 1000 mb height analysis. The MSL data was evaluated separately to obtain printout grids which were then combined with the 1000 millibar printout grids.

Generally, 1970's results concur with previous findings. Of greatest significance was the fact that concurrently and for several days preceding activity over the peninsula as a whole, and also at individual stations, heights are high over North Korea, especially at the 200 mb level. Pressure height thicknesses over that area indicate that the entire air column is 2 1/2° to 3° warmer before active than before inactive days. Present analysis, however, failed to show any relationships with mid-latitude troughs at any level or abnormal effects over or near the Tibetian Peninsula. Preceding activity, the hemispheric analysis yielded an unexplainable picture of slightly higher heights in the lower atmosphere around the hemisphere near 20°N except from 10° to 100°E. At the 500 mb level, heights near 30°N are slightly above average around the globe on active days, while, at the same time the polar vortex shifts slightly toward the North American, northern Atlantic and northwestern European side. These departures from average are at most only 2 dekameters so their significance is uncertain at this time. Sea level data, however, shows a clear relationship between activity produced on the peninsula and the movement of areas of lower pressure westward across the Western Pacific Ocean to position in the South China Sea or over the Phillippines. Figure 1 illustrates this westward movement by the positions of the maximum correlation between the 1000 mb. heights 6, 5, 4, 3, 2 and 1 days before the RI at Pleiku. Correlation coefficients at these points were about -0.5. For activity at Tan Son Nhut the track of slightly lower pressure is near 10°N, while for activity at Udorn it is at 15°N over the China Sea and at 20°N at 140°E. The new

data did not permit back tracking of these minor pressure changes east of about 155°. Other researchers have previously illustrated the westward movement of cloud clusters across the Pacific Ocean through use of successive days of photography. This was further investigated adding credibility to the pressure and cloudiness correlations found at points east of the peninsula. Thicknesses indicated that the disturbed areas, on the average, were cool at low levels and warm aloft. As these surface disturbances move westward, low-level pressures also increase over the South China coast to cause easterly winds over that area. The resulting East-West trough is called the monsoonal trough and extends from Northern India eastward to the China Sea. Pressures south of this trough also fall during activity, so the pressure gradients south of the trough only increase slightly with activity. On inactive days, the trough is very weak or missing altogether.

V. Application of the Above Findings to Give Objective Forecasts of Future Activity

1. RI limits corresponding to different tertiles.

RI values are calculated on a day-to-day basis in order to verify activity. Radar echoes are plotted on polar coordinate paper and through the use of an area calculator (planiometer) averages are computed and the tertiles are determined from Table 2 which is based on data from June-August 1966 plus June-September 1967 and 1968 for Tan Son Nhut and June-September 1967 and 1968 for Pleiku, Ubon and Udorn.

Table 1. Correlations, r, between noontime coded cloudiness and $\overline{RI}$, number of pairs, n, and coordinates of position of the maximum correlation

RI predict period (LT)		r	n	Center 4°x4° position °N	°E
	Tan Son Nhut (based on June - Aug 66, June - Sept. 67 and 68 data)				
1230-1430	same day	.32	193	11	105
1530-1730	" "	.36	196	10	104
1830-2030	" "	.47	184	9	113
2130-2330	" "	.48	186	9	114
1230-2330	" "	.50	191	9	113
1230-2330	Day + 1	.35	182	11	116
1230-2330	Day + 2	.24	188	7	113
1230-2330	Day + 3	.29	179	6	114
	Pleiku (Based on June - Sept 1967 and 68 data)				
1230-1430	same day	.45	151	13	105
1530-1730	" "	.38	152	16	109
1830-2030	" "	.37	167	13	105
2130-2330	" "	.43	163	12	106
1230-2330	" "	.45	173	13	105
1230-2330	Day + 1	.42	145	13	115
1230-2330	Day + 2	.38	143	12	115
1230-2330	Day + 3	.36	165	15	107
	Ubon (based on June - Sept 1967 and 68)				
1230-1430	same day	.42	156	15	108
1530-1730	" "	.36	159	17 16	108
1830-2030	" "	.40	164	15	108
2130-2330	" "	.37	167	14	107
1230-2330	" "	.46	168	15	108
1230-2330	Day + 1	.36	168	16	108
1230-2330	Day + 2	.44	156	18	111
1230-2330	Day + 3	.47	157	17	112

Table 1. Continued

$\overline{RI}$ predict period (LT)		r	n	Center 4°x 4° position	
				°N	°E
Udorn (based on June - Sept 1967 and 1968)					
1230-1430	same day	.43	154	16	104
1530-1730	" "	.24	154	16	106
1830-2030	" "	.36	163	15	105
2130-2330	" "	.35	163	17	104
1230-2330	" "	.41	163	15	105
1230-2330	Day + 1	.34	141	13	114
1230-2330	Day + 2	.27	134	18	116
1230-2330	Day + 3	.21	124	15	118

Table 2 Average RI, 1230-2330LT vs tertile

	Tertile 1	Tertile 2	Tertile 3
Tan Son Nhut	$\geq$ 17.70	7.01-17.69	$\leq$ 7.00
Pleiku	$\geq$ 11.75	5.41-11.74	$\leq$ 5.40
Ubon	$\geq$ 10.50	4.06-10.49	$\leq$ 4.05
Udorn	$\geq$ 14.70	5.61-14.69	$\leq$ 5.60

Average afternoon tertiles were not computed unless at least nine of the hourly values were known.

2. Variables tested

In order to derive useful equations the following variables were tried in a stepwise multiple regression program:

a. Noontime cloudiness averaged over a 4°x4° square at a key geographical position.

b. The MSL pressure gradient at 00Z, stations 48652-48914, in tenths of a mb.

c. The 00Z MSL pressure minus 1000, at a key grid point, or station.

d. Tertile trend (day-2 to day-1)

e. Tertile recurrence (day-1) to forecast day.

f. "Super"-trend (day-3 to day-2 to day-1). This was designed to build in a 4 day cycle.

Tests to date indicate that variables a, b and c are useful for calculating tertiles.

3. Equations for forecasting tertiles

From the data period June - September 1967 and 1968 the following equations appear to be useful. After computation of a tertile number to the nearest tenth, a table is entered to give the probabilities of any tertile for the forecast period; these values can also be compared with those found if recurrence alone is used. The tertile number calculated from the equation also serves to give some indication of extreme activity or inactivity if it is very low or very high respectively.

FOR TAN SON NHUT:

Day + 1

Tertile = $-0.53C + 0.14P + 0.01\Delta p + 1.10$

where:

C = average coded noontime cloudiness (3) over $4^{o}x4^{o}$ square centered at 12N, 115E

P = 00Z MSL pressure minus 1000 mb at 8N, 124E

Δp = 00Z MSL pressure gradient in tenths of a mb, stations 48657 minus 48914

Probabilities of a tertile 1, 2 or 3 day from the forecast tertile quantity are as follows probabilities by recurrence day-1 to day+1 are in parentheses.

Probabilities

Forecast Tertile	Tert 3 (inactive)	Tert 2 (average)	Tert 1 (active)
$\geq$ 2.2	53% (32)	37% (42)	10% (26)
1.9 - 2.1	18% (29)	46% (42)	36% (29)
$\leq$ 1.8	10% (21)	31% (31)	59% (48)

(3) A valid average cloudiness requires that at least 14 of the 16 values be known. Reading and coding the clouds is described on p4, 4th Prog. Rept. Briefly: 1=0-0.2, 2=0.3-0.7 and 3 = 0.8-1.0 coverage. Those areas which appear to consist of transparent cirrus are not counted.

FOR PLEIKU

Day + 1

Tertile = 0.11P - 0.42C - 0.01Δp + 1.68

where P = 00Z MSL pressure minus 1000 mb at 11N, 126E

C = average coded noontime cloudiness over a 4^{o}x4^{o} square centered at 13N, 115E

Δp = 00Z MSL pressure gradient in tenths of a mb, stations 48657 minus 48914

Probabilities of a tertile 1, 2 or 3 day from the forecast tertile quantity are as follows; probabilities by recurrence day-1 to day+1 are in parentheses.

Probabilities

Forecast Tertile	Tertile 3 (inactive)	Tertile 2 (average)	Tertile 1 (active)
$\geq$ 2.3	64% (52)	27% (18)	9% (30)
1.8 - 2.2	32% (34)	30% (26)	38% (40)
$\leq$ 1.7	7% (19)	21% (35)	72% (45)

FOR PLEIKU

Day + 2

Tertile = -0.61C + 0.10P + 1.96

where:

C = average coded noontime cloudiness over a $4^{o}x4^{o}$ square centered at 12N, 115E

P = 00Z MSL pressure minus 1000 mb at 13N, 143E (or at Guam)

Probabilities of a tertile 1, 2 or 3 day from the forecast tertile quantity are as follows; probabilities by recurrence day-1 to day+2 are in parentheses.

	Probabilities		
Forecast tertile	Tertile 3 (inactive)	Tertile 2 (average)	Tertile 1 (active)
$\geq$ 2.4	63% (52)	24% (30)	13% (18)
2.0 - 2.3	27% (32)	54% (38)	19% (30)
$\leq$ 1.9	23% (25)	23% (34)	54% (41)

FOR PLEIKU

Day + 3

Tertile = 0.08P - 0.41C - 0.01Δp + 2.04

where P = 00Z MSL pressure minus 1000 mb at 13N, 143E (or at Guam)

C = average coded noontime cloudiness over a $4^{o}x4^{o}$ square centered at 15N 107E

ΔP = 00Z MSL pressure gradient, in tenths of a mb, stations 48657 minus 48914

Probabilities of a tertile 1, 2 or 3 day from the forecast tertile quantity are as follows: probabilities by recurrence day-1 to day+3 are in parentheses.

	Probabilities		
Forecast tertile	Tertile 3 (inactive)	Tertile 2 (average)	Tertile 1 (active)
$\geq$ 2.2	59% (48)	29% (30)	12% (22)
1.8 - 2.1	26% (28)	36% (40)	38% (32)
$\leq$ 1.7	9% (18)	41% (35)	50% (47)

4. Evaluation of the forecasting equations.

An evaluation of the skill obtained using the above equations to forecast a tertile 1, 2 or 3 day is given in Table 3.

Table 3. Evaluation of equations to forecast tertile 1, 2 or 3 days

Station and forecast time	Correl. Coef. r	n	% correct	Heidke skill score over chance	Heidke skill score over recurrence
Tan Son Nhut Day + 1	.49	94	52	.28	.18
Pleiku Day + 1	.50	102	53	.30	.21
Day + 2	.49	102	57	.37	.26
Day + 3	.48	114	48	.13	.08

The development of equations for other stations and time periods is planned. Unfortunately these equations have not been tested on the independent data of 1969. However this is scheduled.

5. Forecast example

Forecast period: 1230 - 2330 LT next day at Pleiku

a. From 00Z surface map estimate sea level pressure at 11N, 126E to 0.2 mb. Read 1010.0 mb, use 10.0

b. From noontime APT picture read 1 squares of cloudiness for area 11-15N, 113-117E. Average to nearest 0.1; assume reading is 1.0.

c. From 00Z surface map read sea level pressure at stations 48657 and 48914. Determine difference (48657-48914), assume difference = 0.0 mb.

d. Insert values in a, b and c in appropriate equation to read: Tertile = 0.11 x 10.0 - 0.42 x 1.0 - 0.01 x 0.0 + 1.68

e. Compute: Tertile = 2.35

f. Read forecast probabilities from table:

64% for tertile 3 day
27% for tertile 2 day
9% for tertile 1 day

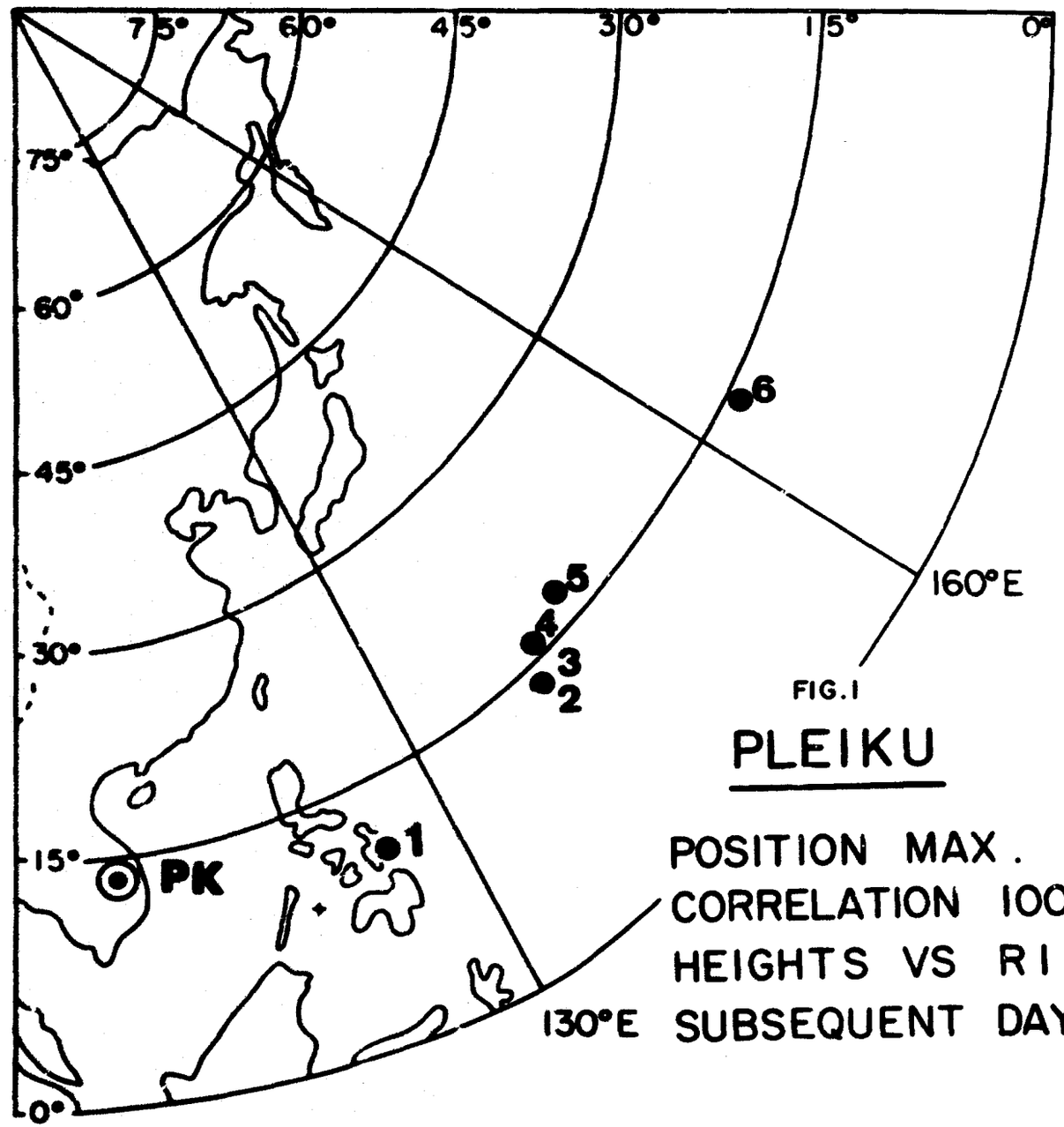

FIG. 1

PLEIKU

POSITION MAX.
CORRELATION 1000 mb
HEIGHTS VS RI
SUBSEQUENT DAYS

AFCRL PHOTO 60-274

Work on this project is continuing.

Project Number: 8624

Problem Number: 1694

Researcher: Mr. J. Couover

SECTION 5

WIND ANALYSIS - UPPER AIR

A large volume of data generated by weather stations throughout the Air Force Network is being gathered, analyzed, and prepared for input. The data is made up of two general categories and falls within the time period of June 1967 through September 1968. The first category consists of pre-processed cards which have been edited and punched at Regis College. The second source of wind information is a collection of ETAC weather observation tapes which have been generated at a central facility. Each tape is a composite of approximately 300 stations reporting in from within the entire network of weather stations.

The primary objective of researchers at AFCRL is to collect all pertinent data sources and establish a complete and accurate data set for each station on a day-by-day status. A complete data set is defined as:

1) station identification block:
    a) block, number
    b) altitude
    c) latitude & longitude
    d) time in hours
    e) date
2) gradient
3) upper air data points (850 mb, 700 mb, 500 mb, 300 mb, 200 mb)

A data point is composed of two parameters, wind direction and velocity.

The final objective is to use these data sets as input to an existing wind analysis program.

The ETAC tapes will be used as a secondary or back-up source of data. If the pre-processed data set is incomplete, then ETAC information will be added to the data set in order to establish a complete record.

A complete and exhaustive analysis of the ETAC tapes must be conducted. A design configuration must be proposed in order to edit and select the variety of data samples which constitute an ETAC tape record. Certain guidelines must be established with respect to data acceptance.

Since magnetic tapes will be the primary source of input, agreement with format required by the wind analysis program must be strictly adhered to.

Data samples from both sources must be categorized and compared.

Sorting and merge techniques must be utilized in generating a master tape with complete and accurate data sets. The work performed under this project is continuing.

Project Number: 8624

Problem Number: 1694

Researcher: Mr. J. Conover

SECTION 6

Windy Acres

The Boundary Layer Branch, Meteorology Laboratory of AFCRL, conducted a project known by the code name WINDY ACRES. This problem was submitted to the Analysis and Simulation Branch (CRMCA) under contract number F19628-70-C-0029, problem number 1764 and project number 8624.

The purpose of this project was to study the distribution of wind speeds on the Windy Acres Tower and the power law index.

Project WINDY ACRES resulted in the creation of magnetic tape records during the summers of 1967 and 1968 at heights of 0.5, 1.0, 2.0, 4.0, 8.0, 16.0, 24.0 and 32.0 meters above ground on an instrumental tower located about 35 miles northwest of Liberal, Kansas. The data was recorded for all eight levels at 1 second intervals for an overall total of 40 hours in 1967, 39 of which are usable, and 50 hours in 1968. The data is given in cm/sec and at a rate of 3600 per hour.

The following tasks were required by the project:

1. To find the distribution of
   (a) 1-second windspeeds at each level.
   (b) 3-second average windspeeds at each level.
   (c) the highest 3-second average windspeeds (or gusts) in 1 minute at each level.
2. Referring to the 99th percentile of the 1-second windspeeds at height h_j as v_j, find
   (a) the average $\bar{v}$ (i/j) of the 1-second windspeeds at each level (h_i = 0.5, 1.0, • • • 32.0 meters) for those seconds when the windspeeds at height hj is v(j).

(b) the ratio of each average $\bar{v}(i/j)$ to v(j).

(c) to estimate by method of least squares, the index p in the "power law" for each key level (hj) given by

$$\frac{\bar{v}(i/j)}{v(j)} = \left(\frac{hi}{hj}\right)^p \qquad \begin{matrix} i = 1, 8 \\ j = 1, 8 \end{matrix}$$

3. Same as 2. except using the 3-second average windspeeds.

4. Referring to the 99th percentile of the highest 3-second average windspeeds in 1 minute at height hj as g(j), find

(a) the average $\bar{v}(i/j)$ of the highest 3-second average windspeeds in 1 minute at each level (h_i = 0.5, 1.0, • • • 32.0 meters) for those seconds when the highest 3-second average windspeeds at height hj is g(j)

(b) the ratio of each average $\bar{v}(i/j)$ to g(j).

(c) to estimate, by method of least squares, the index p in the "power law" for each key level (hj) given by

$$\frac{\bar{v}(i/j)}{g(j)} = \left(\frac{hi}{hj}\right)^p \qquad \begin{matrix} i = 1,8 \\ j = 1,8 \end{matrix}$$

The derivation of the index p by method of least squares is shown below.

GIVEN: $\frac{\bar{v}(i/j)}{v(j)} = \left(\frac{hi}{hj}\right)^p$;

LET: $A_{ij} = \frac{\bar{v}(i/j)}{v(j)}$ and $R_{ij} = \frac{hi}{hj}$;

then $A_{ij} = R_{ij}^p$.

By dropping subscripts for simplicity and clarity purposes, the equation becomes

$$A = R^p.$$

taking logs of both sides,

$$\log A = p \log R \qquad \text{or}$$

$$p \log R - \log A = 0 \quad ;$$

and calling E the error,

$$E = p \log R - \log A.$$

Then by squaring E and expanding the right hand side,

$$E^2 = p^2 (\log R)^2 - 2p \log R \log A + (\log A)^2$$

and setting $\frac{dE^2}{dp} = 0$ for the least squares error

$$\frac{dE^2}{dp} = 2p (\log R)^2 - 2 \log R \log A = 0$$

$\therefore$

$$p = \frac{\log R \log A}{(\log R)^2}$$

Remembering that the subscripts were dropped, by adding them now and substituting back the result is

$$p_{ij} = \frac{\log\left(\frac{hi}{hj}\right) \log\left(\frac{v(i/j)}{v(j)}\right)}{\left[\log\left(\frac{hi}{hj}\right)\right]^2}$$

A very important aspect of this study was to determine the value of p, which relates windspeeds from one height to another height. It was particularly desirable to find p for the high windspeeds.

The ultimate purpose of this study was to improve our climatological knowledge of gusts as it is needed to determine the risks due to strong gusts in structural design and operation of equipment and buildings. Studies under this project are continuing.

Project Number: 8624

Problem Number: 1764

Researcher: Mr. I. Gringorten

SECTION 7

MICROWAVE ACOUSTICS

Radar and communications systems require rapid acquisition and processing of large amounts of data. For a long while this was handled by electromagnetic waves. But electromagnetic devices require large amounts of coaxial cables. The cables are unwieldy as well as inefficient. What is needed are devices which are compact, lossless, and easily accessible. The field of microwave acoustics is able to satisfy these requirements, originally in the form of bulk waves but more recently by surface waves. The shift from bulk devices to surface wave devices has come about because it is practically impossible to vary the delay and quite difficult to manipulate the acoustic energy during transmission through a bulk device. Surface waves, however, have all the desirable properties of bulk waves, as well as being quite accessible for other changes. Microwave acoustics exhibit the potential to develop miniature microwave components for high-speed signal processing and avionics systems. This project is involved with the propagation characteristics of surface waves on general piezoelectric crystals surfaces in the presence of perfect electric and magnetic conductors.

A rectangular co-ordinate system with the X_3 axis perpendicular to the crystal surface and the X_1 axis in the direction of propagation is selected. Various orientations of the crystal surface with respect to the crystal axes are to be considered. In order to accomplish this, the crystal axes must undergo a rotation through the Euler Angles. The matrix defining this rotation is

$$V = \begin{pmatrix} \cos\alpha\cos\gamma - \sin\alpha\cos\beta\sin\gamma & \sin\alpha\cos\gamma + \cos\alpha\cos\beta\sin\gamma & \sin\beta\sin\gamma \\ -\cos\alpha\sin\gamma - \sin\alpha\cos\beta\cos\gamma & -\sin\alpha\sin\gamma + \cos\alpha\cos\beta\cos\gamma & \sin\beta\cos\gamma \\ \sin\alpha\sin\beta & -\cos\alpha\sin\beta & \cos\beta \end{pmatrix}$$

where α, β, γ, are the Euler Angles. The differential equations for mechanical

displacements and electric potential are independent of the surface under consideration, only the values of the coefficients change with the surface orientation, relative to the crystal axes. The tensor quantities of interest, i.e. the elastic constants (c_{ijkl}), piezoelectric constants (e_{ijk}) and the dielectric constants (ϵ_{ij}) are transformed by:

$$c'_{ijkl} = \sum_{r,s,t,u=1}^{3} V_{ir} V_{js} V_{kt} V_{lu} c_{rstu}$$

$$e'_{ijk} = \sum_{r,s,t=1}^{3} V_{ir} V_{js} V_{kt} e_{rst}$$

$$\epsilon'_{ij} = \sum_{r,s=1}^{3} V_{ir} V_{js} \epsilon_{rs}$$

where the primed quantities refer to a rotated co-ordinate system and the unprimed to when the crystal surface and srystal axes systems coincide.

The equations for the components $\bar{U}_1$, $\bar{U}_2$, $\bar{U}_3$ of mechanical displacement and electric potential, φ, are

1
$$\left.\begin{cases} c'_{ijkl} U_{k,li} + e'_{kij} \varphi_{,ki} = \rho \dfrac{\partial \bar{U}_i}{\partial t^2} \quad j = 1,2,3 \\ e'_{ikl} U_{k,il} - \epsilon'_{ik} \varphi_{,ki} = 0 \end{cases}\right\} X_3 > 0$$

2
$$\nabla^2 \varphi = 0 \qquad -h \le z \le 0$$

Considering displacement and potential independent of the X_2 co-ordinate, we are seeking solutions of the form:

$$U_i = \beta_i e^{-\alpha\omega X_3/V_s} e^{i\omega(t - X_1/V_s)} \qquad i = 1,2,3$$

$$\varphi = \beta_4 e^{-\alpha\omega X_3/V_s} e^{i\omega(t - X_1/V_s)}$$

Substituting these solutions into the above differential equations yields a system of four equations in the unknowns β_1, β_2, β_3, β_4. In order for a non-trivial solution to exist the determinant of the coefficients must equal zero, i.e. given a V_s our problem is to find an α such that

$$
\begin{bmatrix}
C_{55}\alpha^2 + 2C_{15}\alpha - C_{11} + \rho v_s^2 & C_{45}\alpha^2 + [C_{14}+C_{56}]\alpha - C_{16} & C_{35}\alpha^2 + [C_{13}+C_{55}]\alpha - C_{15} & C_{35}\alpha^2 + [e_{15}+e_{31}]\alpha - e_{11} \\
C_{45}\alpha^2 + [C_{14}+C_{56}]\alpha - C_{16} & C_{44}\alpha^2 + 2C_{46}\alpha - C_{66} + \rho v_s^2 & C_{34}\alpha^2 + [C_{36}+C_{45}]\alpha - C_{56} & e_{34}\alpha^2 + [e_{14}+e_{52}]\alpha - e_{16} \\
e_{35}\alpha^2 + [C_{13}+C_{55}]\alpha - e_{15} & e_{34}\alpha^2 + [e_{36}+e_{52}]\alpha - e_{56} & e_{33}\alpha^2 + 2e_{35}\alpha - e_{55} + \rho v_s^2 & e_{33}\alpha^2 + [e_{13}+e_{55}]\alpha - e_{15} \\
e_{35}\alpha^2 + [e_{15}+e_{31}]\alpha - e_{11} & e_{34}\alpha^2 + [e_{14}+e_{36}]\alpha - e_{16} & e_{33}\alpha^2 + [e_{13}+e_{15}]\alpha - e_{15} & -e_{33}\alpha^2 - 2e_{13}\alpha + \epsilon_{11}
\end{bmatrix}
$$

has a determinant of zero, where the C's are the elastic constants, the e's the piezoelectric constants, and the ϵ's the dielectric constants. This involves solving an eighth order equation in α. For each α value which has a positive real part we obtain values of $\beta_1, \beta_2, \beta_3, \beta_4$. Since field amplitudes are arbitrary we take $\beta_4 = 1$ and find $\beta_1, \beta_2, \beta_3$, from three of the remaining four homogeneous equations.

Assuming the surface of the crystal is free of stress the mechanical boundary conditions are

$$
T_{3j}\Big|_{x_3=0} = C'_{3jkl}\, U_{k,l} + e'_{k3j}\, \Phi_{,k}\Big|_{x_3=0} = 0 \qquad j = 1,2,3
$$

Now the mechanical displacement and potential may be expressed as a linear combination of fields associated with allowable values of α; thus for $x_3 \geq 0$

$$
U_i = \sum_{j=1}^{4} A^{(j)} \beta_i^{(j)} e^{-\alpha(j)\omega x_3/v_s}\, e^{i\omega(t - x_1/v_s)} \qquad i = 1,2,3
$$

$$5 \qquad \varphi = \sum_{j=1}^{4} A^{(j)} \beta_4^{(j)} \, e^{-\alpha(j)\omega X_3/v_s} \, e^{i\omega(t - X_1/v_s)}$$

while in the interval $h \le X_3 \le 0$ (using equation 1 and the above derived boundary conditions) we get

$$6 \qquad \varphi = \sum_{j=1}^{4} A^{(j)} \beta_4^{(j)} \cosh\left(\frac{\omega h}{v_s}\right) \sin k\left(\frac{\omega}{v_s}(X_3 + h)\right) e^{i\omega(t - X_1/v_s)}$$

Lastly since the component of the normal must be continuous across $X_3 = 0$ the electric displacement is given by

$$D_i = C_{ikl} U_{l,k} - e_{ik} \varphi_{,k} \qquad i = 1, 2, 3$$

$$\vec{D} = -\epsilon_0 \nabla \varphi \qquad -h \le X_3 \le 0$$

Using equations 4, 5, and 6 we get the following set of homogeneous equations for the amplitudes $A^{(j)}$.

$$\sum_{j=1}^{4} \left[\beta_1^{(j)} \left[i C_{15} + \alpha^{(j)} C_{55} \right] + \beta_2^{(j)} \left[i C_{56} + \alpha^{(j)} C_{45} \right] + \beta_3^{(j)} \left[i C_{51} + \alpha^{(j)} C_{11} \right] + \beta_4^{(j)} \left[i e_{15} + \alpha^{(j)} e_{11} \right] \right] A^{(j)} = 0$$

$$\sum_{j=1}^{4} \left[\beta_1^{(j)} \left[i C_{14} + \alpha^{(j)} C_{45} \right] + \beta_2^{(j)} \left[i C_{46} + \alpha^{(j)} C_{44} \right] + \beta_3^{(j)} \left[i C_{41} + \alpha^{(j)} C_{14} \right] + \beta_4^{(j)} \left[i e_{14} + \alpha^{(j)} e_{14} \right] \right] A^{(j)} = 0$$

$$\sum_{j=1}^{4} \left[\beta_1^{(j)} \left[i C_{13} + \alpha^{(j)} C_{53} \right] + \beta_2^{(j)} \left[i C_{36} + \alpha^{(j)} C_{34} \right] + \beta_3^{(j)} \left[i C_{31} + \alpha^{(j)} C_{33} \right] + \beta_4^{(j)} \left[i e_{13} + \alpha^{(j)} e_{33} \right] \right] A^{(j)} = 0$$

$$\sum_{j=1}^{4} \Big[\beta_1^{(j)} \big[i e_{31} + \alpha^{(j)} e_{35} \big] + \beta_2^{(j)} \big[i e_{36} + \alpha^{(j)} e_{34} \big] + \beta_3^{(j)} \big[i e_{35} + \alpha^{(j)} e_{33} \big] - \beta_4^{(j)} \big[i e_{13} + \alpha^{(j)} e_{33} + e_1 \coth\left(\frac{\omega h}{v_s}\right) \big] \Big] A^{(j)} = 0$$

By solving the equation obtained by setting the determinant of the above system equal to zero we obtain the allowable surface wave velocities.

As a by-product of this problem the components of stress, strain, electric displacement, electric potential, electric field, and average power flow are calculated as functions of wx_3. The computer program has the option to print out any or all of these quantities. The applicable equations are to be found in Supplement A.

Project Number: 5635

Problem Number: 1614

Researcher: Capt. A. Slobodnik Jr., U. S. A. F.

Stress

$$\frac{T_{11}}{\omega} = \sum_{j=1}^{4} A^{(j)} e^{-\alpha^{(j)} \omega x_3 / v_s} e^{i\omega(t - x_1/v_s)} \left\{ \beta_1^{(j)} \left[\frac{-i}{v_s} c_{11} - \frac{\alpha^{(j)}}{v_s} c_{15} \right] + \beta_2^{(j)} \left[\frac{-i}{v_s} c_{16} - \frac{\alpha^{(j)}}{v_s} c_{14} \right] + \beta_3^{(j)} \left[\frac{-i}{v_s} c_{15} - \frac{\alpha^{(j)}}{v_s} c_{13} \right] + \beta_4^{(j)} \left[\frac{-i}{v_s} c_{11} - \frac{\alpha^{(j)}}{v_s} c_{31} \right] \right\}$$

$$\frac{T_{12}}{\omega} = \frac{T_{21}}{\omega} = \sum_{j=1}^{4} A^{(j)} e^{-\alpha^{(j)} \omega x_3 / v_s} e^{i\omega(t - x_1/v_s)} \left\{ \beta_1^{(j)} \left[\frac{-i}{v_s} c_{66} - \frac{\alpha^{(j)}}{v_s} c_{56} \right] + \beta_2^{(j)} \left[\frac{-i}{v_s} c_{66} - \frac{\alpha^{(j)}}{v_s} c_{46} \right] + \beta_3^{(j)} \left[\frac{-i}{v_s} c_{56} - \frac{\alpha^{(j)}}{v_s} c_{36} \right] + \beta_4^{(j)} \left[\frac{-i}{v_s} e_{16} - \frac{\alpha^{(j)}}{v_s} e_{36} \right] \right\}$$

$$\frac{T_{13}}{\omega} = \frac{T_{31}}{\omega} = \sum_{j=1}^{4} A^{(j)} e^{-\alpha^{(j)} \omega x_3 / v_s} e^{i\omega(t - x_1/v_s)} \left\{ \beta_1^{(j)} \left[\frac{-i}{v_s} c_{15} - \frac{\alpha^{(j)}}{v_s} c_{55} \right] + \beta_2^{(j)} \left[\frac{-i}{v_s} c_{56} - \frac{\alpha^{(j)}}{v_s} c_{45} \right] + \beta_3^{(j)} \left[\frac{-i}{v_s} c_{55} - \frac{\alpha^{(j)}}{v_s} c_{35} \right] + \beta_4^{(j)} \left[\frac{-i}{v_s} c_{15} - \frac{\alpha^{(j)}}{v_s} e_{35} \right] \right\}$$

$$\frac{T_{22}}{\omega} = \sum_{j=1}^{4} A^{(j)} e^{-\alpha^{(j)} \omega x_3 / v_s} e^{i\omega(t - x_1/v_s)} \left\{ \beta_1^{(j)} \left[\frac{-i}{v_s} c_{12} - \frac{\alpha^{(j)}}{v_s} c_{25} \right] + \beta_2^{(j)} \left[\frac{-i}{v_s} c_{26} - \frac{\alpha^{(j)}}{v_s} c_{24} \right] + \beta_3^{(j)} \left[\frac{-i}{v_s} c_{25} - \frac{\alpha^{(j)}}{v_s} c_{23} \right] + \beta_4^{(j)} \left[\frac{-i}{v_s} e_{12} - \frac{\alpha^{(j)}}{v_s} e_{32} \right] \right\}$$

$$\frac{T_{23}}{\omega} = \frac{T_{32}}{\omega} = \sum_{j=1}^{4} A^{(j)} e^{-\alpha^{(j)} \omega x_3 / v_s} e^{i\omega(t - x_1/v_s)} \left\{ \beta_1^{(j)} \left[\frac{-i}{v_s} c_{14} - \frac{\alpha^{(j)}}{v_s} c_{45} \right] + \beta_2^{(j)} \left[\frac{-i}{v_s} c_{46} - \frac{\alpha^{(j)}}{v_s} c_{44} \right] + \beta_3^{(j)} \left[\frac{-i}{v_s} c_{45} - \frac{\alpha^{(j)}}{v_s} c_{34} \right] + \beta_4^{(j)} \left[\frac{-i}{v_s} e_{14} - \frac{\alpha^{(j)}}{v_s} e_{34} \right] \right\}$$

$$\frac{T_{33}}{\omega} = \sum_{j=1}^{4} A^{(j)} e^{-\alpha^{(j)} \omega x_3 / v_s} e^{i\omega(t - x_1/v_s)} \left\{ \beta_1^{(j)} \left[\frac{-i}{v_s} c_{13} - \frac{\alpha^{(j)}}{v_s} c_{35} \right] + \beta_2^{(j)} \left[\frac{-i}{v_s} c_{36} - \frac{\alpha^{(j)}}{v_s} c_{34} \right] + \beta_3^{(j)} \left[\frac{-i}{v_s} c_{35} - \frac{\alpha^{(j)}}{v_s} c_{33} \right] + \beta_4^{(j)} \left[\frac{-i}{v_s} e_{13} - \frac{\alpha^{(j)}}{v_s} e_{33} \right] \right\}$$

Strain

$$\frac{S_{11}}{\omega} = \sum_{j=1}^{4} \frac{-i}{v_s} A^{(j)} \beta_1^{(j)} e^{-\alpha^{(j)} \omega x_3 / v_s} e^{i\omega(t - x_1/v_s)}$$

$$\frac{S_{22}}{\omega} = 0$$

$$\frac{S_{33}}{\omega} = \sum_{j=1}^{4} \frac{-\alpha^{(j)}}{v_s} A^{(j)} \beta_3^{(j)} e^{-\alpha^{(j)} \omega x_3 / v_s} e^{i\omega(t - x_1/v_s)}$$

$$\frac{S_{12}}{\omega} = \frac{S_{21}}{\omega} = \frac{1}{2} \sum_{j=1}^{4} \frac{-i}{v_s} A^{(j)} \beta_2^{(j)} e^{-\alpha^{(j)} \omega x_3 / v_s} e^{i\omega(t - x_1/v_s)}$$

$$\frac{S_{13}}{\omega} = \frac{S_{31}}{\omega} = \frac{1}{2} \sum_{j=1}^{4} A^{(j)} \left[\frac{-\alpha^{(j)}}{v_s} \beta_1^{(j)} - \frac{i}{v_s} \beta_3^{(j)} \right] e^{-\alpha^{(j)} \omega x_3 / v_s} e^{i\omega(t - x_1/v_s)}$$

$$\frac{S_{23}}{\omega} = \frac{S_{32}}{\omega} = \frac{1}{2} \sum_{j=1}^{4} \frac{-\alpha^{(j)}}{v_s} A^{(j)} \beta_2^{(j)} e^{-\alpha^{(j)} \omega x_3 / v_s} e^{i\omega(t - x_1/v_s)}$$

Electric Field

$$\frac{E_1}{\omega} = \frac{i}{v_s} \sum_{j=1}^{4} A^{(j)} \beta_4^{(j)} e^{-\alpha^{(j)} \omega x_3 / v_s} e^{i\omega(t - x_1/v_s)} = \frac{i}{v_s} \psi$$

$$\frac{E_3}{\omega} = \frac{1}{v_s} \sum_{j=1}^{4} \alpha^{(j)} A^{(j)} \beta_4^{(j)} e^{-\alpha^{(j)} \omega x_3 / v_s} e^{i\omega(t - x_1/v_s)}$$

Electric Displacement

$$\frac{D_1}{\omega} = \sum_{j=1}^{4} A^{(j)} e^{-\alpha^{(j)}\omega x_3/v_s} e^{i\omega(t-x_1/v_s)} \left\{ \beta_1^{(j)} \left[\frac{-i}{v_s} e_{11} - \frac{\alpha^{(j)}}{v_s} e_{15} \right] + \beta_2^{(j)} \left[\frac{-i}{v_s} e_{16} - \frac{\alpha^{(j)}}{v_s} e_{14} \right] + \beta_3^{(j)} \left[\frac{-i}{v_s} e_{15} - \frac{\alpha^{(j)}}{v_s} e_{13} \right] + \beta_4^{(j)} \left[\frac{-i}{v_s} \varepsilon_{11} - \frac{\alpha^{(j)}}{v_s} \varepsilon_{13} \right] \right\}$$

$$\frac{D_2}{\omega} = \sum_{j=1}^{4} A^{(j)} e^{-\alpha^{(j)}\omega x_3/v_s} e^{i\omega(t-x_1/v_s)} \left\{ \beta_1^{(j)} \left[\frac{-i}{v_s} e_{21} - \frac{\alpha^{(j)}}{v_s} e_{25} \right] + \beta_2^{(j)} \left[\frac{-i}{v_s} e_{26} - \frac{\alpha^{(j)}}{v_s} e_{24} \right] + \beta_3^{(j)} \left[\frac{-i}{v_s} e_{25} - \frac{\alpha^{(j)}}{v_s} e_{23} \right] + \beta_4^{(j)} \left[\frac{-i}{v_s} \varepsilon_{21} - \frac{\alpha^{(j)}}{v_s} \varepsilon_{23} \right] \right\}$$

$$\frac{D_3}{\omega} = \sum_{j=1}^{4} A^{(j)} e^{-\alpha^{(j)}\omega x_3/v_s} e^{i\omega(t-x_1/v_s)} \left\{ \beta_1^{(j)} \left[\frac{-i}{v_s} e_{31} - \frac{\alpha^{(j)}}{v_s} e_{35} \right] + \beta_2^{(j)} \left[\frac{-i}{v_s} e_{36} - \frac{\alpha^{(j)}}{v_s} e_{34} \right] + \beta_3^{(j)} \left[\frac{-i}{v_s} e_{35} - \frac{\alpha^{(j)}}{v_s} e_{33} \right] + \beta_4^{(j)} \left[\frac{-i}{v_s} e_{13} - \frac{\alpha^{(j)}}{v_s} \varepsilon_{33} \right] \right\}$$

Power Flow

The flow of complex mechanical power at any point in the piezoelectric medium is given in component form as follows:

$$P_i = -\frac{1}{2} \sum_{j=1}^{3} T_{ij} \dot{U}_j^*$$

The real part of this expression represents the time average power flow at a point.

Since all fields decay exponentially in the x_3 direction there is no net flow of real power in this direction. Thus, only P_1 and P_2 need be considered.

The components of the total time-average power flow are as follows:

$$P_1^t = \int_0^{\infty} \mathrm{Re}[P_1]\,dx_3 = \mathrm{Re}[P_1^t]$$

$$P_2^t = \int_0^{\infty} \mathrm{Re}[P_2]\,dx_3 = \mathrm{Re}[P_2^t]$$

where Re $P_{1,2}$ means the real part of $P_{1,2}$. The final expressions for the complex mechanical power flow P_1 and P_2 are

$$\frac{P_1^t}{\omega} = \frac{1}{2}\sum_{\ell=1}^{4}\sum_{k=1}^{4}\frac{1}{\alpha^{(\ell)}+\alpha^{*(k)}}B^{(\ell)}B^{*(k)}\Big\{\beta_1^{*(k)}\Big[\beta_1^{*(\ell)}\big(c_{11}-j\alpha^{(\ell)}c_{15}\big)+\beta_2^{(\ell)}\big(c_{16}-j\alpha^{(\ell)}c_{14}\big)+\beta_3^{(\ell)}\big(c_{15}-j\alpha^{(\ell)}c_{13}\big)+\beta_4^{(\ell)}\big(c_{11}-j\alpha^{(\ell)}c_{31}\big)\Big]$$
$$+\beta_2^{*(k)}\Big[\beta_1^{(\ell)}\big(c_{16}-j\alpha^{(\ell)}c_{56}\big)+\beta_2^{(\ell)}\big(c_{66}-j\alpha^{(\ell)}c_{46}\big)+\beta_3^{(\ell)}\big(c_{56}-j\alpha^{(\ell)}c_{36}\big)$$
$$+\beta_4^{(\ell)}\big(c_{16}-j\alpha^{(\ell)}c_{36}\big)\Big]$$
$$+\beta_3^{*(k)}\Big[\beta_1^{(\ell)}\big(c_{15}-j\alpha^{(\ell)}c_{55}\big)+\beta_2^{(\ell)}\big(c_{56}-j\alpha^{(\ell)}c_{45}\big)+\beta_3^{(\ell)}\big(c_{55}-j\alpha^{(\ell)}c_{35}\big)$$
$$+\beta_4^{(\ell)}\big(c_{15}-j\alpha^{(\ell)}c_{35}\big)\Big]\Big\}$$

$$\frac{P_2^t}{\omega} = \frac{1}{2}\sum_{\ell=1}^{4}\sum_{k=1}^{4}\frac{1}{\alpha^{(\ell)}+\alpha^{*(k)}}B^{(\ell)}B^{*(k)}\Big\{\beta_1^{*(k)}\Big[\beta_1^{(\ell)}\big(c_{16}-j\alpha^{(\ell)}c_{56}\big)+\beta_2^{(\ell)}\big(c_{66}-j\alpha^{(\ell)}c_{46}\big)+\beta_3^{(\ell)}\big(c_{56}-j\alpha^{(\ell)}c_{36}\big)+\beta_4^{(\ell)}\big(c_{16}-j\alpha^{(\ell)}c_{36}\big)\Big]$$
$$+\beta_2^{*(k)}\Big[\beta_1^{(\ell)}\big(c_{12}-j\alpha^{(\ell)}c_{25}\big)+\beta_2^{(\ell)}\big(c_{26}-j\alpha^{(\ell)}c_{24}\big)+\beta_3^{(\ell)}\big(c_{25}-j\alpha^{(\ell)}c_{23}\big)$$
$$+\beta_4^{(\ell)}\big(c_{12}-j\alpha^{(\ell)}c_{32}\big)\Big]$$
$$+\beta_3^{*(k)}\Big[\beta_1^{(\ell)}\big(c_{14}-j\alpha^{(\ell)}c_{45}\big)+\beta_2^{(\ell)}\big(c_{46}-j\alpha^{(\ell)}c_{44}\big)+\beta_3^{(\ell)}\big(c_{45}-j\alpha^{(\ell)}c_{34}\big)$$
$$+\beta_4^{(\ell)}\big(c_{14}-j\alpha^{(\ell)}c_{34}\big)\Big]\Big\}$$

SECTION 8

THE DIGITAL SOUNDER

A BASIS FOR REAL TIME RECORDING OF IONOSPHERIC PARAMETERS

A need exists for the development of techniques which can specify, in real time, the conditions of the ionospher spanning large areas of the globe. Therefore, the techniques of ionosphere specification must necessarily be able to follow rapid changes in time and space in order to detect the development of geophysical disturbances and to estimate quickly their effects on various communication and surveillance systems.

The systems, such as radio circuits, radar systems, and surveillance systems, that are affected by the conditions of the ionosphere operate in a wide band of frequencies ranging from VLF to VHF. The performance of the systems are adversely affected by the disturbances causing a variety of changes at different frequencies. A real time determination of ionization distribution would make it possible to compute the effects of these disturbances and other deviations from the normal. This knowledge would permit the restoration of proper system functioning in some cases and proper interpretation of the observed phenomena in other cases.

Real time determination of ionization does not necessarily mean real time measurement; although it is an aim of ionospheric research to predict the ionization by inference. However, the direct measurement by fast methods will remain a basic requirement.

1. Limitations of Ionospheric Data Collection Using Conventional Ionosondes

a. The Electron Density Profile

One of the goals of ionospheric data collection is to determine the distribution of electron density versus height and its variation in time and space.

The electron density & profile is basically determined by a radar sounding technique using ionospheric sounders. Narrow RF-pulses are transmitted and propagated upwards, into the ionosphere. Every frequency has a distinct electron density that reflects the wave. The reflected pulse is recorded and measured. The time delay which is measured is used to compute the height of the reflection using a complex theory and knowledge of the underlying ionization. Increasing the radio frequencies permits penetration deeper into the ionosphere, detecting the different layers until a final frequency is transmitted, for which even the highest occurring electron density no longer reflects. The wave escapes into space. Therefore, this technique cannot be used to gather information on the inoization above the maximum.

b. The Interference Problem on Ground Sounders

In the initial years of sounder operations when the transmitted pulse power was quite low, daytime ionograms were generally poorer than those taken at night due to absorption. Increasing the transmitter power improved the situation. However, since the number of commercial radio and communications systems which use the same frequency bands as the ionosondes as well as their transmitted power have multiplied over the past 20 years, the quality of the ionograms at night has deteriorated. Due to the high level of interference, whole bands are useless for ionospheric sounding at night and data have to be interpolated when possible.

c. The Airborne Sounder and its Specific Interference Problems

All the interference problems that must be overcome are multiplied in an aircraft. Nevertheless, there are advantages to an aircraft carrying a sounder over ground stations. First of all, since an aircraft is mobile, it can be used in places where it is difficult or impossible for sounders such as on oceans, in the Arctic, in the tropics or in deserts. Secondly, it can be used to measure

special phenomena, such as those occurring during an eclipse, a nuclear detonation, or associated with magnetospheric phenomena where ground sounders can be installed only with great difficulty and great cost if at all. An airborne sounder cannot replace a net of ground stations; however, since many ionospheric variations are under solar control and move much faster across the earth than the fastest aircraft.

Additional disadvantages of an airborne sounder compared with a ground sounder are displayed schematically in Figure 1. In heavily populated areas, an aircraft is more exposed to the man-made interference than a ground sounder. The reason is due to the fact that the ground sounder has only a small antenna lobe, while the aircraft's antenna pattern includes a lobe pointing downward which is comparable with the one directed upward. The airborne antenna system captures almost twice the energy of any ground sounder because of the ground reflected sky wave.

d. Time Consuming Photo Processing and Tedious Evaluations

The problem of interference, whether man-made or natural, is great in the measurement of ionospheric parameters. It is important to point out that technical limitations in the data recording process of conventional ionosondes are not favorable for real time analysis. The analog signals are recorded on film, processed and interpreted by specialists. In order to obtain spatial characteristics, a net of stations is required. The problem of coordinating various equipments in the same degree of sensitivity conditions and to maintain close contact with data technicians to ensure consistency in interpretation is quite difficult and extremely costly even for a rather thin net of stations.

2. The Digital Ionosonde as a Solution to Existing Problems

a. General

In order to overcome some of the problems mentioned, CRPC (Boundary Interactions Branch) at Hanscom Air Force Base has begun on a program to develop systems

that produce ionospheric data in digital form. In this form, large amounts of data can be handled on a computer.

A proposal to build a digital ionosonde for the aircraft has been funded. This equipment has been named Digisonde 128. The equipment uses phase coding and phase coherent integration as a means to improve signal to noise ratio. This is combined with digital data processing to facilitate high speed operations.

b. Improvement of Signal to Noise Ratio by Phase Coherent Integration and Phase Coding

There are applied detection techniques for conventional sounders that use the energy content of noise and signal, but ignoring the fact that the frequency is known. The technique of phase coherent detection utilizes this information. Figure 2 shows how this is implemented in the digisonde.

The upper line shows a sequence of transmitted pulses, that appear at the receiver output as the "Direct Signal" and a sequence of ionospheric returns. Consecutive echoes of the same order occur at the receiver output with exactly the same time delay and phase with respect to the transmitted signal. The receiver output is sampled by gates which are derived from a frequency standard common to transmitter and receiver. They also have a precise and fixed time delay with respect to transmitted pulses. This means, that the samples of a specific ionospheric echo always have the same phase for one specific height gate, and if they are summed or integrated, enhance each other. In contrast, the phase of the random noise will jump randomly and tend to cancel out in the integration, if enough samples are used.

A range of 128 height increments have been chosen to cover the area of interest, since the integration requires storage and only a limited amount of data can be stored. Greater height ranges than the "Basic Range" can be inspected in less detail by increasing the spacing between sample gates.

The integration process is shown in Figure 3. A separate memory place is provided for the integration of the amplitudes of each of the 128 height ranges. The stored amplitude information, which is initially a "zero" is sequentially fed into a temporary auxilliary storage by precisely timed signals. Next, it is converted into an analog level and, at a time determined by the proper sample gate, is compared with the receiver output. If the receiver output is smaller than the storage value, this value will be modified downwards,or if it is bigger, it will be modified upwards. Phase coherent signals will always have the same amplitude and sign in their respective sample gates, changing the stored information in the same direction, while the noise with random positive and negative amplitudes of varying magnitude tends to cancel. The phase coherent signal amplitude will be approximated rapidly in its specific memory place, while the noise decreases with $1/\sqrt{m}$ as signal statistics can show. The input signal-to-noise ratio of S/N will thus be improved to $\sqrt{m}$ S/N after M Samples, an improvement of 19 decibels for the case of 80 integrations.

Phase coding was used to overcome the coherent interference problem. This type of interference which is caused by radio transmitters can severly disturb the integration process. The worst case of interference which is one with exactly the same frequency as that transmitted by the sounder is illustrated by Figure 4. Line D and E show the interference pattern between pulses and the unwanted radio signal for two specific phases of the transmitted pulses.

The phase switching of the signal phase has been introduced by design and this knowledge can be applied in the summing process by correcting for the phase switch. The idealized example shows complete cancellation of the interference and enhancement of the signal. This is true even if the signal is only a small fraction of the interference amplitude, as long as the receiver is not saturated by

interference. If the decoding sequence is delayed by one full cycle, it is possible to observe higher order multiples.

c. The Digisonde Format

The Digisonde 128 covers a frequency range from 25 KH_z to 16 MHz in 640 steps of 25KHz. The basic frequency increment of 25 KHz can be changed by programs to 50 or 100 KHz increments. Pulse widths of 50, 100, or 150 microseconds are available. The basic integration consists of 80 samples per frequency and height increment, but can be increased in 2^N muitiples. The pulse repetition rate can be selected as 50, 100 or 200 Hz. The fastest possible ionogram between 0 and 16 MHz would be one with a frequency stepping of 100 KHz, an integration of 80 samples and a PRF of 200 Hz. It would require 64 seconds to be recorded. In addition to measuring the amplitude in each height gate in 64 levels, which corresponds to a 1 decibel resolution, the RF-phase is also measured. The 128 amplitude-phase pairs per frequency are combined with time and operational information and are recorded on 1/2 inch computer tape in computer compatible format.

d. Online Printout with Digital Level Presentation

It is essential that an immediate picture of the ionogram is available at the station in order to check for proper gainsetting and frequency, range and to allow for real time determination of specific parameters. Figure 5 shows an example of an ionogram produced with the Digisonde 128. Although the transmitted power was only 500 Watt (it will eventually be 30 KW) and the antenna extremely poor, the quality of the ionogram is considered good and the digital information is readily available for ionogram interpretation. A weighting function is used in the construction of the numerals in order to enhance the recognition of the pattern of the ionospheric trace (the dark area increases linearly with the number). This basically describes the Digisonde as it has been conceived and is being developed. The

new system has potentialities of routine usage on both the ground and in airplanes which go beyond its use as a research tool. However, this would require a substantially larger effort before it can be realized. Only a few of the supplements that could be developed are outlined here:

e. Real Time Availability of Data for Centralized Computer Processing

An extension of the concept of recording the data content of an ionogram in digital form is to connect the sounder with a suitably programmed computer. The computer can determine such ionospheric parameters as the lowest observable frequencies f_{min}, the mimimum virtual heights of the E and F layers, the critical frequencies f_oE and f_oF2 and possibly parameters of the sporadic E-layer. A more complicated process is the separation of the two traces, the O- and x- component of the ionogram, by the computer and a subsequent true height analysis which converts the ionogram into an electron density profile. The computer may also be used to control sounder functions, such as gainsetting, number of necessary integrations and the selection of the frequency scan limits.

An electron density profile requires measurements only on a few selected frequencies, the distribution of which depends on certain ionospheric conditions. This selection could be optimized through the use of a computer and would minimize the operational time of the sounder. This fact is important in cases where sounder interference poses a problem to other systems.

The development of the decoder printer combination has opened the way for real time analysis using computers that are not necessarily close to the transmitter sites. The total data content of an ionogram can be transformed by the decoder through selection and compression into an amount which can be transmitted in real time via telephone wires. This compressed data is the input to a central computer which can interpret the information and update short term predictions.

A net of similar or identical sounders that are all connected to a central processor would ensure standardization of the systems. The continuous monitoring could point out deficiencies of certain stations and perhaps calibration processes could be implemented to allow for proper correlation of the data.

3. Synchronized Net of Sounders

a. Application of Oblique Ionograms

An ionospheric sounder operating at one location can be received by a simultaneously tracking receiver in another place. The oblique ionogram obtained permits the determination of all propagation parameters on the specific circuit. Parameters, such as LUF (lowest usable frequency), MUF (maximum usable frequency) and the different modes as E_s propagation, 1XF, 2XF and other modes can be identified and the effects on transmission of data can be derived. The condition of the ionosphere in the mid-point can also be determined through careful analysis. The first successful attempt to record an ionogram from an aircraft was made at night over a distance of about 2000 km. The systems used were a Granger Transmitter operated at Alta Loma, Texas and the receiver of an airborne Granger System. It is quite possible to have a combination of ground airborne sounders or 2 airborne sounders monitor the ionosphere over inaccessible territory.

b. The Digisonde and Oblique Propagation

The Digisonde concept lends itself immediately for oblique soundings for monitoring the ionospheric conditions. It utilizes the exact timing of the functions and the controlled synthesis of the frequencies using highly stable standards.

4. Computer Programs

The first stage of a major programming effort to handle the Digisonde 128 data tapes has been completed. The existing programs, written in FORTRAN IV

language for the IBM 7094/DCS at AFCRL, allows the printout of the digital ionograms in a variety of formats. Noise suppressing modifications have been incorporated into the program and the results show the feasibility of presenting ionospheric parameters in this digital form. The extraction of parameters has been attempted. Minimum layer heights and critical frequencies versus time have been successfully extracted from suitable actual data. The reformatting of reduced parameters into a format usable by the Digicoder-Xerox Printer combination has been accomplished. This permits the use of the pattern enhancing scheme in the presentation of these data. Figures 6 through 12 are examples of the printed outputs from the Digicoder-Xerox Printer combination and the IBM 7094/DCS.

Project Number: 5631

Problem Number: 1688

Researcher: Mr. Jurgen Buchau

INTERFERENCE PROBLEMS FOR AIRBORNE SOUNDERS

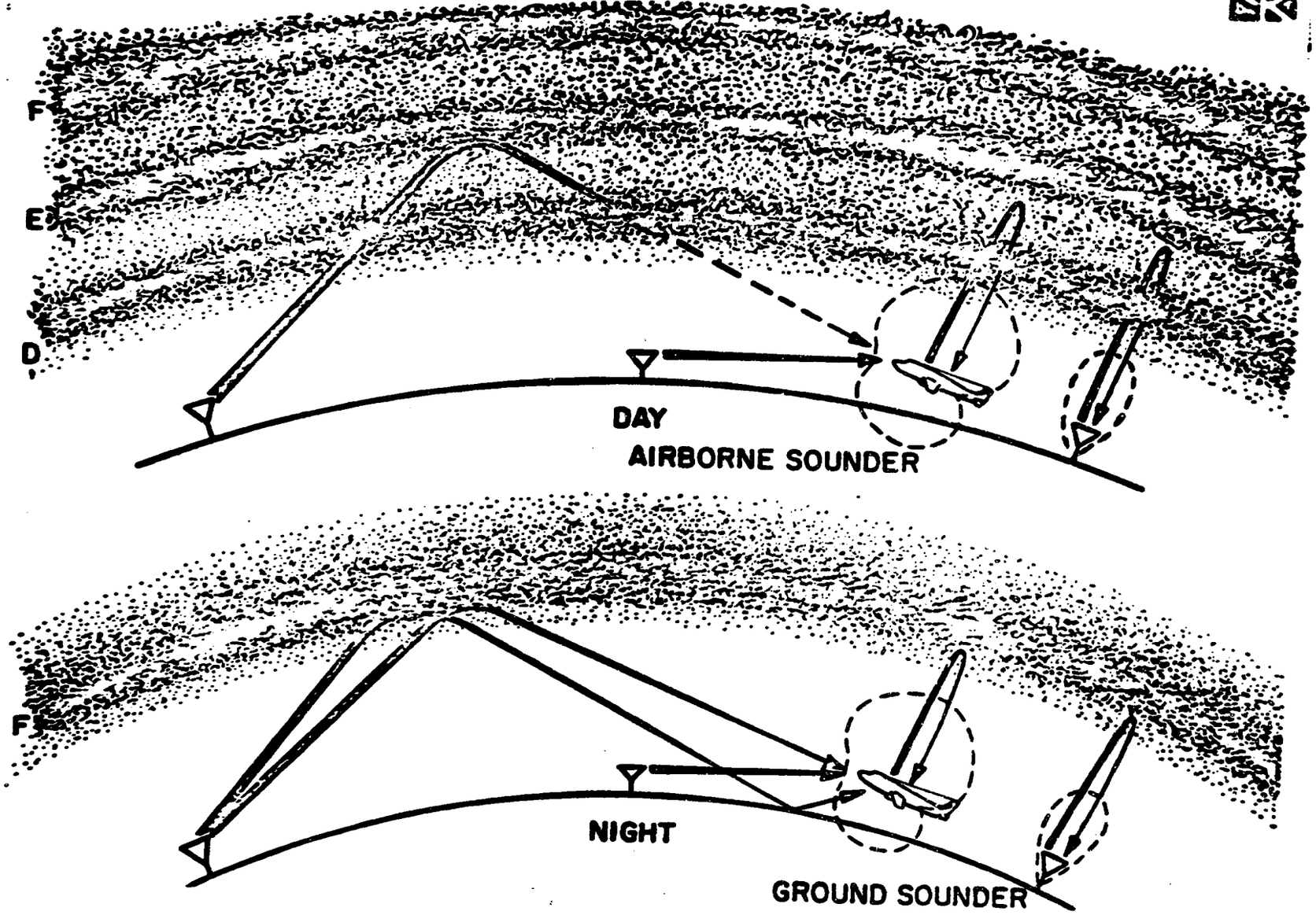

8-10

PRINCIPLE OF PHASECOHERENT GATING

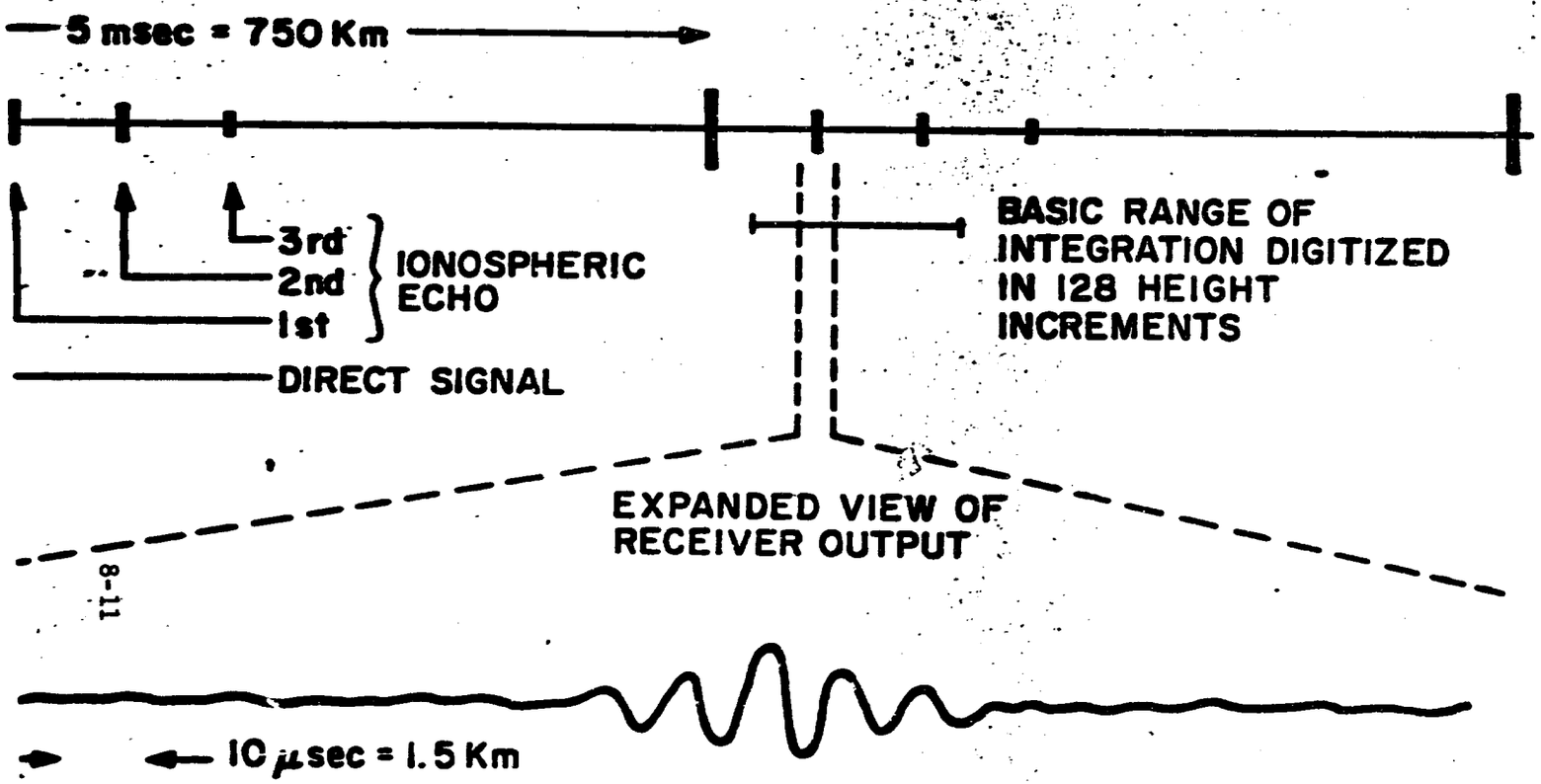

and Cos SAMPLE GATES FOR A HEIGHT RESOLUTION OF 1.5 Km

Fig. 2

SIGNAL TO RANDOM NOISE RATIO IMPROVEMENT BY PHASECOHERENT INTEGRATION

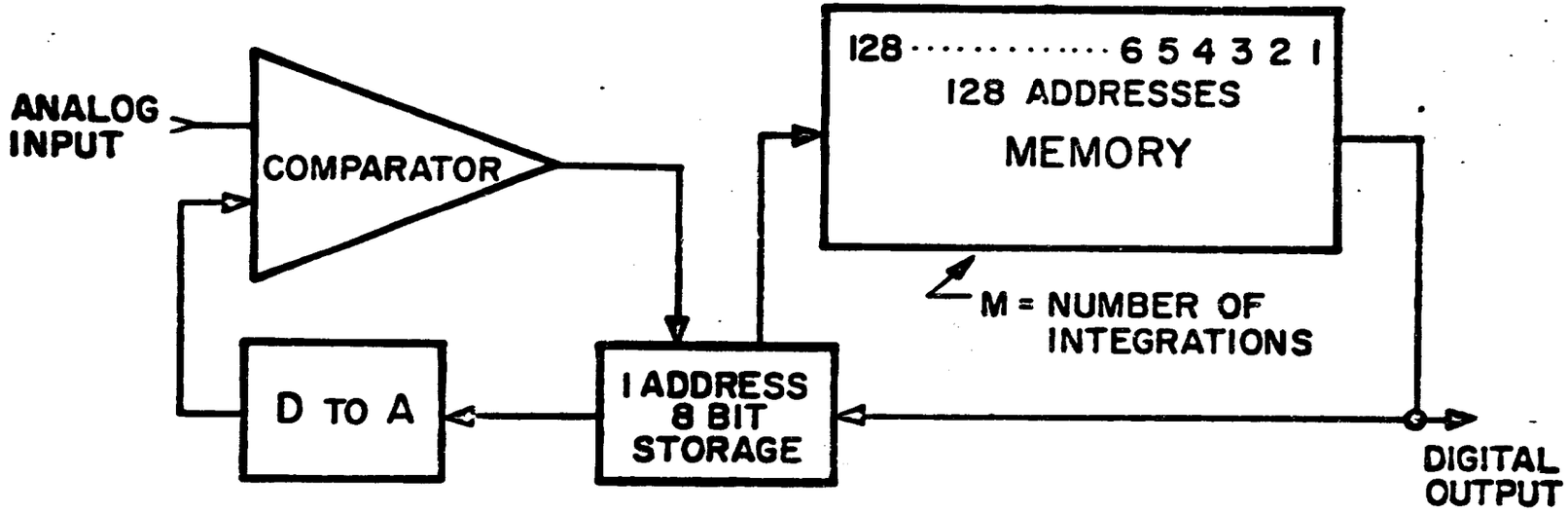

INPUT SIGNAL	S	OUTPUT SIGNAL	S
INPUT NOISE ($\sqrt{N^2}$)	N	OUTPUT NOISE	$N/\sqrt{M}$
SIGNAL TO NOISE	S/N	SIGNAL TO NOISE	$\sqrt{M}\,S/N$

$$\text{IMPROVEMENT} = \text{OUTPUT/INPUT} = \frac{\sqrt{M}\ S/N}{S/N} = \sqrt{M}$$

EXAMPLE $M = 80 \longrightarrow$ IMPROVEMENT $= \sqrt{80}$ OR ~ 20 db

Fig. 3

IMPROVEMENT OF SIGNAL TO COHERENT NOISE RATIO BY PHASECODING AND PHASECOHERENT INTEGRATION

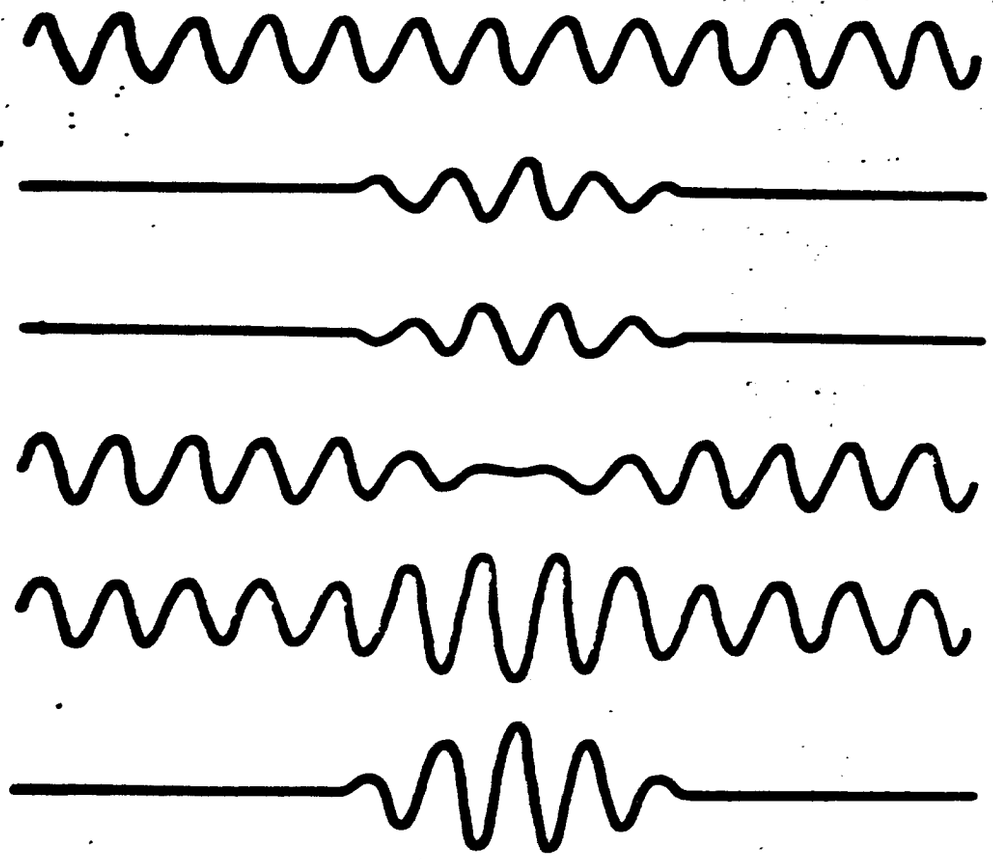

A : COHERENT INTERFERENCE

B : PHASECODED PULSE, $\phi = 0°$

C : PHASECODED PULSE, $\phi = 180°$

D : RECEIVER OUTPUT PULSE B TRANSMITTED

E : RECEIVER OUTPUT PULSE C TRANSMITTED

F : PROCESSED SIGNAL AFTER PHASECOHERENT INTEGRATION. [F = D + (-E)]

Fig: 4

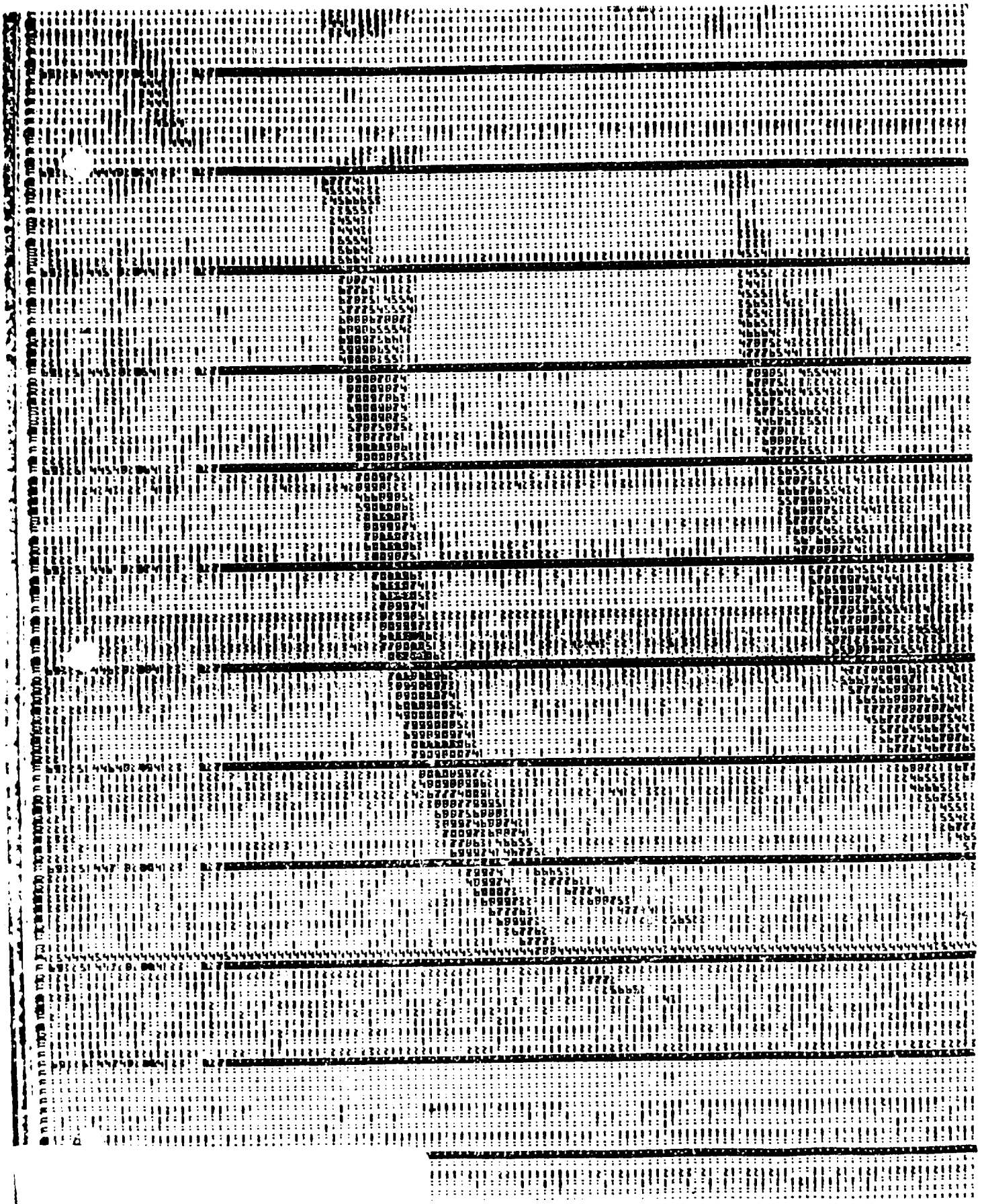

Fig. 5

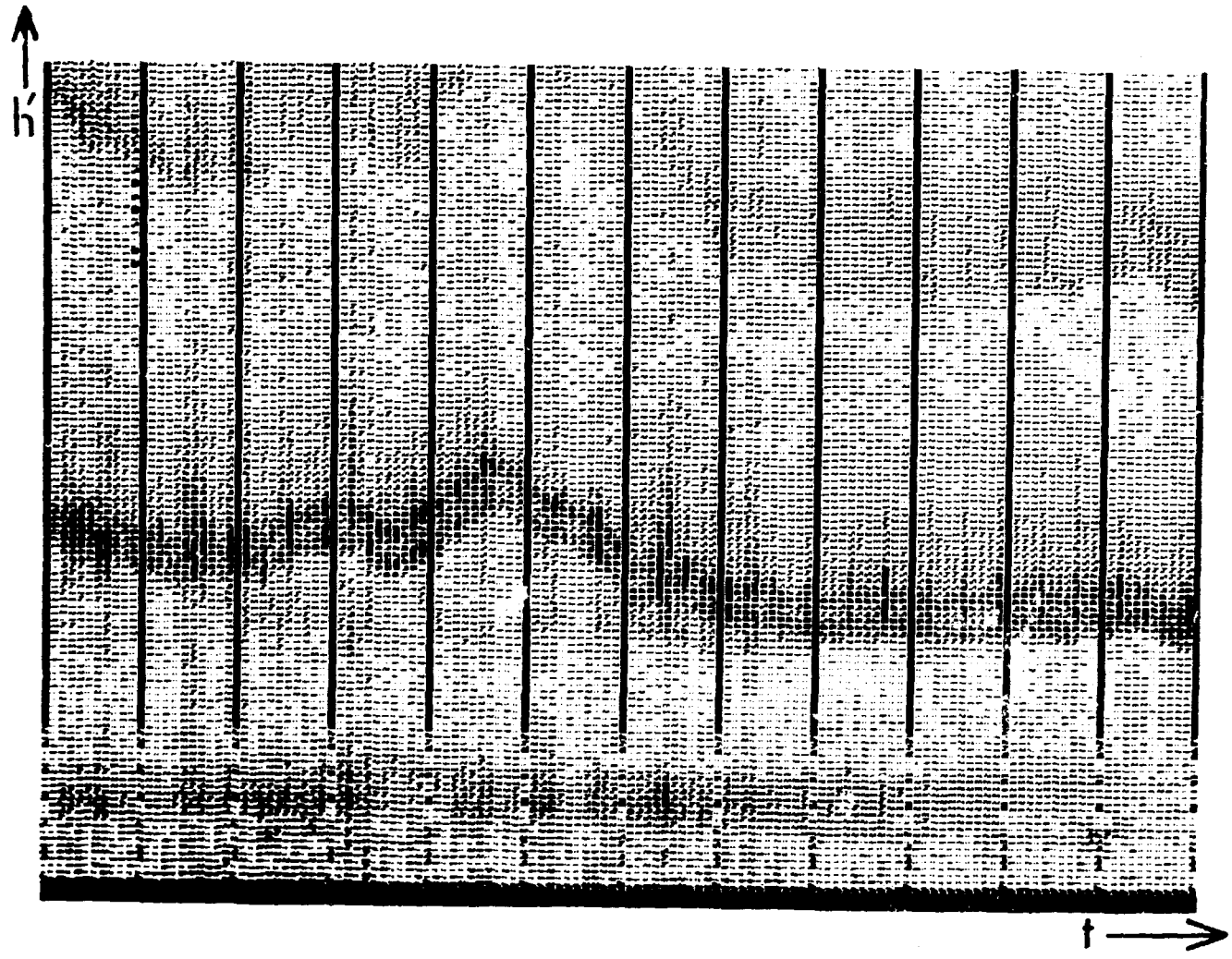

Minimum Heights of E- and F-Layer versus Time

Digicoder Printout

Fig. 6

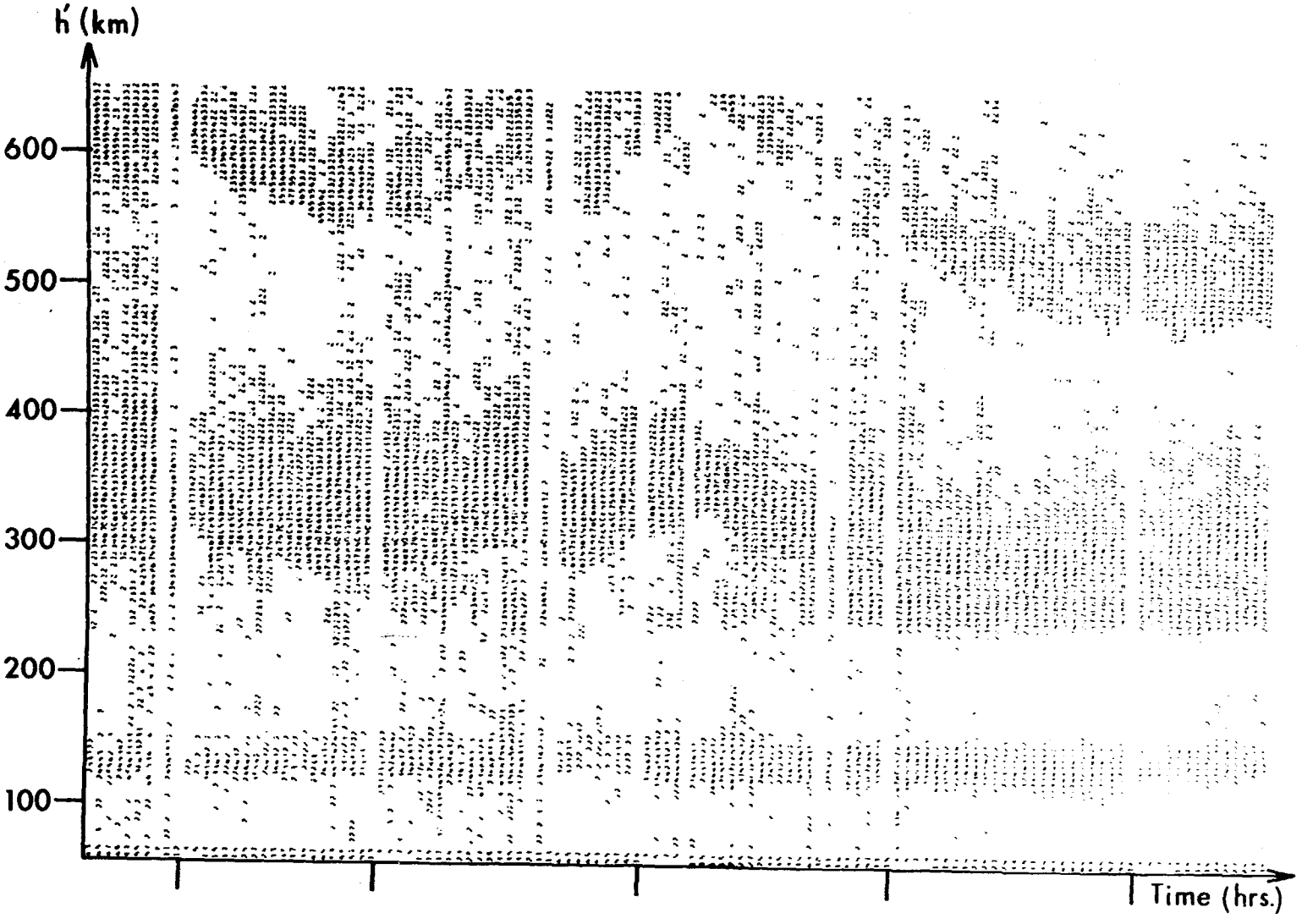

Minimum Heights of E- and F-Layer versus Time

Fig. 7

110-498

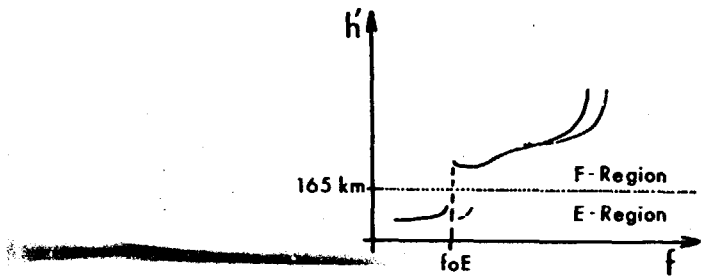

Determination of Critical Frequencies by Computer

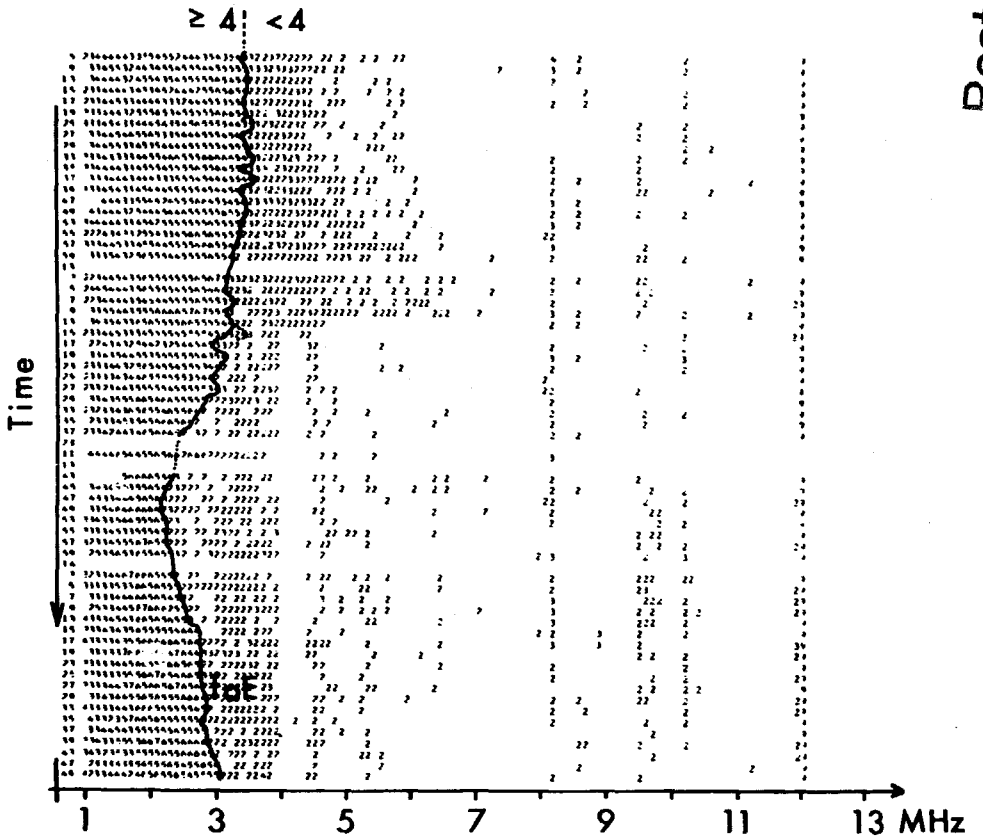

Fig. 5

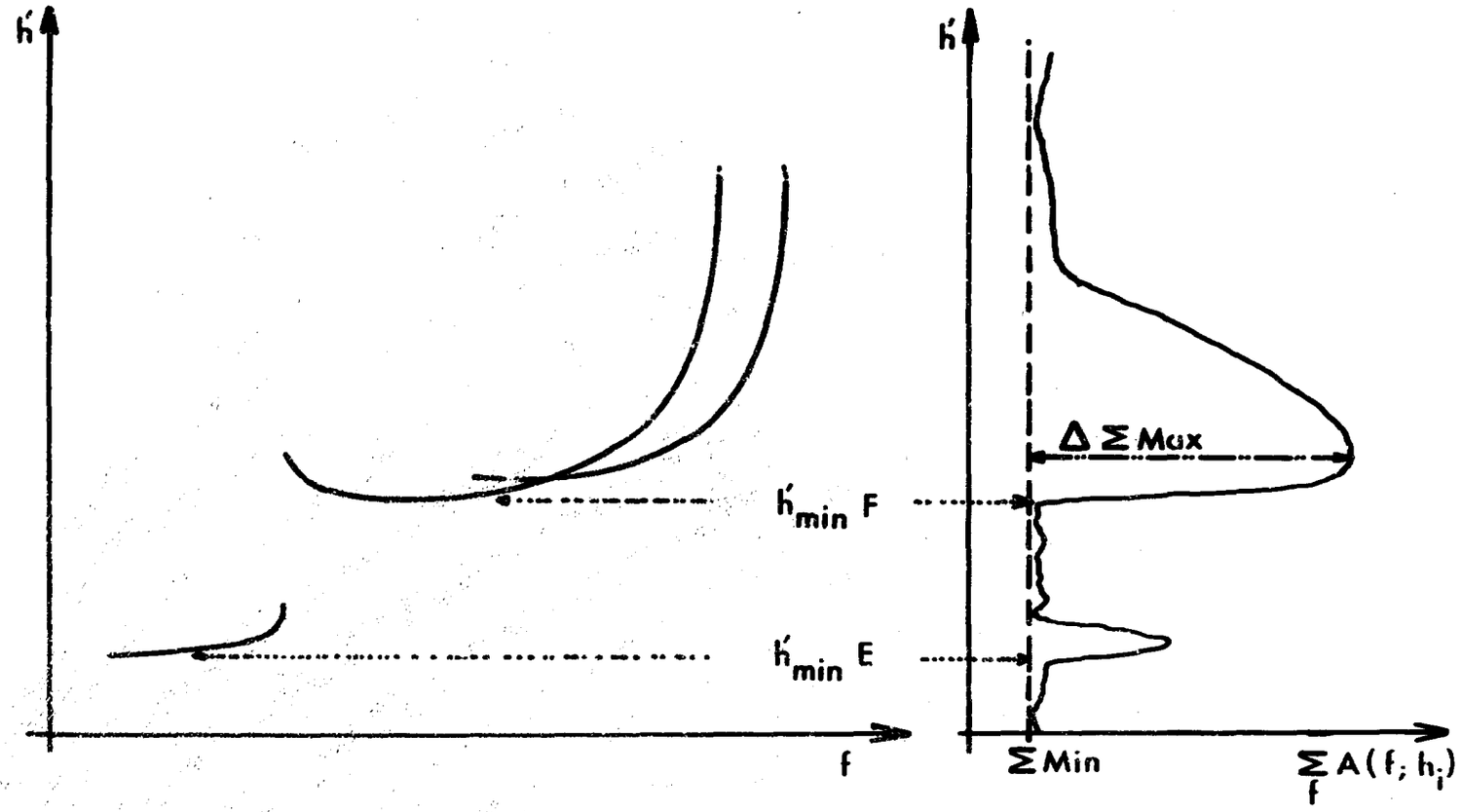

Determination of Minimum Layer-Heights

Fig. 9

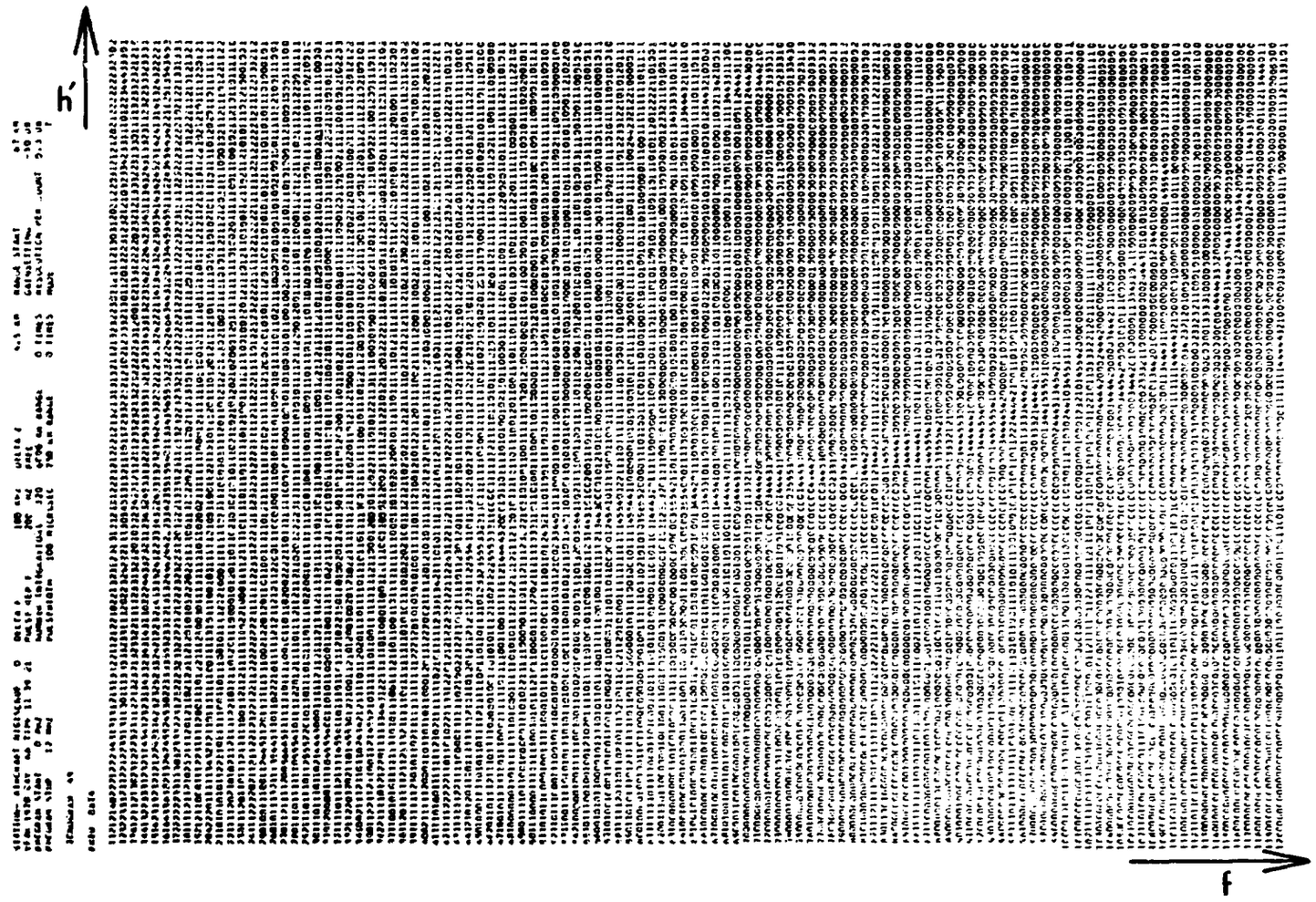

COMPUTER PRINTOUT OF DIGITAL IONOGRAM

NOISEFILTER: 0 dB

Fig. 10

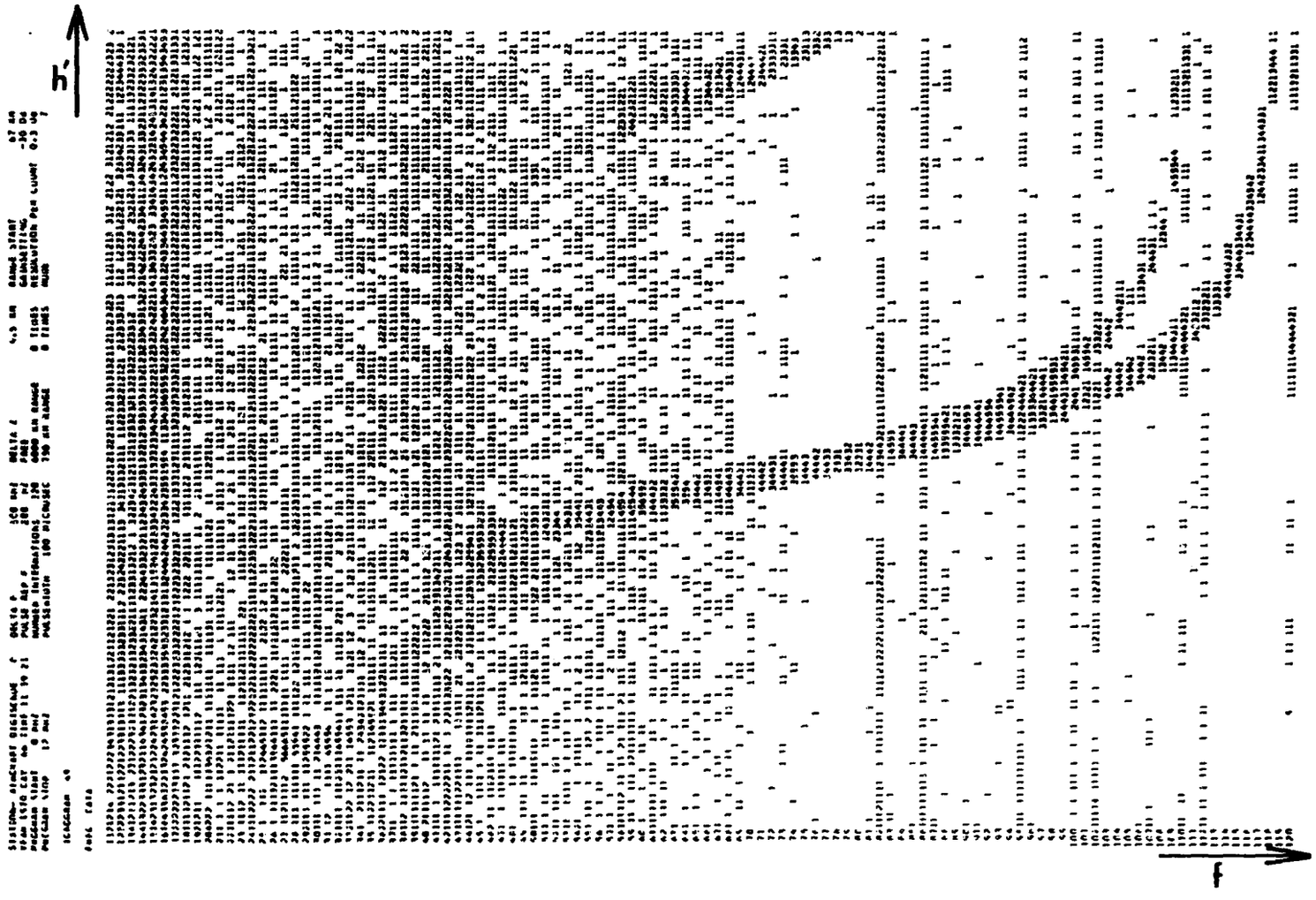

COMPUTER PRINTOUT OF DIGITAL IONOGRAM

NOISEFILTER: 3 dB

Fig. 11

Fig. 12

110-515

COMPUTER PRINTOUT OF DIGITAL IONOGRAM

NOISEFILTER: 6 dB

SECTION 9

ANALYSIS OF RADIO PROPAGATION CONDITIONS OF THE IONOSPHERE

Radio propagation conditions of the ionosphere are being recorded continuously. The primary source of research data is an analog magnetic tape. The purpose of this particular research project is to verify the data samples recorded on the analog tape.

In order to accomplish this task, the analog tape must be converted to a digital tape. The conversion of analog to digital was processed at the Data Reduction Facility at Northeastern University. The format of the digital tape is classified as "DCS-7094 type 1 format". The actual data tape used in the analysis was labeled "DOPLER" and it contained "Ionospheric Doppler Shift" data recorded at the Canadian range on 23rd of November 1968. The sampling rate is 5 KHz (5 kilocycles/sec). A tape record consists of a time word and twenty four (24) data values. The data values represent results from two channels, 5 and 4. The order in which these data points were written on the tape is the staggered mode; 5, 4, 5, 4, etc... 12 values of each. It should be pointed out that one of the program requirements was that as many as four (4) channels may be recorded on future tapes. The data processing program (ATA1) can handle 1, 2, 3, or 4 channels as generated per tape record.

"DCS-7094 type 1 format" will now be described. The data is set up in logical records, each consisting of two control words and a given number of frames of data. The first control word is the number of data words in a frame, including the time word. The second control word is the number of frames in the logical record. These two control words are fixed point or integer numbers. The "end of data" consists of a record of only three (3) words; "1, 1, 0". It is impossible to have a frame of data with only one data word. Such a condition uniquely identifies the "end of data".

The "time" word is a 36 bit word and it is the first word of each frame. It is constructed in the following manner:

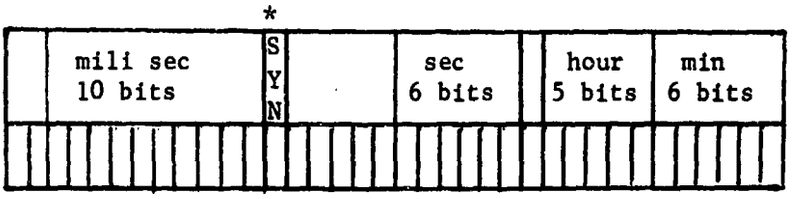

*SYN (13 bit) denotes "synchronization" (1 = not sync, 0 = in sync)

Another program requirement was that unpacking the time word to obtain individual values of hours, minutes, seconds, and miliseconds.

A data processing program (ATA1) was written in FORTRAN IV to run on the Direct Couple System at AFCRL. This program reads the digital tape, unpacks the time word, searches for the proper time segment, converts raw values (voltage) to amplitude, flogs values out of range, prints converted values with time, writes output record, and plots amplitude points graphically on line.

The tape is read by means of a READ TAPE statement as outlined in CEIR 7090 FORTRAN COMPATIBLE FLOATING POINT memo - R. McInerney. Also, the "end of data" and EOF are checked.

By using the "MOD" function and "powers of 2", time information is stripped from the time word.

Input to the program requires a start and stop time. If the time of a particular record does not fall within the time interval, the program either keeps on searching for a starting point or terminates.

The conversion technique is based on input parameters: for each channel, the following information is required; upper and lower tolerances, high and low ranges. The raw data value is converted by the equation:

$$V = \frac{r - tl}{tk} \quad X\ (rgk) + rgl$$

where:

V = converted value

r = raw value to be converted

tl = lower tolerance

rgl = low range

tk = (upper - lower) tolerance

rgk = (high - low) range

The converted value is tested to see if it falls within the range interval specified for each particular channel. If it does not satisfy the limits, the value is flogged at printout.

The on line plot scheme is called SCETCH. This display prints a two coordinate graph. The y coordinate is amplitude value and the x coordinate is the sequential order of signals.

The scope of this task is to show that the analog and digital data tapes are compatible. Once this has been established, the digital data (from ATA1 output tape) will be subjected to power spectrum and cross spectrum analysis.

Project Number: 5631

Problem Number: 1689

Researcher: Dr. C. Rush

SECTION 10

INVESTIGATION OF VARIATIONS OF STRATOSPHERIC AEROSOL THROUGH PHOTOGRAPHIC MEASUREMENTS

In the course of the atmospheric optics research by CROA, photographic twilight measurements for investigations of variations of stratospheric aerosol have been made at several stations. Several films each with about 60 exposures (simultaneously in two wavelength ranges) had to be evaluated. Initially these calculations were done by hand but it was found that this process was much too tedious and to ease the workload a computer program was written to perform all the necessary calculations.

The program was designed to compute the solar elevation from local time and to convert film densities to intensities, taking care of corrections for neutral filter steps, aperture setting and exposure duration.

Since the input to the program was given in terms of the transmission percent, it was necessary first of all to convert from this film transmission percentage to film density. This is done by means of the graph shown in Fig. 1, which gives the relationship between transmission percent and film density for this particular film 12C. Figure 1 also shows how arrays are set up giving corresponding values for transmission percent and film density for the U and G filter ranges. Thus, inserting these arrays into the program we can easity find the density of the film given the transmission percent through a simple interpolation scheme.

Since the area of concern was the film intensity, this final conversion was necessary and the equation is as follows:

$$\bar{\bar{O}}_o = \bar{O}_o + \hat{k} - \log (T/5)$$

where $\bar{O}_o$ is the weighted film density mean, k is a constant depending on the

aperture setting, and T is the exposure duration.

More recently, a plotting routine was added to the program for a more detailed study of these films. The plots consisted of intensity and color ratio versus solar elevation. A sample plot can be seen in Fig. 2.

Project Number: 7621

Problem Number: 1687

Researcher: Mr. F. Volz

TRANSMISSION PERCENT	3	5	10	15	20	30	40	50	60	70	80	90
100 LOG U (DENSITY)	115	100	75	65	58	48	40	30	22	13	5	0
100 LOG G (DENSITY)	150	130	105	92	84	72	63	52	43	33	22	8

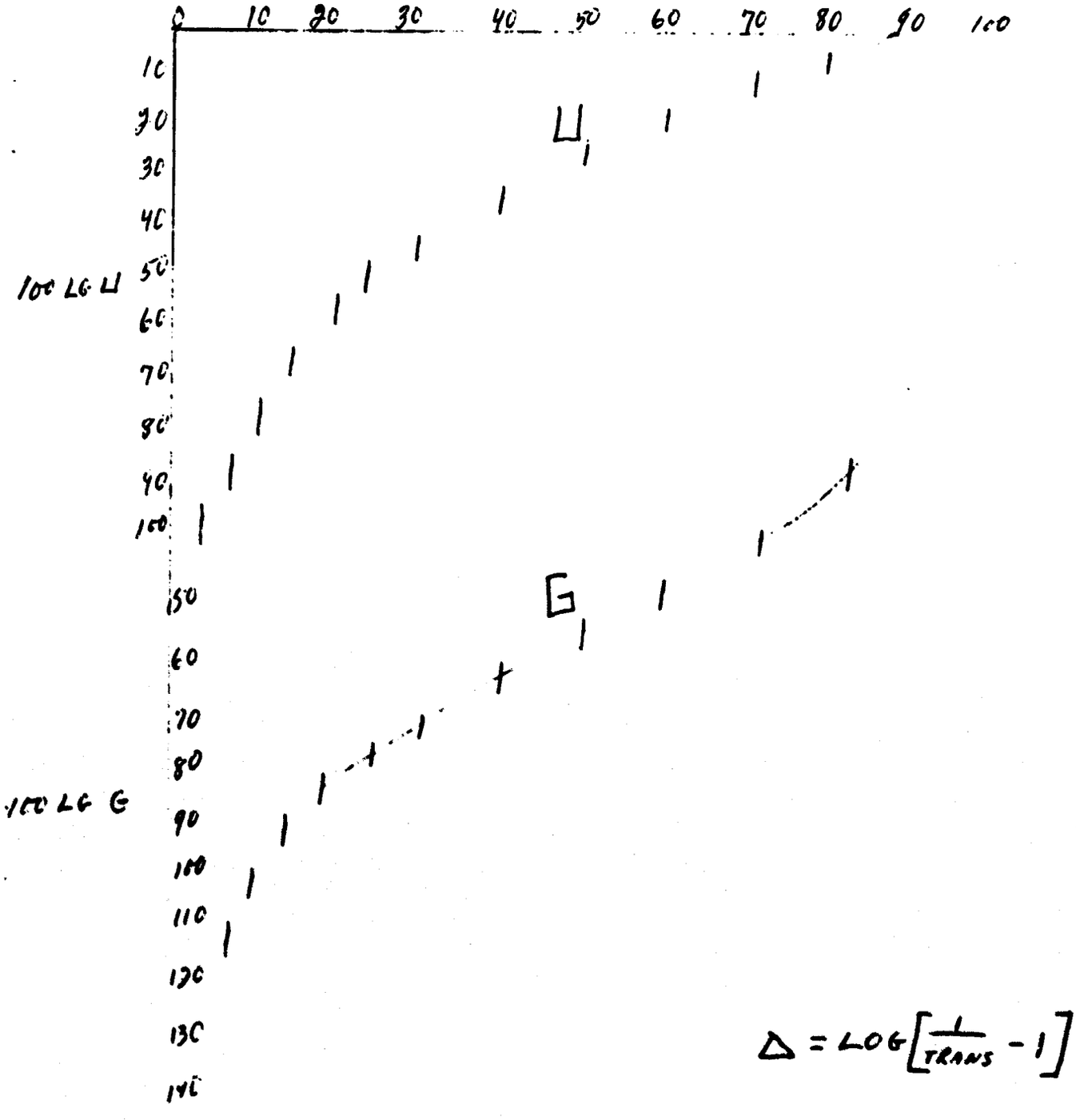

FIG. 1

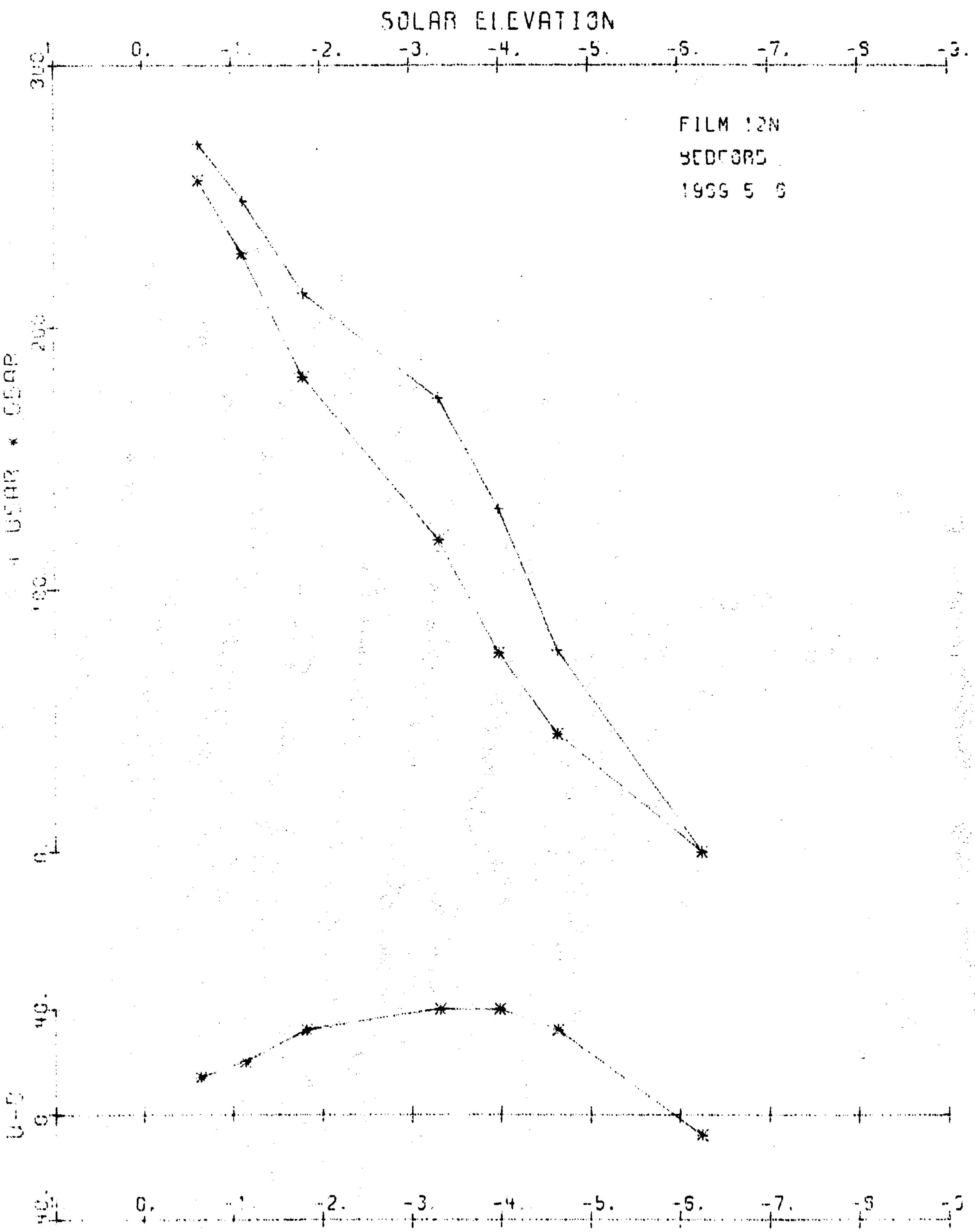

SOLAR ELEVATION
0.
-1.
-2.
-3.
-4.
-5.
-6.
-7.
-8
-9.
FILM 12N
BEDFORD
1969 5 9
+ USAR * CSAR
300
200
100
0
40.
U-C

FIG. 2

SECTION 11

WAVE PROPOGATION IN HOT MAGNETAPLASMAS

Recent work at AFCRL has been concerned with deriving dispersion relations for electromagnetic waves propogating in plasmas immersed in a magnetic field. These dispersion relations can be used to predict how waves progogating in a plasma will attenuate and distort as a function of the parameters characterizing the medium. These investigations are of use in the design of any radio communications system in which waves must propogate through an intervening plasma medium, such as in reentry communications systems and in ionospheric propogation work. Conventional dispersion relations, such as the appletos-Hartree equations, neglect a number of important properties of plasmas that can have an effect on wave propogation. The work at AFCRL is concerned with deriving dispersion relations that are much more accurate and that are valid over a much wider range of plasma parameters than previous theoretical formulas.

The dispersion relations are obtained by solving the Baltzmann kinetic equation using a variety of Fourier transform techniques and perturbation methods. Graphs are available of the propogation constants plotted over a wide range of normalized plasma parameters. The cases of propogation along and across the DC magnetic field lines are investigated in detail. The graphs show the effect of velocity dependent electron-neutral collisions and Coulomb collisions on the propogation constants of the wave. Four graphs are given at the end as a sample of the output generated in support of the research on this project.

The interaction of electromagnetic waves with an infinite, homogeneous plasma is completely described by Maxwell's equations and the constitutive relations. For such a medium, Maxwell's equations may be written in the form

$$\nabla \times \underset{\sim}{E} = -B \qquad (1)$$

$$\nabla \times H = C \qquad (2)$$

where $\underset{\sim}{C}$ = total current density. The constitutive relations express $\underset{\sim}{C}$ in terms of $\underset{\sim}{D}$ and $\underset{\sim}{E}$. For a.c. fields, it is possible to obtain two separate, yet equivalent, models of the plasma by considering the medium to possess either dielectric or conducting properties. For the dielectric model, the electrons and positive ions are considered to form an induced dipole moment as the result of interacting with an externally imposed electric field. The motion of the electrons then gives rise to a polarization vector P = -Ner where N is the electron density, e is the electronic charge, and where the electron displacement r is determined from an equation of motion of the electron. In the following, a subscript will denote the Cartesian component of a vector. Since $D_i = P_i + \epsilon_o E_i$, the total current density C_i is equal to the electric displacement current density D_i. This model yields the constitutive relations.

$$B_i = {}_o H_i$$

$$D_i = P_i + {}_o E_i = E_i$$

For the electrical conductor model of a plasma, the electrons and ions are considered to be free charges that acquire a net drift velocity under the influence of externally imposed fields. Here, the total current density C_i is the sum of a conduction current density $J_i = E_i$ and a free space displacement current density ${}_o E_i$, so that $C_i = E_i + {}_o E_i$. The constitutive relations are completed by the relation: $B_i = {}_o H_i$, since the diamagnetic effect of a plasma at ordinary densities is negligible. When the ion motion is neglected, the conduction current density is given by $J_i = -Nev_i$ where the electron velocity v_i is determined from the equation of motion for the electron. Hence, the conduction current density J_i is exactly equivalent to the polarization current density P_i in the dielectric model. By equating the total current density in the dielectric model to the total current density in the conductor model, the following expression is obtained for the dielectric constant, K:

$$K = 1 + \frac{\sigma}{j\omega\epsilon_o} \qquad (3)$$

where $K = \epsilon/\epsilon_o$, σ = electrical conductivity and the electric field varies in time as exp + (jwt).

In the following presentation, there will be a number of assumptions made about the interaction of the electromagnetic waves with the plasma medium. First, it will be assumed that the plasma is electrically neutral in the absence of any external perturbations. Also, the plasma will be assumed to be weakly ionized, so that electron collisions with the neutral particles will dominate over electron-electron and electron-ion collisions. The signal strength of the electromagnetic fields will be low in order that the kinetic equations may be linearized. For low signal strengths, nonlinear effects such as harmonic generation and self-modulation are negligible. Since the ions are much heavier than the electrons, they respond more slowly to an alternating electric field. It will be assumed that the signal frequencies are sufficiently high so that the ion contribution to the electrical conductivity is negligible.

A fundamental length characterising a plasma is the Debye length, ℓ_D,

$$\ell_D = \sqrt{\frac{\epsilon_o k T_e}{NE^2}}$$

where k = Boltzmann's constant

and T_e = electron temperature.

In considering the influence of many particles upon a test particle introduced into the plasma, it is found that there is a limit to the number of particles that have to be considered in the interaction. Charged particles close to the test particle act as a screen between the test particle and more distant charged particles. The Debye length is the length parameter that characterizes this transition. It will be assumed that the electromagnetic wavelength is much larger than the Debye length $_D$. This is necessary in order to consider the perturbing electromagnetic fields as macroscopic fields. Finally, the plasma temperature will be considered to be sufficiently low so that the particle motion is nonrelativistic

$$k T_e \ll mc^2$$

where

m = electron mass.

It will be shown that first order thermal corrections to a cold plasma are proportional to n^2, where

$\sigma = kT_e/mc^2$ and

n = index of refraction

Hence, for nonrelativistic plasmas, thermal effects are important only when the index of refraction is large.

Special Features of Hot Plasma Theory

There are several different approaches that may be taken in describing the dielectric and/or conduction properties of a plasma. The most appropriate method for a particular problem depends upon the nature of the information desired. The simplest model of a plasma is based upon orbit theory. According to this approach, it is assumed that the individual particles comprising the plasma do not interact with one another and that they do not possess a random thermal motion. The motion of the individual particles is calculated from Newton's equations of motion where the force exerted on each particle is due only to the externally impressed fields.

The well-known expression for the dielectric constant K of a cold isotropic plasma is obtained from the equation of motion of an electron

$$m\underset{\sim}{v} = -e\underset{\sim}{E} . \qquad (5)$$

This equation may be solved for v by assuming E and v vary as exp(+jwt) in time:

$$\underset{\sim}{v} = \frac{je}{mw}\underset{\sim}{E} . \qquad (6)$$

From the fact that the current density is given by

$$J = -Nev = \sigma E ,$$

the conductivity may be expressed in the form

$$\sigma = -j\frac{Ne^2}{mw} . \qquad (7)$$

Substituting Eq. (7) into (3) yields

$$K = 1 - \frac{w_N^2}{w^2} = 1 - X \quad , \tag{8}$$

where $w_N = (Ne^2/m_o)^{1/2}$ is the electron plasma frequency, and

$$X = \frac{w_N^2}{w^2}$$

Although orbit theory is not capable of rigorously taking into account the effect of interparticle collisions, an average collision frequency v is often introduced into the analysis in a heuristic fashion by adding a damping term m v to the left-hand side of the equation of motion (5).

The effect of the thermal motion of the particles cannot be adequately taken into account within the framework of orbit theory. The most direct means of including the effects of thermal motion is to retain the pressure gradient terms that appear in the momentum equations for each plasma constituent. If the wave motion is assumed to be adiabatic, then the continuity equation and the momentum equation for each constituent, together with the electrodynamic equations, form a determined set of equations. By linearizing these equations and looking for solutions that vary in space and time as $\exp j(wt - \underset{\sim}{k} \cdot \underset{\sim}{r})$, where k is the wave number, a dispersion relation between w and k may be obtained. In contrast to the results of orbit theory, the linearized moment equations yield a dispersion relation that includes first order temperature terms. For transverse electromagnetic waves the thermal corrections are negligible except when a d.c. magnetic field is present and the signal frequency is close to the electron cyclotron frequency. On the other hand, for longitudinal waves (in which the direction of propagation is parallel to the electric vector) the effects of finite temperature are important because they provide a mechanism for the propagation of the longitudinal oscillations.

According to the orbit theory description of longitudinal oscillations in a cold plasma, if a group of electrons is slightly displaced from its equilibrium position, a space-charge field will immediately develop tending to drive the

electrons back to their equilibrium position. The momentum they gain will cause them to over-shoot their equilibrium position and a space charge field will again tend to restore them to their equilibrium position. In a cold plasma, this oscillation about their equilibrium position will occur at the plasma frequency, w_N. However, if the electrons are displaced from their equilibrium position and they possess thermal energy, a pressure gradient will develop, tending to accelerate the electrons in the same direction as the space charge electric field. The frequency of these oscillations in a warm plasma is slightly greater than the plasma frequency, and the oscillations now can propagate and carry energy. These oscillations are maintained primarily by the velocity modulation of a small group of electrons that are moving rapidly in the direction of propagation of the wave. This dispersion relation for the electron oscillations is given by

$$w^2 = w_N^2 + k^2 v_{TH}^2$$

where

k = wave number

$v_{TH}^2 = 3kT_e/m$.

When a d.c. magnetic field is present, then it is found that this longitudinal wave can propagate along the magnetic field lines. If the linearized moment equations are used to study the propagation of longitudinal electron waves across the magnetic field lines, then the dispersion relation takes the form exhibited in Figure 1. Here, $w_H = eB/m$ is the electron cyclotron frequency. In this figure, the frequency is normalized to the electron cyclotron frequency and the abscissa, kv_{TH}/w_H, is the ratio of the mean radius of gyration to the wavelength. The analysis based upon the linearized moment equations is not valid if the radius of gyration of the electrons is sufficiently large so that in a single gyration an electron samples a significant portion of the electric field. Hence, the dispersion curves in Figure 1

are valid only for long wavelengths. A more detailed kinetic theory approach is necessary in order to ascertain how these curves must be modified for larger wavenumbers.

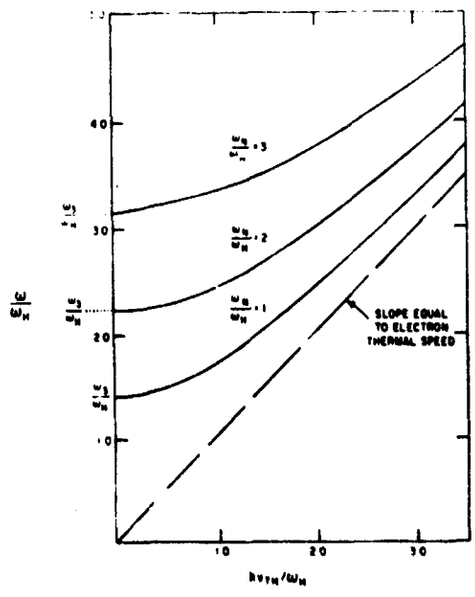

Figure 1. Electron Wave Propagating Across a Magnetic Field Based on the Moment Equations. Higher order temperature effects cause change in dispersion curves $\omega_3 = \sqrt{\omega_H^2 + \omega_N^2}$

For certain types of collision-dominated plasmas in a magnetic field, a conducting fluid model is often simpler and more useful than the model based upon the moment equations for each plasma constituent. For many cosmic and astrophysical plasmas, the time and length scales are so large and the frequencies are so low that the motion of the electrons relative to the ions is unimportant. The important question concerns the motion of an element of conducting fluid viewed as a whole. Thus, there is less information contained in the conducting fluid model of a plasma as opposed to the single constituent moment equations. The equations for the conducting fluid model may be derived from the single constituent moment equations by writing these equations in terms of a mean velocity for the mixture and summing over all the constituents of the gas.

The most general approach to wave propagation in a plasma includes the use of kinetic equations for each plasma constituent. Since only relatively high fre-

quencies are considered in this analysis, only the kinetic equation for electrons is of interest. The kinetic equation describes the behavior of the velocity distribution function, f. This distribution function is defined as the density of points in the six dimensional phase space made up of the three components of the particle's position plus the three components of the particle's velocity. The kinetic equation approach must be used to describe wave propagation in a plasma when information is desired about phenomena that depend explicitly on the velocity spread of the particles.

There are several important effects which occur in a hot magnetoplasma that are absent in a cold plasma. One effect is transconductance, in which the conductivity at a given point in the plasma is not entirely due to the drift velocity of the electrons acquired by the presence of the electric field at that point, but may depend upon the effect of the electric field at neighboring points. This nonlocal effect is due to the fact that the electrons, because of their thermal motion, may move during one period of oscillation of the electric field. This nonlocal, hot magnetoplasma effect may be expressed mathematically as

$$J_i(r, t) = \iint \sigma_{ij}(\underset{\sim}{r} - \underset{\sim}{r}', t-t') \, E_j(r', t) \cdot d^3r'dt' \quad . \tag{10}$$

Another important effect which occurs in a hot plasma involves collisionless wave damping. In an isotropic plasma, longitudinal waves may be damped when the wavelength becomes of the order of a Debye length. This is termed Landau damping and is the result of energy transfer between the longitudinal wave and those particles travelling near the wave phase velocity. This energy transfer is a consequence of the fact that particles travelling slightly slower than the wave phase velocity will gain energy from the wave if they are initially randomly phased with respect to it. Another type of collisionless damping is termed cyclotron damping,

and occurs when a right-hand, circularly-polarized wave is travelling along the magnetic field lines at a signal frequency close to the electron cyclotron frequency. If an electron is gyrating about the magnetic field lines at the cyclotron frequency w_H, and is travelling along the magnetic field lines with a velocity $\pm (v)_{11}$, then in the electron's frame of reference the frequency of the wave is $(w - w_H \pm (v)_{11}k)$, where $(v)_{11}k$ represents the Doppler shift due to the relative motion of the electron and the wave. At the resonant electron velocity $(v)_{11}$ equals $\pm (w - w_H)/k$, the electrons rapidly gain energy at the expense of the electromagnetic wave. This damping results in a finite maximum wave number for propagation of the right-hand wave at the cycletron frequency.

A third important effect which is predicted by the kinetic theory approach involves a modification of the dispersion curves shown in Figure 1 for propagation across the magnetic field. This modification is due to resonant effects that may occur when the Larmor radius (mv_T/w_H) is an integral number of electromagnetic wavelengths. It will be seen that pass bands can exist for longitudinal waves propagating across the magnetic field close to all the harmonics of the cyclotron frequency.

Work under this project is continuing.

Project Number: 4642

Problem Number: 1550

Researcher: Mr. R. Papa

Graph A shows:

$$NU+ = \frac{\gamma_{eff}}{\gamma_0} = \frac{1}{\pi_0}(1-Y)\frac{Re(\sigma^+)}{Im(\sigma^+)}$$

vs y for $y = .4$ to 1.1

Graph B shows:

$$RHO- = \rho + = \frac{(1+y)|\sigma^-|^2}{Im(\sigma^-)}$$

vs y for $y = .4$ to 1.1

Graph C shows:

RE(N) = Re (N_o)

vs X for X = .4 to 1.0

Graph D shows:

IM(N) = Im (N_o)

vs X for X = .4 to 1.0

The parameters characterizing the medium are listed in the upper left corner of each graph.

A

X = 1.500000
Z0 = .500000
Z2 = -.100000
VEE = 1.000000
VCL = .500000
DELTA= .000001

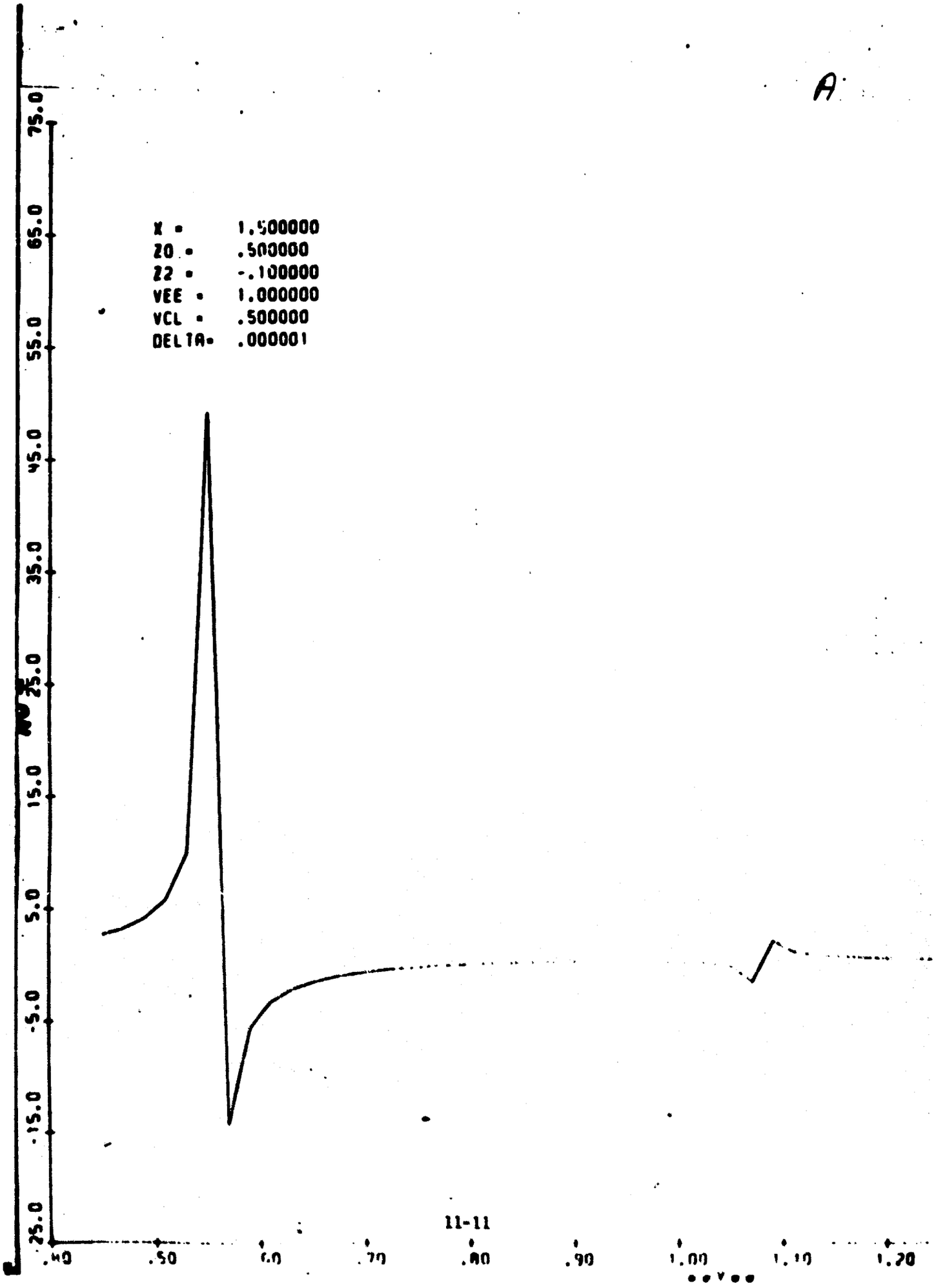

B.

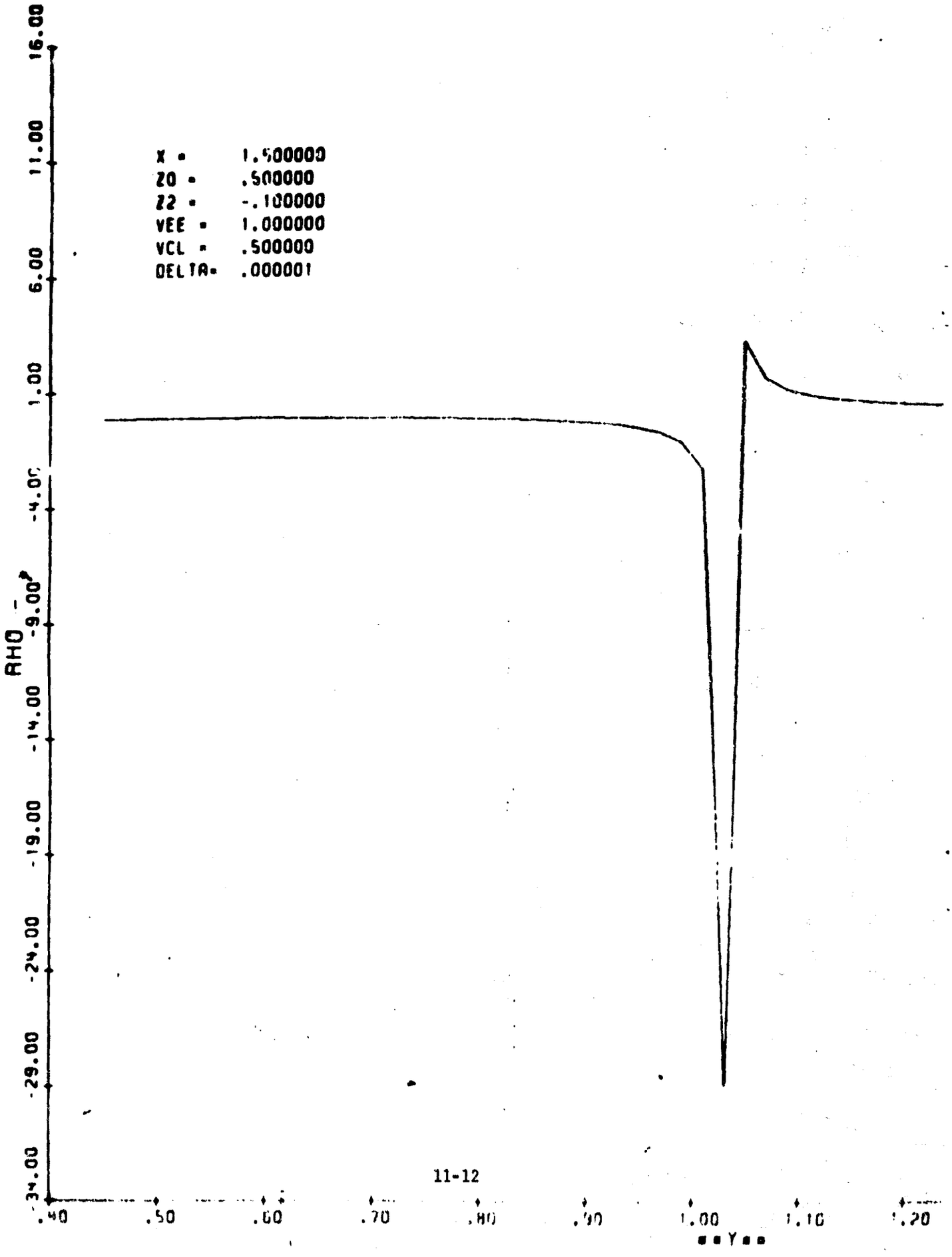
X = 1.500000
Z0 = .500000
Z2 = -.100000
VEE = 1.000000
VCL = .500000
DELTA= .000001
16.00
11.00
6.00
1.00
-4.00
-9.00
-14.00
-19.00
-24.00
-29.00
-34.00
RHO
.40
.50
.60
.70
.80
.90
1.00
1.10
1.20
Y

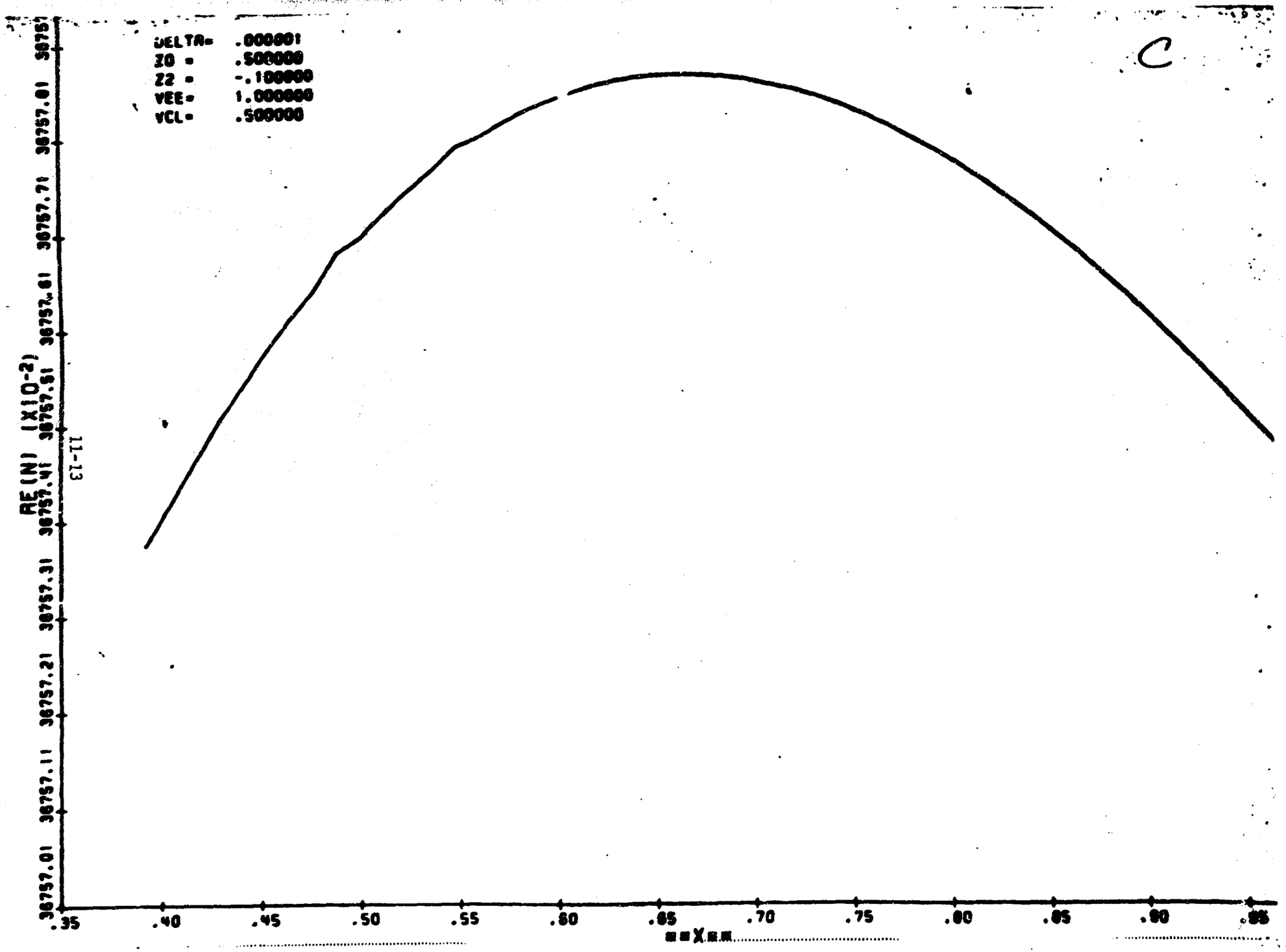
DELTA= .000001
Z0 = .500000
Z2 = -.100000
VEE= 1.000000
VCL= .500000
RE(N) (X10-2)
36757.01
36757.11
36757.21
36757.31
36757.41
36757.51
36757.61
36757.71
36757.81
36757.91
.35
.40
.45
.50
.55
.60
.65
.70
.75
.80
.85
.90
.95
X

C

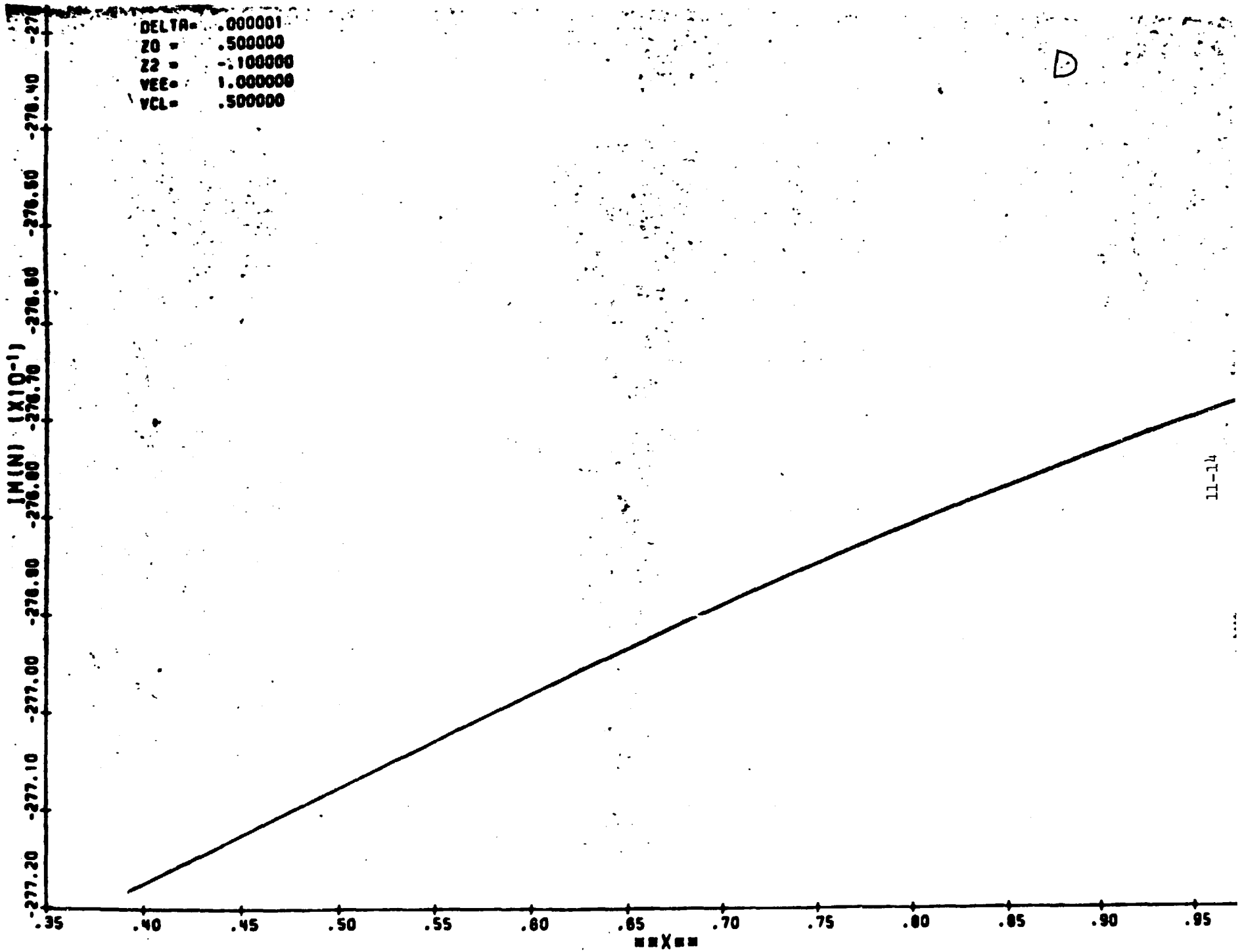
DELTA= .000001
Z0 = .500000
Z2 = -.100000
VEE= 1.000000
VCL= .500000
D
-277.20
-277.10
-277.00
-276.90
-276.80
-276.70
-276.60
-276.50
-276.40
IM(N) (X10⁻¹)
.35
.40
.45
.50
.55
.60
.65
.70
.75
.80
.85
.90
.95
XX
11-14

SECTION 12

SOME MATHEMATICAL PROPERTIES OF AN INTEGRAL EQUATION FOR THREE-BODY SCATTERING

In the past ten years the quantum mechanical three-body problem has received a lot of attention in the literature. The main advance in treating this problem has been the notion that the wavefunction, or the T-matrix, may be decomposed into a sum of three parts. The reason for making this decomposition is the hope of obtaining equations which are tractable, whereas a straightforward approach leads to many difficulties.

The two recent methods for the three-body problem are given in the work of Eyges[1] and Jasperse[2,3], and the work of Faddeev[4] and others[5,6]. Eyges and Jasperse decompose the wavefunction directly, and Faddeev and others decompose the T-matrix directly.

Once the decomposition is made, two questions arise immediately. They are, (1) what are the mathematical properties of the resulting equation?, and (2) is the equation tractable using modern computational methods? In this report, a study of some mathematical properties of Eqn. (16) of reference 3 is presented. This equation describes the simplest model of neutron-deuteron scattering, which still retains the basic features of a more complicated nuclear fission process.

In this first phase of the investigation of Eqn. 16, we have studies the resulting integral operator to determine whether or not it is compact as an operator on a certain Banach space. Knowing that the operator is compact would allow us to apply the classical Fredholm Theory. This theory enables us to say something about the existence and uniqueness of solutions to functional equations. Without an answer to this existence and uniqueness problem, the results of any numerical attempt to solve eqn. 16 would be at best difficult to interpret.

The results to be proved in this report are summarized in Section 1. The main result is negative in character, and shows that no power of a certain operator is compact.

The reader will find the necessary background material in Reference 7. This includes the definition and some properties of Banach spaces, the integration of Banach space valued functions, and the theory of compact operators. For a more thorough treatment of the Fredholm Theory, the reader is advised to consult Reference 8.

References

1. L. Eyges, Phys. Rev. 115, 1643 (1959)

2. J.R. Jasperse and M.H. Friedman, Phys. Rev. 159, 69 (1967)

3. J.R. Jasperse, J. Math. Phys. 9, 1931 (1968)

4. L.D. Faddeev, J.E.T.P. 12, 1014 (1961)

5. C. Lovelace, Phys. Rev. 135, B 1225 (1964)

6. R. Aaron, R.D. Amado, and Y.Y. Tam, Phys. Rev. 140, B 1291 (1965)

7. S. Lang, Analysis II, Addison-Wesley, 1969

8. Kantorovich and Akilov, Functional Analysis in Normed Spaces, Macmillan, 1964

1. The integral equation to be examined is,

$$\frac{g(\eta)}{\beta - i(S - 3/4\,\eta^2)^{1/2}} = (\eta^2 + \eta\cdot\eta_0 + \eta_0^2 - S)^{-1} + \frac{1}{\pi^2}\int \frac{g(\gamma)\,d\gamma}{(\gamma^2+\gamma\cdot\eta+\eta^2-S)(-\beta^2+3/4\gamma^2-S)} \qquad (1.1)$$

where

$$\eta = (\eta_1, \eta_2, \eta_3)$$
$$\eta_0 = (\eta_{01}, \eta_{02}, \eta_{03})$$
$$\gamma = (\gamma_1, \gamma_2, \gamma_3)$$

$\beta \geq 0$, S is on the Cut $-\infty < S < \infty$, and the argument of the square root is chosen to be $\frac{\theta}{2}$, $0 \leq \theta < 2\pi$, $\theta = \arg(S - 3/4\,\eta^2)$. Further, the integral is taken over all of three space, and we also assume that S, β, η_0 are chosen so that $S = -\beta^2 + \frac{3}{4}\eta_0^2$.

For convenience, we set

$$\delta(\eta, \eta_0, S) \equiv \delta(\eta, \eta_0) = (\eta^2 + \eta\cdot\eta_0 + \eta_0^2 - S)$$
$$\gamma(\eta, \beta, S) \equiv \gamma(\eta) = \beta - i(S - 3/4\,\eta^2)^{1/2}$$
$$\psi(\gamma, S, \beta) \equiv \psi(\gamma, S) = -\beta^2 + 3/4\,\gamma^2 - S .$$

(1.1) can now be written,

$$\frac{g(\eta)}{\gamma(\eta)} = \frac{1}{\delta(\eta, \eta_0)} + \frac{1}{\pi^2}\int \frac{g(\gamma)\,d\gamma}{\delta(\gamma, \eta)\,\psi(\gamma, S)} . \qquad (1.2)$$

R^3 will denote Euclidean three-space, while $C_1(R^3)$ will denote the space of continuous bounded complex valued functions, having continuous bounded

first partial derivatives, which are defined on R^3. Also $C_1^0(R^3)$ will denote the subspace of $C_1(R^3)$, which consists of functions which vanish at ∞, and which have vanishing first-partial derivatives at ∞. For $F \in C_1(R^3)$, we define $\|F\| = \max \left\{ \sup |F|, \sup \left|\frac{\partial F}{\partial y_1}\right|, \sup \left|\frac{\partial F}{\partial y_2}\right|, \sup \left|\frac{\partial F}{\partial y_3}\right| \right\}$.

It can be shown that $\|\cdot\|$ is a norm and that with this norm, $C_1(R^3)$ becomes a Banach space, and also that $C_1^0(R^3)$ becomes a closed subspace, and hence, itself a Banach space. If B is a Banach space, we will use $[B]$ to denote the Banach space of bounded linear operators from B into B.

From Appendix I, it is seen that, when $S < 0$, $S(y,y) > 0$. However, $\psi(y,S)$ may vanish. Thus, when $S < 0$, by $\int \frac{g(y)\,dy}{S(y,y)\psi(y,S)}$ we will mean $\lim_{\sigma \to S} \int \frac{g(y)\,dy}{\psi(y,\sigma)S(y,y)}$, where either $\sigma = S - \epsilon \in$ or else $\sigma = S + \epsilon$. The limit in general depends upon the side of the axis from which σ approaches S, but since in both cases the analysis is the same, we will not usually distinguish between the two. For $S < 0$, let K_σ denote the integral operator acting on g, which is given by $K_\sigma g = \int \frac{g(y)\,dy}{S(y,y)\psi(y,\sigma)}$.

For $S < 0$, we will thus understand equation (1.2) to mean

$$\frac{g(x)}{\psi(x)} - \frac{1}{\pi^2} K g = \frac{1}{S(x,x_0)}$$

where $K = \lim_{\sigma \to S} K_\sigma$.

In Section 2, we will show that this is meaningful. In fact, we will show that in both $[C_1(R^3)]$ and $[C_1^s(R^3)]$ $\lim_{\epsilon \to 0} K_\epsilon$ exists, and is compact. This will prove that (1.2) can be viewed as a functional equation in both $C_1(R^3)$ and $C_1^s(R^3)$.

In Section 3, we show that when $\lambda < 1$, and (1.2) is written in operator form as,

$$(I - H)g = \frac{f(\eta)}{s(\eta, \eta_0)}$$

that again, the equation can be viewed as a functional equation in both $C_1(R^3)$ and $C_1^s(R^3)$. This time, however, compactness is lost; we will show that in both $[C_1(R^3)]$ and $[C_1^s(R^3)]$ no power of H is compact. This result is disappointing; for if some power of H were compact, we could apply the generalized Fredholm Theory to gain further information about the solutions (if any) to (1.2).

2. In this section, some theorems will be valid for $C_1^p(R^1)$ $\left([C_1^p(R^1)]\right)$ as well as for $C_1(R^1)$ $\left([C_1(R^1)]\right)$. In most cases, the proofs will be identical (except for an interchange of symbols) and will only be given for $C_1(R^1)$. If, however, this is not the case, then the additional reasoning will appear. Throughout the section, γ will be negative.

Define the operator $C_\gamma(y)$ by $[C_\gamma(y)]\,g = \dfrac{g(\cdot)}{\gamma(y,\cdot)+\gamma(y,\cdot)}$

Thus for each fixed y, $C_\gamma(y)$ takes the function $g(\cdot)$ into the function (of y) $\dfrac{g(y)}{\gamma(y,\cdot)+\gamma(y,\cdot)}$. Clearly $C_\gamma(y)$ takes g into $C_1^p(R^1)$. Since $C_\gamma(y)$ is a linear operator, to show that it is in both $[C_1(R^1)]$ and $[C_1^p(R^1)]$, we need only show it's bounded. An operator F from G into H is contained in $[B]$ if it's linear and if $\|F\| = \sup_{\|x\|\le 1} \|F(x)\| < \infty$.

Lemma 2.1: $C_\gamma(y)$ is contained in both $[C_1(R^1)]$ and $[C_1^p(R^1)]$.

PF: We need only show $\|C_\gamma(y)\| < \infty$. If $g \in C_1(R^1)$ and $\|g\| \le 1$, then $\|[C_\gamma(y)]g\| = \left\| \dfrac{g(\cdot)}{\gamma(y,\cdot)+\gamma(y,\cdot)} \right\| = \left\| \dfrac{1}{\gamma(y,\cdot)+\gamma(y,\cdot)} \right\| < \infty$.

Thus, $\|C_\gamma(y)\| < \infty$.

$y \to C_\gamma(y)$, thus, defines a function from R^1 into a Banach space of linear operators. Now, in a Banach space, a Cauchy sequence has a limit and

hence, under appropriate conditions, a Riemann sum, like $\sum C_\alpha(y_\alpha)\Delta V_\alpha$ will have a limit in the operator space. This is to say that we can integrate certain operator-valued functions with the integral itself coming out as an operator.

More generally, let $F(y)$ be a continuous Banach space-valued function defined on R^3. We have

Theorem 2.2: If A is a measurable subset of R^3, and if $\int_A |F| dy < \infty$ then $\int_A F(y) dy$ exists, and is an element of the Banach space.

Proof: Serge Lang Analysis II.

Let $y, \eta \in R^3$, and let $K(y,\eta)$ be a continuous complex-valued function defined on $R^3 \times R^3$. Now, if for each y, $C(y)$, given by $[C(y)]f = f(y)K(y,\eta)$, is contained in $[C_1(R^3)]$ $\left([L^2(R^3)]\right)$, and as an operator-valued function, is a continuous function of y, we have

Theorem 2.3: Let A be a measurable set in R^3, such that $\int_A \|C(y)\| dy < \infty$, and such that for each fixed η, $\left|\int_A K(y,\eta) f(y) dy\right| < \infty$ when $f \in C_1(R^3)$ $\left(f \in L^2(R^3)\right)$, we have then $\left[\int_A C(y) dy\right] f = \int_A K(y,\eta) f(y) dy$, where we have equality of both sides as functions of $C_1(R^3)$ $\left(L^2(R^3)\right)$

Proof: Fix η, choose $f \in C_1(R^3)$, and let α be a sphere closed in A, such that $\int_{A-\alpha} \|C(y)\| dy < \epsilon$, and $\left|\int_{A-\alpha} K(y,\eta) f(y) dy\right| < \epsilon$

where $\mathcal{C}\mathcal{A}$ denotes the exterior of $\mathcal{A}$. Since $C(y)$ is a continuous function of y, it's uniformly continuous on $\mathcal{A}$; hence, we can partition $\mathcal{A}$ into measurable disjoint subsets $\mathcal{A}_i$ $(i = 1, \ldots, n)$, such that $x, y \in \mathcal{A}_i$ implies

$\|C(x) - C(y)\| < \dfrac{\epsilon}{\text{Vol. of } \mathcal{A}}$, and also so that

$\left| K(x,y)g(y) - K(x,y)g(x) \right| < \dfrac{\epsilon}{\text{Vol. of } \mathcal{A}}$ whenever $x, y \in \mathcal{A}_i$.

In each $\mathcal{A}_i$, choose y_i^*, and define the step maps,

$T : \mathcal{A} \longrightarrow [C_1(R^3)]$ and

$H : \mathcal{A} \longrightarrow \mathbb{C}$ (the complex numbers)

given by

$$\left.\begin{aligned} T(y) &= C(y_i^*) \\ H(y,y) &= K(y_i^*, y) g(y_i^*) \end{aligned}\right\} \quad y \in \mathcal{A}_i$$

We, thus, have for $y \in \mathcal{A}$ that both $\left| H(y,y) - g(y) K(y,y) \right| < \dfrac{\epsilon}{\text{Vol. of } \mathcal{A}}$, and $\| C(y) - T(y) \| < \dfrac{\epsilon}{\text{Vol. of } \mathcal{A}}$.

If $G \in [C_1(R^3)]$ $(G\,y)_y$ will denote Gy evaluated at y.

For convenience, let $\int_{\mathcal{A}} C(y)\, dy = C$ and $\int_{\mathcal{A}} T(y)\, dy = P$.

We have,

$$\left| (Gy)_y - \int_{\mathcal{A}} K(y,y) g(y)\, dy \right| = \left| (Gy)_y - (Py)_y \right| + \left| (Py)_y - \int_{\mathcal{A}} K(y,y) g(y)\, dy \right| \leq$$

$$\| C - T \| \, \| g \| + \left| (Py)_y - \int_{\mathcal{A}} K(y,y) g(y)\, dy \right| \leq$$

$$\|f\|\left(\left\|\int_{C\cap A} C(y)\,dy\right\| + \left\|\int_{C\cap A^c} C(y) - T(y)\,dy\right\|\right) + \left|Pf\right]_\eta - \int_A K(y,\eta) f(y)\,dy\Big| \le$$

$$2\|f\|\epsilon + L. \quad L \equiv \left|Pf\right]_\eta - \int_A K(y,\eta) f(y)\,dy\Big|.$$

Now,

$$L \le \left|Pf\right]_\eta - \int_{A^c} K(y,\eta) f(y)\,dy\Big| + \left|\int_{A^c} K(y,\eta) f(y)\,dy - \int_A K(y,\eta) f(y)\,dy\right| \le$$

$$\left|\left(\sum_{i=1}^{n} C(y_i)\,m(A_i \cap A)\right) f\right]_\eta - \int_{A^c} K(y,\eta) f(y)\,dy\Big| + \left|\int_{C\cap A} K(y,\eta) f(y)\,dy\right| \le$$

$$\left|\sum_{i=1}^{n} K(y_i,\eta) f(y_i)\,m(A_i \cap A) - \int_{A^c} K(y,\eta) f(y)\,dy\right| + \left|\int_{C\cap A} K(y,\eta) f(y)\,dy\right| \le$$

$$\left|\int_{A^c} K(y,\eta) f(y)\,dy - \int_{A^c} K(y,\eta) f(y)\,dy\right| + \left|\int_{C\cap A} K(y,\eta) f(y)\,dy\right| \le \epsilon + \epsilon.$$

Therefore, $\left|Gf\right]_\eta - \int_A K(y,\eta) f(y)\,dy\Big| \le 2\|f\|\epsilon + 2\epsilon.$

But, since ϵ is arbitrary, and η is arbitrary, we have,

$$\left[\int_A C(y)\,dy\right] f = \int_A K(y,\eta) f(y)\,dy.$$

Let $K(y,\eta)$ and $C(y)$ be the same as in the previous theorem.

We have for a measurable set A,

Theorem 2.4 If $\int_A \|C(y)\|\,dy < \infty$, then $\int_A C(y)\,dy$ is compact as a member of $\left[C_1(R^3) \mid \left([C_1^0(R^3)]\right)\right.$.

Proof: For fixed y, $C(y)$ is compact. For, let $\|f_n(y)\| \leq M$

then $C(y)f_n = K(y,y)f_n(y)$, and there exists a sequence n_j, such that

$f_{n_j}(y) \longrightarrow x$, and thus, $\|K(y,y)f_{n_j}(y) - xK(y,y)\| =$

$|f_{n_j}(y) - x| \, \|K(y,y)\| \longrightarrow 0$.

Now, with the notation the same as in the previous theorem,

we have $\| \int_A C(y)dy - \int_{S \cap A} T(y)dy \| \leq \int_{S \cap A} \|C(y) - T(y)\| dy + \int_{CS \cap A} \|C(y)\| dy \leq \epsilon + \epsilon$,

and since $\int_{S \cap A} T(y)dy = \sum_{i=1}^{n} C(y_i)\, u(\Delta_i \cap A)$

(Which is the sum of compact operators), it is compact. But, hence, $\int_A C(y)dy$

is the limit of compact operators, and hence, itself compact.

Definition 2.4: Let f be a Banach space-valued function defined on the interval $[a,b]$, and let $\tau \in [a,b]$. We say that f is pointwise Hölder with index $\mu > 0$ at τ if there exists $\bar{\epsilon} > 0$ and $A > 0$, such that for $x \in [a,b]$, $|x - \tau| \leq \bar{\epsilon}$ implies $\|f(x) - f(\tau)\| \leq A|x - \tau|^{\mu}$.

Theorem 2.5: Let $f(x)$ be a continuous complex Banach space-valued function defined on the interval $[a,b]$, $\tau \in (a,b)$, and λ either $\tau + \epsilon \in (\tau, b]$ or $\tau - \epsilon \in [a, \tau)$, then if f is Hölder at τ of index $0 < \mu \leq 1$, $\lim_{\epsilon \to 0} \int_a^b \frac{f(x)}{x - \lambda} dx$ exists. Further, if τ is an end point and if $f(\tau) = 0$, then again, the limit exists.

Proof: First we assume $\tau \in (a,b)$. Choose an interval $I \subset (a,b)$, such that $\tau \in I$ (but not an end point), and $\| f(x) - f(\tau) \| \leq A |x-\tau|^{\alpha}$ for $x \in I$. Then,

$$\int_a^b \frac{f(x)\,dx}{x-\lambda} = \int_{\bar{I}} \frac{f(x)\,dx}{x-\lambda} + \int_{\epsilon \bar{I}} \frac{f(x)}{x-\lambda}\,dx.$$

Now $\int_{\epsilon \bar{I}} \left(\frac{f(x)}{x-\lambda} - \frac{f(x)}{x-\tau} \right) dx \Big\|^{\cdot} = \int_{\epsilon I} \frac{(\lambda-\tau) f(x)\,dx}{(x-\lambda)(x-\tau)} \leq M |\lambda-\tau| \int_{\epsilon I} \| f(x) \|\,dx.$

where M is a positive constant. It follows that,

$$\lim_{\epsilon \to 0} \int_{\epsilon I} \frac{f(x)\,dx}{x-\lambda} = \int_{\epsilon \bar{I}} \frac{f(x)}{x-\tau}\,dx.$$

Looking at $\int_{\bar{I}} \frac{f(x)\,dx}{x-\lambda}$, we see that,

$$\int_{\bar{I}} \frac{f(x)\,dx}{x-\lambda} = \int_{I} \frac{f(x)-f(\tau)}{x-\lambda}\,dx + \int_{\bar{I}} \frac{f(\tau)\,dx}{x-\lambda}.$$

Now, on I $\| \frac{f(x)-f(\tau)}{x-\lambda} \| \leq \| \frac{f(x)-f(\tau)}{x-\tau} \| = \frac{A|x-\tau|^{\alpha}}{|x-\tau|} = A|x-\tau|^{\alpha-1}$

Further, $\int_I A|x-\tau|^{\alpha-1}\,dx < \infty$, $\frac{f(x)-f(\tau)}{x-\lambda}$ tends to $\frac{f(x)-f(\tau)}{x-\tau}$

almost everywhere on I. Thus, by the dominated convergence theorem,

$$\lim_{\epsilon \to 0} \int_I \frac{f(x)-f(\tau)}{x-\lambda}\,dx = \int_I \frac{f(x)-f(\tau)}{x-\tau}\,dx$$

We now need only show that $\lim_{\epsilon \to 0} \int_{\bar{I}} \frac{f(\tau)}{x-\lambda}\,dx$ exists.

Let $\bar{I} = [c,d]$. $\int_c^d \frac{dx}{x-\lambda} = \int_c^d \frac{x-\tau}{(x-\tau)^2+\epsilon^2}\,dx + i\epsilon \int_c^d \frac{dx}{(x-\tau)^2+\epsilon^2} =$

$$\frac{1}{2}\log\left[\frac{(a-\tau)^2+\epsilon^2}{(c-\tau)^2+\epsilon^2}\right] \pm \left(\operatorname{Arc\,Tan}\left(\frac{a-\tau}{\epsilon}\right) \mp \operatorname{Arc\,Tan}\left(\frac{c-\tau}{\epsilon}\right)\right).$$

This tends to $\log\left[\left|\frac{a-\tau}{c-\tau}\right|\right] \pm \pi$ as $\epsilon \to 0$.

This concludes the proof when τ is not an end point. In the end point case, choose $I \subset [a,b]$ with τ as end point of I. The analysis proceeds as in the first case, except that since $f(\tau) = c$, it is clear that $\lim_{\epsilon \to 0} f(\tau) \int_I \frac{dx}{x-\lambda}$ exists.

Definition 2.6: Let $\Omega \subset R^3$, and let $f(x)$ be a Banach space-valued function defined on Ω. We say that $f(x)$ is uniformly Hölder of index α on Ω if there exists constants A, $\alpha > 0$ independent of x in Ω, such that $x, y \in \Omega$, and $|x-y| < \delta$ implies $\|f(x)-f(y)\| \le A|x-y|^\alpha$.

Let A be an annular region in R^3, given by $0 \le a^2 \le y_1^2 + y_2^2 \le b^2 \le \infty$ where $b > a$. For τ real and $\tau \neq b^2$, let λ equal either $\tau + i\epsilon$ or $\tau - i\epsilon$. If $f(y)$ is a complex Banach space-valued function defined on A, we have

Theorem 2.7: If $\tau \neq a^2$, if $f(x)$ is uniformly Hölder on A, and if for some $\epsilon > 0$ $\int_A \left\| \frac{f(y)}{y_1^2 - \lambda^2} \right\| dy < \infty$, then $\lim_{\epsilon \to 0} \int_A \frac{f(y)\,dy}{y_1^2 - \lambda}$ exists. Further, if $\tau = a = c$, then again the limit exists.

Proof: First assume $\tau \notin [a^2, b^2]$. For all $y \in A$ $\frac{f(y)}{y^2-\lambda} \to \frac{f(y)}{y^2-\tau}$,

and further, $\int_A \left\| \frac{f(y)}{y^2-\lambda} \right\| dy \le \int_A \left\| \frac{f(y)}{y^2-\tau} \right\| dy =$

$$\int_A \frac{\|f(y)\|}{|y^2-\lambda^2|} \frac{|y^2-\lambda^2|}{|y^2-\tau|} dy = M \int_A \frac{\|f(y)\|}{|y^2-\lambda^2|} dy < \infty$$

where M is a bound on $\frac{|y^2-\lambda^2|}{|y^2-\tau|}$ in A . So, by the dominated convergence theorem, $\lim_{\epsilon \to 0} \int_A \frac{f(y)\,dy}{y^2-\lambda} = \int_A \frac{f(y)\,dy}{y^2-\tau}$

Next, assume $\tau \in [a^2, b^2]$, $\tau \neq a^2, b^2$. Break A up into two regions,

A_1 given by $a^2 \le y^2 \le \tau + \bar{c}^2 < b^2$; A_2 given by $\tau + \bar{c}^2 \le y^2 \le b^2$

By the above, we know that $\lim_{\epsilon \to 0} \int_{A_2} \frac{f(y)\,dy}{y^2-\lambda}$ exists.

Now $$\int_{A_1} \frac{f(y)\,dy}{y^2-\lambda} = \int_{a^2}^{\tau+\bar{c}^2} \frac{r^{1/2} \int_0^{2\pi} \int_0^{\pi} \frac{f(y) \sin\phi}{2} d\phi\, d\theta}{r-\lambda} dr$$

where we have set $y = r^{1/2}(\cos\theta \sin\phi, \sin\theta \sin\phi, \cos\phi)$

The Jacobian of this transformation is $\frac{r^{1/2} \sin\phi}{2}$

Thus, by Theorem 2.5, $\lim_{\epsilon \to 0} \int_{A_1} \frac{f(y)\,dy}{y^2-\lambda}$ will exist if we can show

that $r^{-1/2} G(r) \equiv r^{1/2} \int_0^{2\pi} \int_0^{\pi} \frac{f(y) \sin\phi\, d\phi\, d\theta}{2}$ is a continuous function

of r, which is pointwise Holder at $r = \tau$. Let r_1 be arbitrary in $[a^2, \tau+\sigma]$

Set $y = r^{1/2}(\cos\theta \sin\phi, \sin\theta \sin\phi, \cos\phi)$ and

$y_1 = r_1^{1/2}(\cos\theta \sin\phi, \sin\theta \sin\phi, \cos\phi)$ Then,

$$\left\| \int_0^{2\pi} \int_0^{\pi} \frac{f(y) - f(y_1)}{2} \sin\phi \, d\phi \, d\theta \right\| \leq$$

$$\int_0^{2\pi} \int_0^{\pi} \frac{\| f(y) - f(y_1) \|}{2} \, d\phi \, d\theta$$

Now there exists A^*, $\sigma > 0$, such that $|x - x_1| < \sigma$ and $x, x_1 \in A$ imply that $\| f(x) - f(x_1) \| \leq A^* |x - x_1|^{\mu}$

Choose $|r - r_1| < \sigma^2$. We have then $\sigma > |r - r_1|^{1/2} \geq |r^{1/2} - r_1^{1/2}| =$ $|y - y_1|$ independent of θ and ϕ. Thus, for $|r - r_1| < \sigma$,

$$\int_0^{2\pi} \int_0^{\pi} \frac{\| f(y) - f(y_1) \|}{2} \, d\phi \, d\theta \leq \int_0^{2\pi} \int_0^{\pi} \frac{A^* |r^{1/2} - r_1^{1/2}|^{\mu}}{2} \, d\phi \, d\theta =$$

$$\pi^2 A^* |r^{1/2} - r_1^{1/2}|^{\mu} \leq \pi^2 A^* |r - r_1|^{\mu/2}$$

This proves that $G(r)$ is continuous on $[a^2, \tau+\sigma]$ and pointwise Holder at τ. The inequality $|r^{1/2} - r_1^{1/2}| \leq |r - r_1|^{1/2}$ shows that $r^{1/2}$ is pointwise Holder at r_1 in $[a^2, \tau+\sigma]$. It is easy to show that if $g(r)$ is complex-valued and $f(r)$ is Banach space-valued, and if both are pointwise Holder

at r_1, then $g(r)\phi(r)$ is also pointwise Holder. It follows then that $r^{1/2}Q(r)$ is a continuous function of r which is pointwise Holder at $r = \tau$.

Finally, if $a^2 = \tau = 0$, we proceed as in the preceding case; the last step being to show $\int_\epsilon^\sigma \frac{r^{1/2}Q(r)\,dr}{r-\lambda}$ attains a limit as $\epsilon \to c$.

This limit exists by Theorem 2.5, because $r^{1/2}Q(r)$ evaluated at zero is zero.

This concludes the proof.

Let $K(y,\eta)$ be defined on $R^3 \times R^3$. Assume $O(y) \in C_1(R^3)$ $\left(C_1^a(R^3)\right)$, where $\left[\overline{O(y)}\right]_y = g(y)K(y,\eta)$ We have

Theorem 2.8 If $K(y,\eta)$ and all its first and second partial derivatives are uniformly bounded and continuous on $R^3 \times R^3$, then $O(y)$ is a uniformly Holder function from R^3 into $\left[\overline{C_1(R^3)}\right]$ $\left(\left[\overline{C_1^a(R^3)}\right]\right)$.

Lemma 2.9: Let $U(y)$ be a complex-valued function defined on R^3. Assume the partial derivatives exist and satisfy $|U_{y_i}| \le M$ $i = 1,2,3$ uniformly throughout R^3, then $|U(y) - U(x)| \le 6M|x-y|$

Proof:

$|U(y) - U(x)| \equiv |U(y_1,y_2,y_3) - U(x_1,x_2,x_3)| \le |U(y_1,y_2,y_3) - U(y_1,y_2,x_3)| +$
$|U(y_1,y_2,x_3) - U(y_1,x_2,x_3)| + |U(y_1,x_2,x_3) - U(x_1,x_2,x_3)|$. Now if $U = h + ig$ then $|U(y_1,y_2,y_3) - U(y_1,y_2,x_3)| \le |h(y_1,y_2,y_3) - h(y_1,y_2,x_3)| +$

$$| g(y_1, y_2, y_3) - g(y_1, y_2, x_3) | \leq 2M | x_3 - y_3 | \leq 2M | x - y |$$

This completes the proof, since the other two terms in above inequality are also less than $2M|x-y|$

Proof of Theorem 2.8: $\| (C(y) - C(x)) g \| = \| g(y) K(y,\eta) - g(x) K(x,\eta) \| \leq$

$$\| g(y) K(y,\eta) - g(y) K(x,\eta) \| + \| g(y) K(x,\eta) - g(x) K(x,\eta) \| =$$

$$| g(y) | \, \| K(y,\eta) - K(x,\eta) \| + | g(y) - g(x) | \, \| K(x,\eta) \| \leq$$

$$| g(y) | \, \| K(y,\eta) - K(x,\eta) \| + M | g(y) - g(x) | \leq$$

$$\| g \| \, \| K(y,\eta) - K(x,\eta) \| + 6M \| g \| \, | x - y |$$

where M is a bound on K and its first and second partials. Now

$| K(y,\eta) - K(x,\eta) | \leq 6M | x - y |$ and

$| K_{\eta_i}(y,\eta) - K_{\eta_i}(x,\eta) | \leq 6M | x - y |$. Thus,

$\| K(y,\eta) - K(x,\eta) \| \leq 6M | x - y |$.

Hence $\| C(y) - C(x) \| = \sup_{\|g\| \leq 1} \| (C(y) - C(x)) g \| \leq$

$12M | x - y |$

This completes the proof.

We now show that K in (1.3) is compact in both $[C_1(R^3)]$ and $[C_1^0(R^3)]$. In what follows $[C_1(R^3)]$ can simply be replaced by $[C_1^0(R^3)]$.

In Lemma 2.1, we saw that $C_r(y) \in [C_1(R^3)]$. Taking

$K(y,\eta) = \frac{1}{\delta(y,\eta)\psi(y,\sigma)}$ Theorem (2.8) implies that $O_\sigma(y)$ is uniformly Holder, and hence, a continuous function of y. Below, we shall show that $\int \| O_\sigma(y) \| dy < \infty$. Thus, from Theorem (2.3), we see that $K_\sigma = \int O_\sigma(y)\, dy$.

Theorem (2.4) then shows us that K_σ is compact.

Let $O(y)g = \frac{g(y)}{\delta(y,\eta)}$.

Theorem (2.8) shows that $O(y)$ is uniformly Holder. Setting $\lambda = \frac{1}{3}\rho^2 + \frac{1}{3}\tau$ and $\tau = \frac{1}{3}\rho^2 + \frac{1}{3}\delta$ we have $K_\sigma = \int O_\sigma(y)dy = \int \frac{O(y)dy}{\psi(y,\sigma)} = \frac{1}{3}\int \frac{O(y)dy}{y^2 - \frac{1}{3}(\rho^2+\tau)} = \frac{1}{3}\int \frac{O(y)dy}{y^2 - \lambda}$.

In Theorem (2.7) take $A = R^3$. It then follows that $\lim_{\epsilon \to 0} K_\sigma$ exists.

Thus, K is the limit of compact operators, and hence, is itself compact.

It remains only then to show that $\int \| O_\sigma(y) \| dy < \infty$.

Now $\| O_\sigma(y) g \| = \left\| \frac{g(y)}{(y^2 + y\cdot\eta + \eta^2 - \delta)(-\rho^2 + \frac{3}{4}y^2 - \sigma)} \right\| \leq$

$$\frac{\| g(y) \|}{|-\rho^2 + \frac{3}{4}y^2 - \sigma|} \left\| \frac{1}{y^2 + y\cdot\eta + \eta^2 - \delta} \right\|$$

From Appendix I we see that for some $M, a > 0$

$$\left| \frac{1}{y^2 + y\cdot\eta + \eta^2 - \delta} \right| \leq \frac{1}{M(y^2 + \eta^2 + a)} \leq \frac{1}{M(y^2 + a)}.$$

Further, $\left| \frac{\partial}{\partial \eta_i} \left(\frac{1}{\xi^2 + \xi \cdot \eta + \eta^2 - s} \right) \right| = \frac{|2\eta_i + \xi_i|}{|\xi^2 + \xi \cdot \eta + \eta^2 - s|^2} \leq$

$\frac{|2\eta_i + \xi_i|}{M^2(\xi^2 + \eta^2 + a)^2} \leq \frac{K}{M^2(\xi^2 + \eta^2 + a)} \leq \frac{K}{M^2(\xi^2 + a)}$

where K is a bound on $\frac{|2\eta_i + \xi_i|}{(\xi^2 + \eta^2 + a)}$

Thus, there exists positive constants c, d such that

$\|C_s(\xi)f\| \leq \frac{\|f\| C}{(\xi^2+d)|-s^2+\frac{3}{4}\xi^2-s|}$ Hence, $\|C_s(\xi)\| = \sup_{\|f\|=1} \|C_s(\xi)f\| \leq$

$\frac{C}{(\xi^2+d)|-s^2+\frac{3}{4}\xi^2-s|} \leq \frac{cc_1}{(\xi^2+d)(\xi^2+d_1)}, \quad d_1, c_1 > 0.$

Therefore, $\int \|C_s(\xi)\| d\xi < \infty.$

3. We now write (1.2) in the form,

$$f(\eta) - \frac{1}{\pi^n} \int \frac{\hat{\tau}(\eta) f(\xi) d\xi}{s(\xi,\eta) + (\xi,\eta)} = \frac{\hat{\tau}(\eta)}{s(\xi,\eta)}$$

Let τ be either $s + ic$ or $s - ic$, $s < c$, and define $H_\tau f =$

$$\int \frac{\hat{\tau}(\eta) f(\xi) d\xi}{s(\xi,\eta) + (\xi,\eta)}$$

Theorem 3.1: H_τ is contained in both $[C_1(R^1)]$ and $[C_1(R^1)]$

Proof: We know that $K_\tau f$ is continuous with continuous partials; hence, the same is true for $H_\tau f = \hat{\tau}(\eta) K_\tau f$. Further, there exists positive constants a, b, M, M_1, c, d, such that $|(H_\tau f)(\eta)| \leq (a|\eta| + b)\|f\| \int \frac{d\xi}{M(\xi^2+\eta^2+c)M_1(\xi^2+d)} =$

$(a|\eta| + b)\|f\| \int_{-\infty}^{\infty} \int_{-\infty}^{\infty} \int_{-\infty}^{\infty} \frac{r^2 \sin\phi \, d\phi \, d\theta \, dr}{MM_1(r^2+\eta^2+c)(r^2+d)} \leq \frac{4\pi\|f\|}{MM_1}(a|\eta| + b) \int_{-\infty}^{\infty} \frac{dr}{r^2+\eta^2+c} =$

$$\frac{4\pi \|f\|}{M_1 M_2} \frac{(a|\eta|+b)\,\pi/2}{\sqrt{\xi^2+c}} \leq \|f\| \angle \qquad (3.1)$$

where $\angle$ is some positive constant.

Also, $\left| \frac{\partial}{\partial \xi_j} (H_\sigma f)(\eta) \right| = \frac{\partial}{\partial \xi_j} \int \frac{f(x)\, e^{-2\pi i x\cdot\eta}}{\sigma(x,\eta)\,\psi(x,\eta)} +$

$$\sigma(\eta) \int \frac{\partial}{\partial \xi_j} \left(\frac{f(x)}{(x^2+\xi_1^2+\xi_2^2+\xi_3^2)\,\psi(x,\eta)} \right) = \frac{\partial}{\partial \xi_j} (H_\sigma f)(\eta) + (1+|\eta|) \int \frac{-(x_j+\xi_j) f(x)\, e^{-2\pi i x\cdot\eta}}{\sigma(x,\eta)\,\psi^2(x,\eta)\,[(x+\xi_1)^2+\xi_2^2+\xi_3^2]}$$

The differentiation under the integral sign could be justified, but for the sake of brevity, we omit the details.

Let b_1 be a bound on $\left| \frac{\partial \psi}{\partial \xi_j} \right|$. The first term in the sum is equal to $\frac{\partial}{\partial \xi_j} \frac{\hat{\sigma}(\eta)(H_\sigma f)(\eta)}{\hat{\sigma}(\eta)} = \frac{\partial}{\partial \xi_j} \cdot \frac{1}{\hat{\sigma}(\eta)} \cdot (H_\sigma f)(\eta)$, and by (3.1), it is bounded by

$$\frac{b_1 \|f\| \angle}{|\hat{\sigma}(\eta)|} \qquad (3.2)$$

The second term is bounded by $\frac{\|f\|(a|\eta|+b)}{M_1^2} \int \frac{(2|\eta|+|\xi|)\, e^{-2\pi i x\cdot\eta}}{(x^2+\xi_1^2+\xi_2^2+\xi_3^2)^2 (x^2+c)} \leq$

$$\frac{\|f\|(a|\eta|+b)}{M_1^2} \int \frac{2|\eta|+|\xi|}{(x^2+\xi_1^2+\xi_2^2+\xi_3^2)^{1/2}} \cdot \frac{2}{(x^2+c)^{1/2}} \cdot \frac{1}{(x^2+\xi_1^2+\xi_2^2+\xi_3^2)} \cdot \frac{1}{(x^2+c)}\, dx \leq$$

$$\frac{\|f\|(a|\eta|+b)\, M_2}{M_1^2 (x^2+c)^{1/2}} \int \frac{dx}{(x^2+\xi_1^2+\xi_2^2+\xi_3^2)(x^2+c)} \qquad (3.3)$$

where M_2 is a bound on $\frac{2|\eta|+|\xi|}{(x^2+\xi_1^2+\xi_2^2+\xi_3^2)^{1/2}}$.

(3.3) is bound by $\dfrac{\|g\|\left(a|\eta|+b\right)M_2}{M M_1^{-}(\eta^2+c)^{1/2}} \cdot \dfrac{2\pi^2}{\sqrt{\eta^2+c}}$ (3.4)

(3.4) and (3.2) imply that there exists a positive constant M^*, such that $\left|\dfrac{\partial}{\partial \eta_i}(H_\sigma g)(\eta)\right| \le \dfrac{M^*\|g\|}{\sqrt{\eta^2+c}} \le \dfrac{M^*\|g\|}{c}$ (3.5)

(3.1) and (3.5) imply that $H_\sigma \in [C_1(R^2)]$. (3.5) also shows that when $g \in C_c^\infty(R^2)$, $\dfrac{\partial}{\partial \eta_i}(H_\sigma g)(\eta)$ vanishes at ∞. So, to show that $H_\sigma \in [C_1(R^2)]$ it remains to show that when g vanishes at ∞, $H_\sigma g$ vanishes at ∞.

For $g \in C_c^\infty(R^2)$ write $(H_\sigma g)(\eta) = \int_{S_\epsilon} \dfrac{\tau(\eta)\, g(y)\, dy}{\tau(y,\eta)\,\psi(y,\tau)}$

$+ \int_{(S_\epsilon)^c} \dfrac{\tau(\eta)\, g(y)\, dy}{\tau(y,\eta)\,\psi(y,\tau)}$ where S_ϵ is a sphere, centered at the origin, in whose complement $|g(y)| < \epsilon$. As before, we have positive constants, such that

$\left|\dfrac{\tau(\eta)\, g(y)}{\tau(y,\eta)\,\psi(y,\tau)}\right| \le \dfrac{\|g\|(a|\eta|+b)}{M_1(y^2+\eta^2+c)^{M_1}(y^2+d)} \le$

$\dfrac{\|g\|(a|\eta|+b)}{M M_1 d(\eta^2+c)}$. Thus, $|I_\epsilon(\eta)| \le \left|\int_{S_\epsilon} \dfrac{\tau(\eta)\, g(y)\, dy}{\tau(y,\eta)\,\psi(y,\tau)}\right| \le$

$\dfrac{\|g\|}{M M_1 d} \dfrac{a|\eta|+b}{\eta^2+c}$ ... over S_ϵ

Also $\left|\int_{(S_\epsilon)^c} \dfrac{\tau(\eta)\, g(y)\, dy}{\tau(y,\eta)\,\psi(y,\tau)}\right| \le \int \dfrac{|\tau(\eta)|\, dy}{|\tau(y,\eta)|\,|\psi(y,\tau)|} \le \epsilon L$ ... (3.1).

As a consequence, $\left|(H_\sigma g)(\eta)\right| \leq \left|I_\epsilon(\eta)\right| + \epsilon L$. So that given $\bar{\sigma} > 0$, pick ϵ such that $\epsilon L < \bar{\sigma}/2$, and then choose γ so that $|\eta| > \gamma$ implies $|I_\epsilon(\eta)| < \bar{\sigma}/2$. It follows that for $|\eta| > \gamma$

$$\left|(H_\sigma g)(\eta)\right| \leq \bar{\sigma}.$$

This concludes the proof.

To show that $\lim_{\epsilon \to 0} H_\sigma$ exists, we first write $H_\sigma = H_{\sigma 1} + H_{\sigma 2}$, where $H_{\sigma 1} g = \int_{S^*} \frac{\hat{\tau}(\eta)\, g(y)\, dy}{S(y,\eta)\, \psi(y,\tau)}$, and S^* is a closed sphere centered at the origin, which contains all zeros (if any) of $\psi(y,S)$ as interior points. We now show that $H_1 \equiv \lim_{\epsilon \to 0} H_{\sigma 1}$ exists and is compact in both $[C_1(R^3)]$ and $[C_1^c(R^3)]$. In the following argument $[C_1(R^3)]$ can be replaced by $[C_1^c(R^3)]$.

Let $C_\tau(y)\, g = \frac{\hat{\tau}(\eta)\, g(y)}{S(y,\eta)\, \psi(y,\tau)}$.

It is easy to see that $C_\tau(y) \in [C_1(R^3)]$. Theorem 2.8 can be applied to show that $C_\tau(y)$ is a continuous function of y, and hence, since S^* is bounded, $\int_{S^*} \|C_\tau(y)\|\, dy < \infty$. Now theorem (2.3) can be applied to give $H_{\sigma 1} = \int_{S^*} C_\tau(y)\, dy$, while Theorem (2.4) shows that $H_{\sigma 1}$ is compact.

Let $C(y)g = \frac{\Upsilon(\eta)\, g(y)}{S(y,\eta)}$. Theorem (2.8) shows that $C(\cdot)$ is uniformly Holder on Λ^3. Setting $\lambda = \frac{4}{3}\sigma^2 + \frac{4}{3}\Upsilon$ and $\tau = \frac{4}{3}\sigma^2 + \frac{4}{3}S$ we have $H_{\Upsilon 1} = \int_{S^*} C_\Upsilon(y)\,dy = \int_{S^*} \frac{C(y)\,dy}{\Phi(y,\Upsilon)} = \frac{4}{3}\int_{S^*} \frac{C(y)\,dy}{y^2 - \frac{4}{3}(\sigma^2+\Upsilon)} = \frac{4}{3}\int_{S^*} \frac{C(y)\,dy}{y^2-\lambda}$

In Theorem (2.7), take $A = S^*$. It follows that $\lim_{\epsilon \to 0} H_{\Upsilon 1} = H_1$ exists, and is compact.

Define $H_2 g = \int_{\epsilon S^*} \frac{\Upsilon(\eta)\, g(y)\, dy}{S(y,\eta)\,\Phi(y,S)}$.

$$\left| (H_{\tau 2} g)(\eta) - (H_2 g)(\eta) \right| = \left| \int_{\epsilon S^*} \frac{\Upsilon(\eta)(\tau - S)\, g(y)\, dy}{S(y,\eta)\,\Phi(y,S)\,\Phi(y,\tau)} \right| \leq$$

$$|\tau - S| \int_{\epsilon S^*} \frac{|\Upsilon(\eta)|\, \|g\|\, dy}{M_1(y^2 + \eta^2 + c) M_1(y^2 + d_1) M_2(y^2 + d_2)} \leq$$

(where $M_1, M_2, c, d_1, d_2, M_2$ are positive constants).

$$\frac{|\tau - S|\, \|g\| (a|\eta| + b)}{M M_1 M_2} \int_{\epsilon S^*} \frac{dy}{(y^2 + \eta^2 + c)(y^2 + d_1)(y^2 + d_2)} \leq$$

(Note that M_1 and d_2 may be chosen independent of τ near S.)

$$\frac{|\tau - S|\, \|g\| (a|\eta| + b)\, 4\pi}{M M_1 M_2 d_2} \int_0^\infty \frac{dr}{r^2 + \eta^2 + c} \leq$$

$L \|g\| |\tau - S|$, where L is some positive constant. (3.6)

Also, $\left| \frac{\partial}{\partial \eta_i} (H_{\tau 2} g)(\eta) - \frac{\partial}{\partial \eta_i} (H_2 g)(\eta) \right| = \left| \frac{\partial}{\partial \eta_i} \int_{\epsilon S^*} \frac{\Upsilon(\eta)(\tau - S)\, g(y)\, dy}{S(y,\eta)\,\Phi(y,S)\,\Phi(y,\tau)} \right| \leq$

$$\left| \frac{\partial \hat{\tau}}{\partial \eta_i} \int_{\mathcal{S}^2} \frac{(\tau - s)\, g(y)\, dy}{f_p(y) f(s)} \right| + \left| \hat{\tau}(\eta) \frac{\partial}{\partial \eta_i} \int_{\mathcal{S}^2} \frac{(\tau - s)\, g(y)\, dy}{f_p(y)\, s(y,\eta)\, \psi(y,s)\, \psi(y,\tau)} \right|$$

If L_1 is a bound on $\left| \frac{\partial \hat{\tau}}{\partial \eta_i} \right|$, (3.6) implies that the first term is

bounded by $\frac{b_1 L \|g\| |\tau - s|}{|\hat{\tau}(\eta)|} \leq L_1 \|g\| |\tau - s|$ (3.7)

where L_1 is positive.

The second term is equal to $\left| \hat{\tau}(\eta) \int_{\mathcal{S}^2} \frac{(-2\eta_i - y_i)(\tau - s)\, g(y)\, dy}{f_p(y) \left(s(y,\eta)\right)^2 \psi(y,s)\, \psi(y,\tau)} \right| \leq$

$$(a|\eta| + b)|\tau - s| \|g\| \int_{\mathcal{S}^2} \frac{|2\eta_i| + |y_i|\ dy}{M^2 (y^2 + \eta^2 + c)^2 M_1 (y^2 + d_1) M_2 (y^2 + d_2)} \leq$$

$$\frac{(a|\eta| + b)|\tau - s| \|g\| M_3}{M^2 M_1 M_2 d_2} \int \frac{dy}{(y^2 + \eta^2 + c)(y^2 + d_1)} \qquad (3.8)$$

where M_3 is bound on $\frac{2|\eta_i| + |y_i|}{(y^2 + \eta^2 + c)}$.

But (3.8) is bounded by $\|g\| |\tau - s| L_2$, where L_2 is a positive constant. This result together with (3.7) implies that there exists an

$L^* > c$, such that $\left| \frac{\partial}{\partial \eta_i} \left(H_{\sigma_2} g \right)(\eta) - \frac{\partial}{\partial \eta_i} \left(H_2 g \right)(\eta) \right| \leq \|g\| L^* |\sigma - s|$ (3.9)

Since H_τ, H_{σ_1} are both in $\left[C_1(R^3)\right]$ and $\left[C_1^\circ(R^3)\right]$, the same is true for H_{σ_2}. Now, if we choose a countable sequence $\sigma_n \to s$, we have, from (3.6) and (3.9), for all g in $C_1(R^3)$ $\left(C_1^\circ(R^3)\right)$ that $H_{\sigma_n} g$ converges to $H_2 g$. It follows from a corollary to the uniform boundedness principle

(Lang Analysis II) that H_2 is contained in both $[C_1^0(R^3)]$ and $[C_1(R^3)]$, and since $\| H_2 - H_{\sigma 2} \| = \sup_{\|g\| \le 1} \| (H_2 - H_{\sigma 2}) g \| \le L^{**} |\sigma - s|$, $L^{**} > 0$, we have $\lim_{\epsilon \to 0} H_{\sigma 2} = H_2$.

Thus, $\lim_{\epsilon \to 0} H_\sigma = H_1 + H_2 = H$ is contained in both $[C_1(R^3)]$ and $[C_1^0(R^3)]$, and further, H_1 is compact in both operator spaces.

In both $[C_1(R^3)]$ and $[C_1^0(R^3)]$ we have

Theorem 3.2. H is not compact.

Proof: Let $g_n(y) = e^{-y^2/n}$ It is easily seen that there exists a constant $L > 0$, such that $\|g_n\| \le L$. Now, for fixed η, we claim $\lim_{n \to \infty} (H_2 g_n)(\eta) = (H_2 g^*)(\eta)$, where we take $g^*(\eta) = 1$. For, in $\mathcal{S}^*$,

$$\left| \frac{\hat{\tau}(\eta) g_n(y)}{S(y,\eta) \psi(y,s)} \right| \le \frac{\hat{\tau}(\eta) L}{M(y^2+\eta^2+c) M_1 (y^2+d)} \le \frac{\hat{\tau}(\eta) L}{M M_1 (y^2+c)(y^2+d)}$$, which

(M, M_1, C, d are appropriate positive constants.)

is an integrable function of y over $\mathcal{S}^*$, and

$$\lim_{n \to \infty} \frac{\hat{\tau}(\eta) g_n(y)}{S(y,\eta) \psi(y,s)} = \frac{\hat{\tau}(\eta) g^*(y)}{S(y,\eta) \psi(y,s)} \quad \text{for all } y \in \mathcal{S}^*.$$

It follows from the dominated convergence theorem that

$$\lim_{n \to \infty} (H_2 g_n)(\eta) = (H_2 g^*)(\eta).$$

Examining $H_2 g^*$, we find, for all η $|(H_2 g^*)(\eta)| =$

$$\int_{CS^*} \frac{\Upsilon(\eta)\,dy}{\Gamma(y,\eta)\,\Psi(y,\eta)} \geq \Upsilon(\eta) \int_{CS^*} \frac{dy}{M_2(y^2+\eta^2+c_2)M_3(y^2+d_2)}$$

(for appropriate $M_2, c_2, M_3, d_2 > c$) $= \dfrac{\Upsilon(\eta)}{M_2 M_3} \displaystyle\int_{CS^*} \frac{dy}{(y^2+\eta^2+c_2)(y^2+d_2)}$

$$= \frac{\Upsilon(\eta)}{M_2 M_3} \int_{\rho}^{\infty}\int_{c}^{2\pi}\int_{c}^{\pi} \frac{r^2 \sin\phi\, d\phi\, d\theta\, dr}{(r^2+\eta^2+c_2)(r^2+d_2)}$$ where ρ is the radius

of S^n. This last term is equal to $\dfrac{\Upsilon(\eta)}{M_2 M_3} 4\pi \displaystyle\int_{\rho}^{\infty} \frac{r^2\,dr}{(r^2+\eta^2+c_2)(r^2+d_2)} \geq$

$$\frac{4\pi}{M_2 M_3}\Upsilon(\eta) \int_{\rho}^{\infty} \frac{r^2\,dr}{(r^2+\eta^2+c_2)\,r^2(\alpha+1)}$$

(where on $[\rho, \infty)$ $\alpha r^2 \geq \alpha\rho > d_2$)

$$= \frac{4\pi\Upsilon(\eta)}{M_2 M_3(\alpha+1)} \int_{\rho}^{\infty} \frac{dr}{(r^2+\eta^2+c_2)} = \frac{4\pi\Upsilon(\eta)}{M_2 M_3(\alpha+1)} \left[\frac{\operatorname{Arc\,tan} \frac{r}{\sqrt{\eta^2+c_2}}}{\sqrt{\eta^2+c_2}} \right]_{\rho}^{\infty}$$

$$= \frac{K\,\Upsilon(\eta)}{\sqrt{\eta^2+c_2}} \left(\pi/2 - \operatorname{Arc\,tan} \frac{\rho}{\sqrt{\eta^2+c_2}} \right), \quad K > c.$$

Now, $\lim_{|\eta| \to \infty} \dfrac{\Upsilon(\eta)}{\sqrt{\eta^2+c_2}} = \lim_{|\eta| \to \infty} \dfrac{\rho + \sqrt{\frac{3}{4}\eta^2 - 5}}{\sqrt{\eta^2+c_2}} = \sqrt{3/4}$

Therefore, for large $|\eta|$

$$|(H_1 g^*)(\eta)| \geq \left(K\sqrt{3/4}\right) \pi/4 > c.$$

We will have shown that H_2, and hence H, is not compact if we show no subsequence $\{H_2 g_{n_k}\}$ converges. So, assume $H_2 g_{n_k}$ converges.

to say f . i.e. $\| H_2 g_{n_\kappa} - f \| \to 0$. Now, since $H_2 g_{n_\kappa} \in C_1^\circ(R^3)$, f must also be in $C_1^\circ(R^3)$. But, for each η we must have $f(\eta) = \lim_{\kappa \to \infty} (H_2 g_{n_\kappa})(\eta) = (H_2 g^*)(\eta)$. This implies that for large η $|f(\eta)| = |(H_2 g^*)(\eta)| \geq K\left(\frac{\sqrt{3}}{2}\right) \frac{\pi}{4}$, which contradicts the fact that $f \in C_1^\circ(R^3)$. Thus, $H_2 g_{n_\kappa}$ does not converge. This concludes for proof.

In both $\left[C_1(R^3)\right]$ and $\left[C_1^\circ(R^3)\right]$, we have

Theorem 3.3. If $n \geq 1$ H^n is not compact.

Proof: We use the fact that if A is a compact operator, then for any bounded operator K , AK and KA are also compact. It follows that $H^n = (H_1 + H_2)^n$ will not be compact if and only if H_2^n is not compact.

Let j be a positive integer. We first show that for fixed η $\lim_{n \to \infty} (H_2^j g_n)(\eta) = (H_2^j g^*)(\eta)$, where $g^*(\eta) \equiv 1$. In the proof of Theorem 3.2 we have this for $j = 1$. So, assuming it holds for $j-1$, we show it holds for j .

Let $f_{nj}(\eta) = (H_2^j g_n)(\eta)$ and $f_j(\eta) = (H_2^j g^*)(\eta)$.

Then $(H_2^j g_n)(\eta) = (H_2 f_{n,j-1})(\eta) = \int_{G S^4} \frac{\tau(\eta) f_{n,j-1}(y)\, dy}{s(y,\eta)\, \psi(y,s)}$.

Now $\|f_{n,j-1}\| = \|H_2^{j-1} g_n\| \le \|H_2^{j-1}\| \|g_n\| \le L_j$,

where L_j is a positive constant. Thus, for $g \in \mathcal{S}^*$ and some M, M_1, $c, d > 0$ we have $\left| \frac{\hat{\tau}(\eta) f_{n,j-1}(y)}{\tau(y,\eta)\psi(y,s)} \right| = \frac{\hat{\tau}(\eta) L_n}{M(y^2+c) M_1(y^2+d)}$ which is integrable over $\mathcal{S}^*$.

Further, for each $g \in \mathcal{S}^*$ $\lim_{n\to\infty} \frac{\hat{\tau}(\eta) f_{n,j-1}(y)}{\tau(y,\eta)\psi(y,s)} = \frac{\hat{\tau}(\eta) f_{j-1}(y)}{\tau(y,\eta)\psi(y,s)}$

Thus, by the dominated convergence theorem, for fixed η

$$\lim_{n\to\infty} (H_2^j g_n)(\eta) = \lim_{n\to\infty} (H_2 f_{n,j-1})(\eta) = (H_2 f_{j-1})(\eta) = (H_2^j g^*)(\eta).$$

Secondly, we show that $H_2^j g^* \notin C_1^\infty(R^3)$ $j = 1, 2, \ldots$. We have, in Theorem 3.2, proved this when $j = 1$.

Now, since $\frac{g^*(y)\hat{\tau}(\eta)}{\tau(y,\eta)\psi(y,s)} > c$ in $\mathcal{S}^*$, we must have $(H_2 g^*)(\eta) > c$ and similarly, it follows that $(H_2^j g^*)(\eta) > c$ $j = 1, 2, 3, \ldots$ We know from the proof of theorem 3.2, that $H_2 g^*$ is bounded away from 0 at ∞.

So assume that $H_2^{j-1} g^*$ is bounded away from 0 at ∞. It must then be bounded away from zero throughout R^3; that is, there must exist $\alpha_{j-1} > 0$ such that $(H_2^{j-1} g^*)(\eta) > \alpha_{j-1}$. Thus $(H_2^j g^*)(\eta) = (H_2 f_{j-1})(\eta) \ge (H_2 \alpha_{j-1})(\eta) = \alpha_{j-1}(H_2 g^*)(\eta) \ge \alpha_{j-1}\alpha_1 > 0$. Therefore,

$$H_2^j g^* \notin C_1^\infty(R^3)$$

Now, if $\|H_2^j g_{n_k} - f\| \to 0$, then f would have to be $H_2^j g^*$, and

at the same time $f \in C_1^\infty(R^3)$. Since this is impossible, H_2^1 is not compact.

This concludes the proof.

Project Number: 5621

Problem Number: 1529

Researcher: Dr. J. Jasperse

Appendix I

Lemma: Let $A, B \in R^3$ and S be real or complex; then if either $Re\, S < C$ or $Im\, S \neq C$, there exists $a, M_1, M_2 > C$, such that

$$M_1 (A^2 + B^2 + a) \leq | A^2 + A \cdot B + B^2 - S | \leq M_2 (A^2 + B^2 + a)$$

Proof: $A^2 + A \cdot B + B^2 \geq A^2 + B^2 - 2|A||B| = (|A| - |B|)^2 \geq$

C with equality possible

only if $|A| = |B|$. Now, if $|A| = |B|$ then $A^2 + A \cdot B + B^2 = |A|^2 (2 + \cos\theta)$

, where θ is angle between A and B.

On $R^3 \times R^3$ let $F(A,B) = A^2 + A \cdot B + B^2$. Let U be the surface of the unit sphere in Euclidean $R^3 \times R^3$. Then if $(A,B) \in U$, and $|A| = |B|$, we have $|A|^2 = 1/2$, and hence, $|A|^2 (2 + \cos\theta) \neq C$. It follows that for $(A,B) \in U$, $F(A,B) > C$.

Thus, since U is compact, there exists $m, M > C$, such that for $(A,B) \in U$ $m \leq F(A,B) \leq M$. Further, for arbitrary (A,B), we have $(A,B) = (\lambda A_1, \lambda B_1)$ where $A_1^2 + B_1^2 = 1$ and $\lambda^2 = A^2 + B^2$. Now, $F(A,B) = \lambda^2 F(A_1, B_1)$. Hence, $\lambda^2 m = F(A,B) \leq \lambda^2 M$ or $m(A^2 + B^2) \leq F(A,B) \leq M(A^2 + B^2)$

For $(A,B) \neq C$, we have $m \leq \dfrac{F(A,B)}{A^2 + B^2} \leq M$. Now, choose $a > C$, and let $|(A,B)| = \sqrt{A^2 + B^2}$

For $|(A,B)|^2 \geq L$, we have $\frac{|F(A,B)-S|}{A^2+B^2+a} \leq \frac{F(A,B)}{A^2+B^2} + \frac{|S|}{A^2+B^2} \leq$

$M + \frac{|S|}{L}$, and if L is large enough we have $\frac{F(A,B)}{A^2+B^2+a} - \frac{|S|}{A^2+B^2+a} \leq$

$\frac{|F(A,B)-S|}{A^2+B^2+a}$ and $\frac{|F(A,B)-S|}{A^2+B^2+a} \geq \frac{F(A,B)}{2(A^2+B^2)} - \frac{|S|}{2(A^2+B^2)} \geq$

$\frac{m}{2} - \frac{|S|}{2L}$.

Now choose L so that $M + \frac{|S|}{L} \leq 2M$ and $\frac{m}{2} - \frac{|S|}{2L} \geq \frac{m}{4}$

We thus have for $|(A,B)|^2 \geq L$, $\frac{m}{4} \leq \frac{|F(A,B)-S|}{A^2+B^2+a} \leq 2M$.

For $|(A,B)|^2 \leq L$, $\tilde{m} \leq \frac{|F(A,B)-S|}{A^2+B^2+a} \leq \tilde{M}$

for some $\tilde{M}, \tilde{m} > 0$. Let $M_2 = \max[2M, \tilde{M}]$

$M_1 = \min[\tilde{m}, m/4]$

We have, thus, for all (A,B)

$$M_1(A^2+B^2+a) \leq |F(A,B)-S| \leq M_2(A^2+B^2+a)$$

SECTION 14

REFERENCES

1. Lund, Iver A. and Marvin P. Meyer, Rainfall, Soil Moisture and Trafficability in the Vicinity of Saigon, Air Force Surveys in Geophysics, No. 219, May 1970.

2. L. Eyges, Phys. Rev. 115, 1643 (1959)

3. J. R. Jasperse and M. H. Friedman, Phys. Rev. 159, 69 (1967)

4. J. R. Jasperse, J. Marsh, Phys. 9, 1931 (1968)

5. L. D. Faddeev, J.E.T.P. 12, 1014 (1961)

6. C. Lovelace, Phys. Rev. 135, B1225 (1964)

7. R. Aaron, R. D. Amado, and Y. Y. Tam, Phys. Rev. 140, B1291 (1965)

8. S. Lang, Analysis II, Addison-Wesley, 1969

9. Kantorovich and Akilov, Functional Analysis in Normed Spaces, Macmillan, 1964

SECTION 13

CONTRIBUTORS

The writers express their thanks to Miss Eunice C. Cronin, Analysis and Simulation Branch (SUYA), AFCRL Computation Center, Air Force Cambridge Research Laboratories, and to Mr. Vincent J. Mazzio, Contract Monitor, whose technical guidance and experience were invaluable in the preparation of this report.

In addition, the authors would like to thank the following AFCRL research personnel who provided valuable information for preparation of this report.

Mr. J. Buchau
Mr. J. Conover
Mr. I. Gringorten
Dr. J. Jasperse
Mr. I. Lund
Mr. R. Papa
Dr. C. Rush
Mr. F. Volz
Capt. A. Slobodnik, Jr.

Unclassified
Security Classification

DOCUMENT CONTROL DATA - R&D

(Security classification of title, body of abstract and indexing annotation must be entered when the overall report is classified)

1. ORIGINATING ACTIVITY (Corporate author)	2a. REPORT SECURITY CLASSIFICATION
Analysis & Computer Systems, Inc. Building 6 Second Avenue, Northwest Park Burlington, Massachusetts 01803	Unclassified 2b. GROUP

3. REPORT TITLE

MATHEMATICAL ANALYSIS AND COMPUTER ORIENTED ENVIRONMENTAL STUDIES

4. DESCRIPTIVE NOTES (Type of report and inclusive dates)

Scientific. Final. September 1969 through August 1970 Approved 23 December 1970

5. AUTHOR(S) (First name, middle initial, last name)

Donald J. Armstrong, Edward D. Conway, Carolyne M. Mandell
John A. Carbone, Peter W. Lindstrom

6. REPORT DATE	7a. TOTAL NO. OF PAGES	7b. NO. OF REFS
September 1970	133	9

8a. CONTRACT OR GRANT NO.	9a. ORIGINATOR'S REPORT NUMBER(S)
F19628-70-C-0029 b. PROJECT, TASK, WORK UNIT NOS. N/A N/A N/A c. DOD ELEMENT 61102F d. DOD SUBELEMENT 681300	9b. OTHER REPORT NO(S) (Any other numbers that may be assigned this report) AFCRL-70-0581

10. DISTRIBUTION STATEMENT

1-This document has been approved for public release and sale; its distribution is unlimited.

11. SUPPLEMENTARY NOTES	12. SPONSORING MILITARY ACTIVITY
TECH, OTHER	Air Force Cambridge Research Laboratories (SUM) L. G. Hanscom Field Bedford, Massachusetts 01730

13. ABSTRACT

This report is the concluding scientific report to record the status and progress of Scientific Analytical Investigations, the preparation of Computer Programs, Data Reduction, and the development of mathematical and computer techniques in support of Environmental Research and other various aspects of the physical sciences concerning the upper atmosphere.

During the year covered by this report, the 50 completed programs ranged in complexity and size from conversion of programs from one language or computer system to another, to analysis and development of a large system of analytical programs.

DD FORM 1 NOV 65 1473

Unclassified
Security Classification

14. KEY WORDS	LINK A		LINK B		LINK C	
	ROLE	WT	ROLE	WT	ROLE	WT
Climatology						
Trafficability						
Areal Precipitation						
Geopotential Height						
Clouds						
Wind Analysis						
Strain						
Microwave Acoustics						
Recording of Ionosphere Parameters						
Radio Propagation Conditions						
Photographic Measurements						
Hot Magnetoplasmas						
Three-Body Scattering						
Integral Equation						